論文 / 著書情報
Article / Book Information

題目(和文)	
Title(English)	In-plane switching behavior of liquid crystals on high density polymer brushes
著者(和文)	佐藤治
Author(English)	OSAMU SATO
出典(和文)	学位:博士(工学), 学位授与機関:東京工業大学, 報告番号:乙第4168号, 授与年月日:2018年5月31日, 学位の種別:論文博士, 審査員:戸木田 雅利,扇澤 敏明,宍戸 厚,川内 進,松本 英俊
Citation(English)	Degree:Doctor (Engineering), Conferring organization: Tokyo Institute of Technology, Report number:乙第4168号, Conferred date:2018/5/31, Degree Type:Thesis doctor, Examiner:,,,,
学位種別(和文)	博士論文
Type(English)	Doctoral Thesis

In-plane switching behavior of liquid crystals on high density polymer brushes

A Dissertation Presented

by

Osamu Sato

to

Department of Chemical Science and Engineering

School of Materials and Chemical Technology

Tokyo Institute of Technology

Tokyo Japan

2018

In-plane switching behavior of liquid crystals on high density polymer brushes

Contents

Chapter 1

General Introduction

1-1 Motivation

The liquid crystal display (LCD) was put to practical use as a display for calculators and digital watches at the beginning of the 1970s. Taking advantage of their features of thinness, light weight, and low power consumption, LCDs not only acted as substitutes for cathode-ray tubes (CRTs) but also enabled many new applications. The LCD industry has now grown to be a huge industry, which accounts for about 90 % of displays[1].

During the above-mentioned period of rapid development of the LCD industry, the image quality of LCDs also improved quickly. When the thin-film transistor LCD (TFT LCD) was put to practical use in the early 1990s, the key issues with respect to the image quality of LCDs were the viewing angle characteristics and moving pictures. The former issue was resolved by the development of new LCD modes with the wide viewing angle characteristics such as an in-plane switching (IPS) mode[2] and a multi-domain vertical alignment (MVA) mode[3]. The latter issue was overcome via driving technology such as the overdriving[4], blinking backlight[5], and double-speed driving techniques accompanied by frame interpolation technology[6], in addition to improvements in the liquid crystal materials and the LC panel design. At present, the image quality of LCDs has reached a level equivalent to that of the CRT and the plasma display panel (PDP).

On the other hand, the LCD industry is approaching the plateau of the S-curve[7], i.e., the maturation period. Innovative improvements in technology and cost reduction are becoming difficult. Moreover, the LCD industry is faced with a situation in which the functionality and

performance levels of products exceed the level that customer's request[8], and the choice of the direction of development is also becoming very difficult from the point of view of value. In addition, organic light emitting diode displays (OLEDs) have been put to practical use. In recent years, the LCD industry has thus been faced with a situation in which it must overcome the de facto standard of competition within the display industry. The development of innovative LCDs that can demonstrate differentiation from conventional LCDs and meet the challenge of the OLEDs is strongly desired in the LCD industry.

Against such a background, with the aim of creating innovative LCDs, I have introduced a new concept that changes the common idea of a conventional LCD completely: the practical use of an anchoring free state and the development of this new LCD mode by means of IPS driving. In this thesis, the results of basic research toward the realization of a stable zero anchoring state of the azimuth angle direction using a high-density polymer brush, which serves as a basis for the realization of the new LCD mode, are reported. In addition, an outline of the new LCD mode with IPS driving, which utilizes an anchoring free state of the azimuth angle direction for the first time at practical level in the history of the LCD, and improvements in the innovative characteristics of the new LCD mode are also reported.

1-2 Background

1-2-1 The Principle and Structure of the LCD[9,10]

A liquid crystal is defined as a state in which long-distance order in molecular orientation exists, although there is no long-distance order in the center of gravity of molecules[11]. A liquid crystal is a unique material that combines mobility and various forms of anisotropy such as anisotropy of its dielectric constant and refractive index.

An LCD is a display that exploits electro-optical characteristics in which the optical properties of a liquid crystal change under the influence of an electric field, and is a non-light emitting type display that does not emit light by itself.

Although various kinds of LCD exist, three types of classification are possible from the viewpoint of functional structure (Figure 1-1). The first type of classification is based on the light source. Unlike spontaneous light-emitting type displays such as CRTs and PDPs, an LCD cannot emit light by itself but needs a light source for the display of a picture. The second form of classification is based on the LCD mode, and is also a classification based on the state of orientation of the liquid crystals and the principle that generates optical modulation on the application of a voltage: optical rotation, birefringence, optical interference, light scattering, etc. The third type of classification is based on the driving system: static addressing, active matrix addressing. According to the kind of application and the required specifications, an LCD is designed by combining technologies chosen from these three categories. For example, the following combinations exist: transmissive type, IPS mode, and amorphous silicon (a-Si) TFT[12] in the LCD television; transflective (semi-transmissive) type, electrically controlled birefringence (ECB) mode[13], and low-temperature polycrystalline silicon (LTPS) TFT[14] in the mobile phone; and reflective type, twisted nematic (TN) mode[15], and static driving in the pocket calculator.

Henceforth, I will explain the principle and structure of LCDs, focusing on TN LCDs, which have been widely used over a long period of time. As shown in Figure 1-2, a TN LCD consists of a liquid crystal cell in which the liquid crystal is filled between two glass substrates and a backlight unit. A color filter (CF) is formed on a front glass surface, and the TFT electrodes, which consist of TFTs, gate, source, drain electrodes, and pixel electrodes made of indium tin oxide (ITO), and storage capacitances, are formed on the surface of a backboard.

TFTs are formed at the intersection of the gate and source electrodes, and the gate, source, and drain electrodes of the TFTs are connected to the gate, source, and pixel electrodes, respectively. Common electrodes made of solid ITO are located on the CF. One pixel consists of red, green, and blue sub-pixels, and a TFT is formed in every sub-pixel. The CF has a coloring function, and the TFT electrodes play the role of transmitting an electrical signal from the driving circuit to each sub-pixel. Moreover, an alignment layer is formed on the TFT electrodes and the common electrode, the space between the two glass substrates is filled with the liquid crystal, and polarizers are attached to the back of the two glass substrates. The dimming function (optical shutter function) is realized by the liquid crystal, polarizer, and alignment layer, and the component that acts as the optical shutter is referred to as the LC cell. The backlight plays the role of the light source and consists of light sources such as a cold-cathode fluorescent lamp or light-emitting diode, a light guide plate, diffusion films, a light reflector, and prism sheets.

The display in an LCD is obtained as follows. A picture signal is changed into a driving signal, which is used for driving the LCD, in the driving circuit. The driving signal is transmitted to sub-pixels through various electrodes, and a voltage is applied to the sub-pixels. When a voltage is applied to a sub-pixel, the alignment of the liquid crystals changes according to the strength of the voltage, and the intensity of the light entering from the backlight unit is adjusted. Various brightness and colors can be obtained by additive color mixing by adjusting the light volume for every red, green, and blue sub-pixel.

1-2-2 History of the Research and Development of LCDs[9,16,17]

The liquid crystal was discovered by Reinitzer, who was a botanist from Austria, in 1888[18]. Research into liquid crystals started when he requested the German physicist Lehmann to carry out a detailed analysis[19]. The invention of the first LCD was performed by Heilmeier et

al. at RCA Laboratories in the United States in 1962[20]. The basic principle of LCDs, namely, the optical shutter that controls the light intensity of liquid crystal molecules, was first produced at this time. This basic principle has not changed until now.

The first display mode, which was developed by Heilmeier et al., was dynamic scattering (DS) mode[20]. In DS mode, although the liquid crystal layer is transparent when the voltage is off, when the voltage is on the liquid crystal layer becomes opaque owing to the light scattering, because of the turbulent flow of liquid crystal molecules. The LCD that Heilmeier et al. created was a reflective type and had a structure that sandwiched a nematic liquid crystal (NLC) between a backboard with a reflective electrode and a frontboard with transparent electrodes[20]. After the development of DS mode, new LCD modes were successively developed such as guest-host mode[21] in 1968, ECB mode[13] in 1970, TN mode[15] in 1971, and a prototype of the present IPS mode[22] in 1973. DS mode was the first among these five display modes, which were all proposed during the same period, to be put to practical use, and was put on the market as a display for calculators by Sharp in 1973. However, DS mode never became the mainstream in LCDs owing to its high power consumption, difficulties in visivility in segmented displays, and a limit to the number of scanning lines in dot-matrix driving.

After it transpired that DS mode had limits, TN mode came to attract attention. TN mode was put on the market by Suwa Seikosha (Seiko Epson) as a display for a wristwatch in 1973. Although Schadt and Helfrich first reported the transmissive type in 1971, the reflective type of TN LCD with a reflector on the backboard was employed in many applications such as digital watches and calculators after its practical utilization. Although the driving system of TN mode was a static driving in the first stage, a dynamic driving system came to be used afterwards. These are the prototypes of TN mode, which is one of the mainstream display modes used at present and was employed in portable games machines, etc., in the 1980s.

Then, TN mode developed into the dot-matrix display from the segmented display. At that time, discussions regarding which system should be selected in order to produce dot-matrix displays had already taken place. The principle of the active matrix system was proposed by Lechner et al. at RCA Laboratories in 1971[23]. In this proposal, three systems were successfully commercialized or underwent examination for practical use, namely, the diode address, TFT address, and plasma address methods. The first trial production run using the TFT address method was reported by Brody et al. at Westinghouse Research Laboratories in the United States[24]. However, because the crystal structure of CdSe which was used for TFTs was unstable, this method did not result in commercial utilization. Utilization of the TFT system found itself in an impasse temporarily until silicon thin-film technology was invented in the 1980s.

From the above background, development progressed in the direction toward the realization of a dot-matrix display using a passive matrix system. Although the production of a dot-matrix display using a passive matrix was first considered in DS mode, its utilization was first realized in TN mode. The first trial product incorporating a dot-matrix TN LCD was developed by Hitachi in 1976[25]. Hitachi also developed a reflective-type dot-matrix TN LCD in 1978. However, because the voltage ratio between on and off states was small in TN mode, the maximum number of scanning lines in TN mode LCD was limited to 50 to 100. To enable further enlargement and higher resolution, new technical innovations were required.

The discovery of super-twisted nematic (STN) mode solved the problem of the above-mentioned TN mode. In order to increase the number of scanning lines, Waters et al. at the Royal Signals and Radar Establishment in the United Kingdom and Scheffer at Brown Boveri Research Center in Switzerland proposed making the voltage–transmittance characteristic curve steep in 1983[26,27]. In 1984, Scheffer et al. announced the development of STN mode, in which the twist angle of the liquid crystal was made to be 270 ° and the voltage–transmittance

characteristic curve was made steep[28,29]. Scheffer et al. formed the alignment layer by a vapor deposition method. After Hitachi succeeded in developing an STN LCD by a rubbing method in 1986[30], this structure became standard in STN mode. Although STN mode gave rise to blue or yellow colors, the color output was whitened by stacking two panels. A laptop computer equipped with a two-layer STN panel was put on the market by Seiko Epson in 1988. Then, instead of stacking two panels, a new whitening technique in which retardation films were attached to the STN panel was developed, and products using the new technique were put on the market by Seiko Epson, Hitachi, and Sharp, etc., in 1988.

For the colorization of LCDs, Uchida of Tohoku University proposed a technique using a micro-color filter[31]. This method is also used at present. The colorization of LCDs proceeded in TFT LCDs in advance of STN mode, because there was no solution applicable to black and white displays in STN mode at that time. After a monochrome display was obtained in STN mode, as mentioned above, colorization also progressed in STN mode[32-34]. In trial products using TFT LCDs in the second half of the 1980s, in addition to a TFT and a CF, an edge light-type backlight was already used[35,36]. The basic structure of present TFT LCDs was already completed.

The TFT system is a form of active matrix system and was developed in order to prevent crosstalk, which was seen in passive matrix LCDs such as TN or STN mode. As mentioned above, because CdSe was used for early TFTs, the crystal structure was unstable and this method did not result in commercial utilization. Eighteen years after the invention of the TFT, after the method of using a silicon thin film was proposed, examination of the utilization of the TFT system commenced. An a-Si TFT was made as an experiment by Le Comber et al. at Dundee University in the United Kingdom in 1979[12], and an LCD with an a-Si TFT was produced in 1980[37]. Hitachi made an LTPS TFT as an experiment in 1980[14]. The first product

using a TFT system was an LCD television with a high-temperature polycrystalline silicon (HTPS) TFT put on the market by Seiko in 1984. The first product with an a-Si TFT system was an LCD television developed by Matsushita Electric Industrial in 1986. After that, in a-Si TFT systems development proceeded toward the enlargement of the screen size. A typical example was a 14-inch a-Si TFT LCD announced by Sharp in 1989.

The TFT LCD industry was established after a laptop computer with an a-Si TFT color LCD was launched in 1991. Although TN mode was used in early TFT LCDs, it had the problem that the viewing angle was narrow. In order to overcome this problem, Hitachi developed IPS mode in 1995[2]. Then, Fujitsu, Sanyo, and Samsung developed MVA mode[3] in 1997, electrically tilted vertical alignment (EVA) mode[38] in 1997, and patterned vertical alignment (PVA) mode[39] in 1998, respectively. Moreover, Hyundai developed fringe field switching (FFS) mode as a technique that increased the transmittance of IPS mode in 2001[40]. By the development of these new modes, the viewing angle characteristics of LCDs were improved drastically. After the solution of the viewing angle problem, the a-Si TFT-LCD dominated the monitor market at the end of the 1990s and the television market at the beginning of the 21st century and, as a result, the LCD industry has grown to be a huge industry. An outline of the history of the development of LCDs is shown in Table1-1.

1-2-3 Outline and Issues of IPS LCD

Among the several LCD modes that have been proposed, IPS mode LCDs have now become widely used because of their outstanding viewing angle characteristics, i.e., uniform grayscale levels and colors over a wide range of viewing angles[2]. The interdigital electrode method, which formed the origin of IPS mode, was reported by Soref at the Sperry Research Center in the United States[22]. Then, an LCD using IPS mode was announced with a wide

viewing angle characteristic, in which comb-shaped electrodes were used and an in-plane electric field was applied to the liquid crystals[41]. Furthermore, Kondo et al. at Hitachi succeeded in the development of a TFT IPS LCD in 1995[2]. LCDs came to be recognized as displays that could compete with CRTs.

Although an electric field is applied between the substrates (perpendicular to the substrates) in TN mode or VA mode, it is applied almost parallel to the substrates in IPS mode. As a result, liquid crystal molecules transfer from a homogeneous to a twisted orientation in a plane parallel to the substrates in IPS mode on the application of a voltage. Figure 1-3 shows the structure of an IPS LCD for comparison with TN mode (Figure 1-4) and MVA mode (Figure 1-5). TFT, pixel electrodes, etc. are formed in a lower substrate and the common electrode is formed in an upper substrate in TN mode or MVA mode. However all electrodes including TFT, and comb-shaped electrodes (pixel and common electrodes), etc. are formed in a lower substrate in IPS mode, and comb-shaped electrodes that apply the in-plane electric field are formed for every sub-pixel. The liquid crystals are aligned homogeneously parallel to the substrates. The easy axis of liquid crystal alignment is arranged to coincide with the polarization axis of one of the polarizing plates, which are arranged in a cross-Nicol configuration.

The change in the transmittance of the IPS LCD upon the application of a voltage is represented by Equation 1.1:

$$I = I_0 \sin^2(2\theta) \sin^2(\frac{\pi \Delta n d}{\lambda}) \tag{1.1}$$

The transition to a twisted orientation from a homogeneous alignment corresponds to a change in the value of $\sin^2(2\theta)$ in Equation 1.1, and the value of $\sin^2(\frac{\pi \Delta n d}{\lambda})$ in Equation 1.1 hardly changes, because the liquid crystal molecules rotate in a plane parallel to the substrates. For this reason, a wide viewing angle characteristic with little change in color is achieved in IPS mode. However, if the direction of rotation of liquid crystals is only in one way, changes in color from

yellowish to bluish according to the angle between the visual axis and the screen occur. This issue was improved by the formation of bent comb-shaped electrodes and the coexistence of two domains, in which the direction of rotation of liquid crystals differed, in a sub-pixel[42]. Whereas IPS mode has an outstanding viewing angle characteristic, it has a higher driving voltage and lower transmittance than TN mode. The lower transmittance is attributed to the fact that in IPS LCDs light above the electrodes is not transmitted because a longitudinal electric field is formed above the comb-shaped electrodes and the liquid crystals cannot rotate in a sufficiently horizontal plane.

Because the transmittance of an LCD has a significant influence on the power consumption of a range of products, the improvement of transmittance is an important factor in IPS mode. FFS mode was developed in order to improve the transmittance of IPS mode. Because FFS mode uses an in-plane electric field parallel to the substrates, as does IPS mode, it exhibits an excellent viewing angle characteristic equivalent to that of IPS mode. The difference between FFS mode and IPS mode lies in the structure of the electrodes. In FFS mode, the solid common electrode and the comb-shaped electrodes, which consist of ITO, are arranged through an insulating layer. A fringe field is formed between the common electrode and the comb-shaped electrodes by making the distance between these electrodes smaller than both the distance between the comb-shaped electrodes and the cell thickness. Liquid crystals are made to rotate in a plane parallel to the substrates by the fringe field (Figure1-6). Because the fringe field is formed at a peripheral location on the comb-shaped electrodes, a large portion of the liquid crystals above the comb-shaped electrodes can rotate horizontally. FFS mode can substantially increase the aperture ratio in comparison with IPS mode[40]. However, superior transmittance in FFS mode is restricted to the field of high-resolution LCDs for smart phones, etc. The transmittance of an LCD is determined by the aperture ratio and the permeability of

many laminated layers in the direction of transmission of light. Although FFS mode is advantageous with respect to the aperture ratio, it is disadvantageous with respect to permeability, because the insulating layer and the ITO common electrode layer have been added to those used in IPS mode. In a high-resolution LCD, because the area ratio of the comb-shaped electrodes occupying a sub-pixel is large, the transmittance of FFS mode, which can allow light to penetrate above the comb-shaped electrodes, is higher than that of IPS mode. On the other hand, in an LCD with low resolution, because the area ratio of the comb-shaped electrodes occupying a sub-pixel is not so large, the influence of permeability declines owing to the increase in the sizes of the insulating layer and the ITO common electrode, which counteracts the improving effect of the larger aperture ratio. As a result, in an LCD that is not so high-resolution the transmittance in IPS mode is higher than that in FFS mode. Moreover, if the capability of the photolithography method used in a large substrate is taken into consideration, it is difficult to make the width of the comb-shaped electrodes less than the level used at present and an improvement in permeability in FFS mode cannot be expected.

Thus, regardless of the resolution of an LCD, the invention of a new technique that increases the transmittance of IPS LCDs is strongly desired to reduce their power consumption.

1-2-4 The Role of Anchoring in LCDs

Anchoring between the liquid crystal and the interface is indispensable in all the LCD modes currently put to practical use. Uniform orientation of the liquid crystal and recovery to the initial orientation state of the liquid crystal after removal of the applied voltage are achieved by anchoring between liquid crystal molecules and the interface. Present LCDs cannot perform a predetermined function if anchoring does not take place between liquid crystal molecules and the interface.

Anchoring between liquid crystal molecules and the interface is brought about by an alignment material and orientation processing. In general, polyimide (PI) is used as the alignment material in order to enable strong anchoring to take place. The liquid crystal molecules are aligned uniformly in a predetermined direction by a rubbing[43] or photo-alignment method[44] in an LCD mode in which the initial direction of orientation of liquid crystal molecules is horizontal to the substrate, such as TN, STN, IPS, FFS, and surface-stabilized ferroelectric liquid crystal (SS-FLC) modes[45]. Although there is no necessity for rubbing in a mode in which the initial direction of orientation of liquid crystal molecules is perpendicular to the substrate, such as MVA and PVA modes, a treatment that fixes the pre-tilt angle of liquid crystal molecules by forming a polymer layer on the surface of the alignment film is sometimes performed with the aim of an improvement in the response time or the contrast ratio[46]. On the other hand, anchoring between liquid crystal molecules and the interface is a fundamental factor in the existence of the threshold voltage in the Freedericksz transition[47] of LCD. Taking the converse point of view, if anchoring does not take place between liquid crystal molecules and the interface, a threshold voltage does not occur in LCDs and the orientation of the liquid crystal can not only be changed by a very low voltage, but the orientation at the time of application of the voltage can also be maintained after removal of the voltage. In other words, it can be expected that an innovative LCD that combines the advantages of ultralow voltage driving performance and a memory characteristic can be obtained.

1-2-5 Application to LCD of a Weak Anchoring State

Practical use of a weak anchoring state has also been considered in previous work. Nehring et al. at the Brown Boveri Research Center predicted, by theoretical calculations of TN mode, that the driving voltage would decline and the response time in the voltage-on state

would shorten as the strength of anchoring became low; however, the response time in the voltage-off state would lengthen. Moreover, they also predicted that the twist state would become unstable and that bi-stability would appear when the strength of anchoring became less than a certain level[48].

Bryan-Brown et al. at the Defense Evaluation and Research Agency found out that the strength of anchoring at the interface decreased when a minute quantity of the oligomer was dissolved in the liquid crystal[49]. They produced a TN LCD that had weak anchoring at interfaces by the following procedure: they produced the cell by attaching two substrates that had fine concavo-convex structures on each surface so that they might mutually intersect perpendicularly, and injected the liquid crystal, in which a minute quantity of the oligomer was dissolved, into the cell. In their LCD the threshold voltage decreased in contrast to that in a conventional TN LCD into which the liquid crystal without the oligomer was injected, and the response time in the voltage-on state was shortened. However, the response time in the voltage-off state was lengthened, as Nehring et al. had predicted.

Bryan-Brown et al. also proposed a new LCD mode, namely, voltage-controlled twist (VCT) mode[50]. In VCT LCD mode, a fine concavo-convex structure with low surface energy was formed in one substrate and a rubbed PI surface was formed in another substrate. The two substrates were attached so that the longitudinal direction of the fine concavo-convex structure and the direction of rubbing might mutually intersect perpendicularly, and a liquid crystal with negative dielectric anisotropy was injected between the two substrates. However, the liquid crystal molecules on the fine concavo-convex structures with low surface energy aligned perpendicularly to the substrate, whereas the liquid crystal molecules on the rubbed surface aligned horizontally to the substrate. As a result, the liquid crystal molecules changed their alignment direction gradually from a planar orientation on the rubbed PI surface to a vertical

orientation on the surface of the fine concavo-convex structure with low surface energy in the absence of an applied voltage. Because the dielectric anisotropy of the liquid crystal was negative, when an electric field was applied in a direction vertical to the substrates, the liquid crystal molecules on the surface of the fine concavo-convex structure changed their director in the direction horizontally to the substrate. Moreover, they aligned in the direction parallel to the longitudinal direction of the fine concavo-convex structure when a voltage beyond a certain threshold was applied. In other words, the liquid crystal molecules transferred to a 90 ° twisted orientation from the rubbed PI surface toward the surface of the fine concavo-convex structure. VCT LCD mode not only achieved a steep electro-optic characteristic curve and a high contrast ratio equivalent to that of TN mode, but also shortened the response time in comparison with IPS mode[50]. On the other hand, the viewing angle in VCT mode is considered to be intrinsically narrower than that in IPS mode, because the orientation of liquid crystal molecules transferred to a planar orientation from a hybrid orientation on the application of a voltage.

Thus, although the practical use of weak anchoring at the interface has the potential to enable the development of innovative LCDs, almost all previous works about the practical use of weak anchoring considered so far concerned a longitudinal electric field system. This is because the formation of the comb-shaped electrodes is complicated and the IPS system was considered to be disadvantageous, when compared with the longitudinal electric field system, in respect of its cost. On the other hand, LCDs using the IPS system such as IPS and FFS modes are currently applied in many fields because they have extremely wide viewing angle characteristics and uniform grayscale levels and colors over a large range of viewing angles; moreover, their technical completeness is high. Hence, the use of the IPS system based on weak anchoring at the interface is expected to enable the development of innovative LCDs that take

advantage of the merits of having weak anchoring at the interface for LCDs and eliminates the disadvantages for LCDs of the longitudinal electric field system.

1-2-6 Achieving of a Weak Anchoring Surface by Polymer Coating or Mixing Method

Weak anchoring at the interface has been repeatedly achieved in previous studies via the technique of applying polymer materials to a substrate. These substrates with applied polymer materials exhibited a weak anchoring state at high temperatures[51-54]. When a cell filled with NLCs between these two substrates slowly annealed from the isotropic to the nematic phase, the liquid crystals adopted a planar orientation. When an external field, such as a magnetic field, was applied while this annealing occurred, the liquid crystals were uniformly oriented. When the cell was cooled, the uniformly oriented state was fixed, and the coated polymer surface displayed a strong anchoring state. The coated polymer interface assumed a viscoelastic state, and the liquid crystals gradually rotated to the direction of an external field under external influence at intermediate temperatures. These temperatures fell between the temperatures at which the polymer interface exhibited strong and weak anchoring characteristics, respectively[55-58]. In contrast, it is unavoidable that the coated polymer materials mix with the liquid crystals to a certain extent, causing them to be exfoliated from the substrate. For these reasons, the technique of applying polymer materials to a substrate cannot be used to achieve a stable weak anchoring surface.

Weak anchoring at the interface has also been achieved by mixing certain substances into the liquid crystal. Bryan-Brown et al. achieved weak anchoring at the interface by dissolving a minute quantity of the oligomer in the liquid crystals[49]. Yamamoto et al. succeeded in producing a zero-azimuth anchoring interface at which an anchoring force in the direction of an azimuthal angle does not exist although a force exists in an angular direction[59]. To accomplish this, they

produced a cell filled with NLCs containing a minute quantity of dissolved polystyrene (PS) and a block co-polymer consisting of PS and liquid-crystalline polymer between two substrates that were treated to have an affinity with the liquid layer. Liquid/liquid crystal phase separation occurred in the cell, and the liquid layer segregated on both these treated substrates. As a result, a structure, with a sandwiched liquid crystal layer between the liquid layers, was formed. Herein, the block co-polymer played a role in stabilizing the liquid/liquid crystal phase separation. Because the liquid crystal layer existed on the liquid layer, the liquid crystals were restricted in the angular direction; however, they could freely rotate in the azimuth-angle direction. In contrast, the zero-azimuth anchoring state was obtained only over a narrow temperature range by dissolving certain substances in the liquid crystals. For every liquid crystal type, it is impractical to select the specific substances and their amounts to be mixed into the liquid crystals.

1-2-7 The Interaction of Polymer Brushes and Liquid Crystals

Polymer brushes have the potential to overcome the above-mentioned issues. Polymer brushes are produced by surface graft polymerization, in which polymer chains are tethered at one end to a substrate and grow perpendicularly to the substrate. The wettability and water repellency of a surface can be changed by forming polymer brushes of a length of a few hundred nanometers on the surface. Moreover, frictional, adhesive, and antifouling properties, etc., can be improved drastically by the appropriate design of the chemical structure of brush chains. Thus, the polymer brush has been actively studied as a new method of surface treatment in recent years. Polymer brushes are classified as dilute brushes (below 0.01 chains/nm^2), semi-dilute brushes (0.01 - 0.1 chains/nm^2), and concentrated (high density) brushes (above 0.1 chains/nm^2), according to the graft density. Fukuda and Tsujii et al. succeeded in forming

polymer brushes with a high graft density, which was increased to 0.1 - 0.7 chains/nm^2, in which the length and distribution of the chains were controlled on the surface of the inorganic material[60,61]. They discovered many new characteristics of the high density brushes, which were not observed in semi-dilute brushes, via systematic research. In their solvent-swollen state, the polymer chains are highly extended, the thickness of the high density brush reached 80 - 90 % of its full length, and the high density polymer brushes proved highly resistant to compression[62]. However, they also have ultralow surface friction properties, i.e., almost no frictional resistance[63,64]. The high density polymer brushes exhibit a distinct size exclusion effect, which prevents the entry of molecules larger than a certain size into the brushes and inhibits the adsorption of bio-related materials such as proteins[65]. Moreover, the high density polymer brushes are even incompatible with the same kind of polymers when free in the molten state[66]. In addition, silica particles with the high density brushes grafted on their surface provide exceptionally good dispersibility in solvents. They form a semi-colloidal crystal at a gas–liquid interface and develop structural color[67,68].

I expected that either of the following two states would be obtained when the high density polymer brushes were used as an orienting film for liquid crystals, because the high density polymer brushes display a size exclusion effect and polymer chains are tethered at one end to a substrate. The first supposition assumes the case in which liquid crystal molecules cannot enter into polymer brushes owing to the size exclusion effect of the high density brushes. When liquid crystals align perpendicularly to the surface of polymer brushes, a loss of entropy takes place because liquid crystal molecules have to arrange their terminals at the interface with polymer brushes. However, when liquid crystals align parallel to the surface of polymer brushes, a loss of entropy does not occur because there is no necessity for liquid crystal molecules to arrange their terminals at the interface with polymer brushes. Therefore, liquid crystal molecules are

considered to align horizontally on the high density polymer brushes. In this case, it is expected that the interaction between liquid crystals and polymer brushes becomes very small, because liquid crystal molecules contact polymer brushes in the state near their point of contact and the strength of anchoring between liquid crystals and polymer brushes becomes close to zero. On the other hand, the second supposition assumes the case in which liquid crystal molecules enter into polymer brushes. In this case, it is considered that a stable liquid crystal swelling layer is formed at the interface between liquid crystals and polymer brushes, because polymer chains are tethered at one end to a substrate and cannot dissolve in liquid crystals. It is expected that the liquid crystal swelling layer assumes a pseudo-liquid state in which liquid crystal molecules can move freely, because the glass transition temperature (T_g) of polymer brushes at the liquid crystal swelling layer decreases sharply depending on the selection of liquid crystals and polymer brushes. It was shown by Yamamoto et al. that the restraining force in the direction of the azimuthal angle applied to liquid crystal molecules at the interface between the liquid crystal and liquid is zero[59]. It is considered that a near-zero anchoring state can be attained by obtaining a stable pseudo-liquid state at the interface of liquid crystals and polymer brushes using high density polymer brushes.

1-3 Research Objectives

The purpose of this thesis is to investigate the following three subjects:

1) Elucidation of the anchoring behavior between the high density polymer brushes and NLCs;

2) Achievement of a zero-azimuth anchoring state using the high density polymer brushes; and

3) Creation of a new LCD mode driven by IPS that utilizes the zero-azimuth anchoring state

1-4 Research Methods

A series of examinations in this study was performed using an LC cell in which NLCs were injected between two glass substrates, one of which had comb-shaped ITO electrodes for IPS driving, and the other had photospacers. Moreover, the high density polymer brushes were formed on the substrates as an alignment layer. The temperature dependence of anchoring behavior and the strength of azimuthal anchoring at the interface between polymer brushes and liquid crystals were examined on the basis of the results of electro-optical measurements made at various temperatures. LC cells using polymer brushes that had different T_g values and different compatibility with liquid crystals were produced. The influence that the T_g value of polymer brushes and the compatibility between polymer brushes and liquid crystals had on the azimuthal anchoring coefficient (A_2) of the polymer brush interface was examined using these LC cells. The achievement of a zero-azimuth anchoring state at room temperature was also examined.

In addition, the development of a new LCD mode that utilized the zero-azimuth anchoring state driven by IPS was examined. On the basis of the knowledge acquired by the above-mentioned examination, poly(hexyl methacrylate) (PHMA) brushes were used as the alignment layer and the optimization of the structure and optical design of the LC cell was examined. The electro-optical properties of the new mode of LCD were measured and its operational mechanism was also examined.

1-5 Organization of the Thesis

This thesis consists of five chapters. Chapter 1 forms the general introduction. First of all, the motivation of this research is described. Next, as the background of this research, the principle, structure, and research and development history of LCDs, the role of anchoring in

LCDs, and the interaction between polymer brushes and liquid crystals are reviewed, taking into account previous studies. Furthermore, on the basis of this background, the goal of this research is stated and a research method is described.

In chapter 2, the temperature dependence of anchoring at the interface between polymer brushes and liquid crystals is examined. LC cells were produced using high-density poly(methyl methacrylate) (PMMA) and PS brushes as an alignment layer (PMMA-B cell and PS-B cell, respectively), and the temperature dependence of the change in transmittance when the LC cells were driven in IPS mode at various temperatures for a long time was measured. From the results of the measurements, it was clarified that PMMA and PS brushes displayed a strong anchoring property equivalent to that of rubbed PI near room temperature and a viscoelastic property at high temperature. In addition, when the PS-B cell was cooled to form a nematic phase from an isotropic phase, liquid crystals aligned parallel to the comb-shaped electrodes immediately after transferring to the nematic phase. This result showed that the interface of PS brushes assumed a near-zero-azimuth anchoring state near 110 °C.

In chapter 3, the influence that the T_g value of polymer brushes and the compatibility between polymer brushes and liquid crystals has on the A_2 value of the polymer brush interface is examined. LC cells were produced using high-density PMMA, poly(ethyl methacrylate) (PEMA), PHMA, and PS brushes as an alignment layer (PMMA-B cell, PEMA-B cell, PHMA-B cell, and PS-B cell, respectively), and the A_2 value of the polymer brush interface at various temperatures was determined from the threshold voltage when the LC cells were driven in IPS mode at various temperatures. Our results demonstrated that the value of A_2 was affected by the glass transition temperature (T_g) of the grafted polymers and decreased with an increase in temperature, but decreased when the compatibility of the polymer with the NLC was high. In addition, liquid crystals in the PHMA-B cell aligned along the comb-shaped electrodes after a

slight push owing to the unevenness of the brush surface. The PHMA-B cell was driven at a threshold voltage of one-fifth that of a conventional cell. These results demonstrated that the interface of PHMA brushes assumed a near-zero-azimuth anchoring state at room temperature.

In chapter 4, on the basis of the knowledge acquired in chapter 3, the development of a new LCD mode utilizing zero-azimuth anchoring state, which achieves innovative improvements in characteristics, is examined. An LC cell in which PHMA brushes and rubbed PI were used as alignment layers for each substrate exhibited a significant reduction in driving voltage and a substantial increase in maximum transmittance and contrast ratio when compared with a conventional IPS LCD. Such a drastic improvement in transmittance was achieved because NLCs above the comb-shaped electrodes rotated toward the electric field direction on the application of a voltage and the light above the electrodes transmitted.

Chapter 5 represents the conclusion of this thesis.

References

1. *LCD Market 2013 Vol.1: Present Aspect & Future Outlook* (Fuji Chimera Research Institute, Tokyo, 2013). [in Japanese]
2. Oh-e, M., Ohta, M., Aratani, S., & Kondo, K. Principles and characteristics of electro-optical behavior with in-plane switching mode. Asia Display 95, 577-580 (1995).
3. Ohmuro, K., Kataoka, S., Sasaki, T., & Koike, Y. Development of super-high-image-quality vertical-alignment-mode LCD. SID'97 Digest, 845 (1997).
4. Okumura, H., & Fujiwara, H. A new low image-lag drive method for large-size LCTVs, SID Symposium Digest of Technical Papers 23, 601-604 (1992).
5. Hirakata, J., Shingai, A., Tanaka, Y., Ono, K., & Furuhashi, T. Super TFT-LCD for Moving Picture Images with the Blink Backlight System, SID international Symposium Digest of Technical Papers, 990-993 (2001).
6. Itoh, G., Mishima, Nao. & Ohwaki, K. Software and Hardware Technologies for High-Quality Moving Images on LCD TVs. Toshiba review 62 (8), 26-30 (2007).
7. Foster, R. *Innovation: The Attcker's Advantage* (Pan Books, London, 1986).
8. Nobeoka, K., ITO, M. & Morita, H. Failure to Capture Value Because of Commoditization-the Case of Digital Home Electronics. RIETI Discussion Paper Series 06-J017 (2006). [in Japanese]
9. Matsumoto, S. *Ekisho display gijyutsu- active matrix LCD [Liquid crystal display technology: Active Matrix LCDs]* (Sangyo tosyo, Tokyo, 1996). [in Japanese]
10. Naemura, S. *Hajimeteno ekisho display gijyutsu [Liquid crystal display technology for beginners]* (Kogyo Chosakai, Tokyo, 2004). [in Japanese]
11. Iwayanagi, S. *Ekisho [Liquid crystals]* (Koritsu Shuppan, Tokyo, 1984). [in Japanese]

12. Le Comber, P. G., Spear, W. E., & Ghaith, A. Amorphous-silicon field-effect device and possible application. Electronics Letters 15 (6), 179-181 (1979).

13. Hass, W., Adams, J., & Flannery, J. B. AC-field-induced grandjean plate texture in mixtures of roomtemperature nematics and cholesterics. Physical Review Letters 24 (11), 577-578 (1970).

14. Matsui, M., Shiraki, Y., Katayama, Y., Kobayashi, K.L.I., Shintani, A., & Maruyama, E. Polycrystalline-silicon thin-film transistors on glass. Applied Physics Letters 37 (10), 936-937 (1980).

15. Schadt, M., & Helfrich, W. Voltage-dependent optical activity of a twisted nematic liquid crystal. Applied Physics Letters 18 (4), 127-128 (1971).

16. Kawakami. H. Ekisho display wo hatten saseta kihon gijyutsu wo tool kara kaisetsu [Basic technologies which the liquid crystal displays were developed: explanation from tools] in *Flat-panel display 2001* (ed. Nikkei Microdevices) 96-110 (Nikkei Business Publications, Tokyo, 2000). [in Japanese]

17. Uchida, T. Ekisho display : saishin no shinten [Liquid crystal displays : the latest technological developments] Proceedings of lecture meeting in Japanese Liquid Crystal Conference 2007, 42-61 (2007). (in Japanese).

18. Reinitzer, F. Beiträge zur Kenntniss des Cholesterins. Monatshefte für Chemie und verwandte Teile anderer Wissenschaften 9, 421-441 (1888).

19. Lehmann, O. Über fliessende Krystalle, Zeitschrift für Physikalische Chemie 4, 462-472 (1889).

20. Heimeier, G. H., Zanoni, L. A., & Barton, L. A. Dynamic scattering : A new electrooptic effect in certain classes of nematic liquid crystal. Proceedings of the IEEE 56 (7), 1162-1171 (1968).

21. Heimeier, G. H., & Zanoni, L. A. Guest-host interactions in nematic liquid crystals: A new electro-optic effect. Applied Physics Letters 13 (3), 91-92 (1968).

22. Soref, R. A. Interdigital field-effect liquid cristal displays. SID International Symposium Digest of Technical Papers, 34-35 (1973).

23. Lechner, B. J., Marlowe, F. J., Nester, E. O., & Tults, J. Liquid crystal matrix displays. Proceedings of the IEEE 59 (11), 1566-1579 (1971).

24. Brody, T. P., Asars, J. A., & Dixon, G. D. A 6”×6” 20 lines-per-inch liquid crystal display panel.1973 SID International Symposium Digest of Technical Papers, 179 (1973).

25. Kawakami, H., Nage, Y., & Kaneko, E. Matrix addressing technology of twisted nematic liquid crystal display. SID-IEEE Record of Biennal Display Conference, 50-52 (1976).

26. Waters, C. M., Brimmell, V., & Raynes, E. P. Highly multiplexable dyed liquid crystal displays. Japan Display ’83, 396-399 (1983).

27. Scheffer, T. J. Liquid crystal display with high multiplex rate and wide viewing angle. Japan Display ’83, 400-403 (1983).

28. Scheffer, T. J., & Nehring, J. Optimization of contrast ratio in reversed-polarizer transmissive-type twisted nematic display. Journal of Applied Physics 45, 908-914 (1984).

29. Scheffer, T. J., Nehring, J., Kaufmann, M., Amstutz, H., Heimgartner, D., & Eglin, P. 24×80 character LCD panel using the supertwisted birefringence effect. SID International Symposium Digest of Technical Papers, 120-123 (1985).

30. Kinugawa, K., Kando, Y., & Kanasaki, M. 640×480 pixel LCD using highly twisted birefringence effect with low pretilt angle. 1986 SID International Symposium Digest of Technical Papers, 122-125 (1986).

31. Uchida, T. A liquid crystal multicolor display using color filters. Proceedings of European Display Conference 1981, 39-42 (1981).

32. Kimura, N., Shinomiya, T., Yamamoto, K., Ichimura, Y., Nakagawa, K., Ishii, Y., & Matsuura, M. Multicolor display by double-layered dupertwisted nematic LCD. 1988 SID International Symposium Digest of Technical Papers, 49-52 (1988).

33. Koh, H., Sawada, K., Ohgawara, M., Kuwata, T., Tsubota, H., Akatsuka, M., & Matsuhiro, K. A 960×240 pixel multicolor supertwisted-nematic display. 1988 SID International Symposium Digest of Technical Papers, 53-56 (1988).

34. Watanabe, H., Okumura, O.,Wada, H., Ito, A., Yazaki, M., Nagata, M., Takeshita, H., & Morozumi, S. Full-color LCD with neutralized STN (NTN). 1988 SID International Symposium Digest of Technical Papers, 416-419 (1988).

35. Ueda, F., Ideno, H., & Horikiri., K. Men shoumei souchi [Surafce lighting equipment]. Japanese Unexamined Patent Application Publication No. Sho57-128383 (1982.08.09).

36. Mizobe, T. Back light souchi [Back light equipment] Japanese Unexamined Utility Model Application Publication No. Sho61-145979 (1986.09.06).

37. Snell, A. J., Mackenzie, K. D., Spear, W. E., & Le Comber, P. G. Application of amorphous silicon field effect transistors in addressable liquid-crystal display panels. Applied Physics 24, 357-362 (1980).

38. Koma, N., & Nishikawa, R. Development of a high-quality TFT-LCD for projection displays. SID Symposium Digest, 461-464 (1997).

39. Kim, K. H., Lee, K. H., Park, S. B., Song, J. K., Kim, S. N., & Souk, J. H. Domain divided vertical alignment mode with optimized fringe field effect. Proceedings of Asia Display 98, 383-386 (1998).

40. Lee, S. H., Lee, S. L., Kim, H. Y., Kim, J. M., Hong, S. H., Jeong, Y. H., Park, C.H., Choi, Y.J., Lee, J.Y., Koh, J.W., & Park, H.S. 18.1" Ultra-FFS TFT LCD with super image quality and fast response time. SID Symposium Digest, 484-487 (2001).

41. Baur, G., Kiefer, R., Klausmann,H., & Windscheid,F. In-Plane Switching: A Novel Electro-optic Effect. Liquid Crystals Today 5 (3), 12-13 (1995).

42. Kondo, K. Recent IPS Alpha Technologies and Future Possibilities. Hitachi Hyoron 88 (10), 830-831 (2006).

43. Aoyama, H., Yamazaki, Y., Matsuura, N., Mada, H., & Kobayashi, S. Alignment of Liquid Crystals on the Stretched Polymer Films. Molecular Crystals and Liquid Crystals 72 (4), 127-132 (1981).

44. Schadt, M., Schmitt, K., Kozinkov, V. & Chigrinov, V. Surface-induced parallel alignment of liquid crystals by linearly polymerized photopolymers, Japanese Journal of Applied Physics 31, 2155-2164 (1992).

45. Clark, N. A., & Lagerwall, S. T. Submicrosecond bistable electro-optic switching in liquid crystals. Applied Physics Letters 36, 899-901 (1980).

46. Hanaoka, K., Nakanishi, Y., Inoue, Y., Tanuma, S., Koike, Y., & Okamoto, K. A New MVA-LCD by Polymer Sustained Alignment Technology. SID Symposium Digest of Technical Papers 35 (1), 1200-1203 (2004).

47. Fredericks, V., & Zolina, V. Forces causing the orientation of an anisotropic liquid. Transactions of the Faraday Society 29, 919-930 (1933).

48. Nehring, J., Kmetz, A.R., & Scheffer,T.J. Analysis of week-boundary-coupling effects in liquid-crystal displays. Journal of Applied Physics 47 (3), 850-857 (1976).

49. Bryan-Brown, G.P., Wood, E.L., & Sage, I.C. Weak surface anchoring of liquid crystals. Nature 399, 338-340 (1999).

50. Bryan-Brown, G.P., Brown, C.V., Sage, I.C., & Hui, V.C. Voltage-dependent anchoring of a nematic liquid crystal on a grating surface. Nature 392, 365-367 (1998).

51. Nemoto, F., Nishiyama, I,. Takanishi, Y., & Yamamoto, J. Anchoring and alignment in a liquid crystal cell: self-alignment of homogeneous nematic. Soft Matter 8 (45), 11526-11530 (2012).

52. Syed I. M, Carbon G, Rosenblatt C, & Wen B. Planar degenerate substrate for micro- and nanopatterned nematic liquid-crystal cells. Journal of Applied Physics 98, 034303 (2005).

53. Oswald, P., Dequidt, A., & Żywociński, A. Sliding planar anchoring and viscous surface torque in a cholesteric liquid crystal. Physical Review E 77, 061703 (2008).

54. Nespoulous M, Blanc C, & Nobili M. Ultraweak azimuthal anchoring of a nematic liquid crystal on a planar orienting photopolymer. Japanese Journal of Applied Physics 102, 073519 (2007).

55. J´anossy, I. Kinetics of director gliding on a polymer-liquid-crystal interface. Physical Review E 81, 031714 (2010).

56. Vetter P, Ohmura Y, & Uchida T. Study of Memory Alignment of Nematic Liquid Crystals on Polyvinyl Alcohol Coatings, Japanese Journal of Applied Physics 32, L1239-L1241 (1993).

57. Stoenescuab D.N, Dozovac I, & Martinot-Lagardea Ph. Long-Time Behavior of the Azimuthal Anchoring Strength and Easy Axis Gliding of Nematic Liquid Crystal. Molecular Crystals and Liquid Crystals Science and Technology. Section A 351, 427-434 (2000).

58. Yamaguchi, R., & Sato, S. Molecular Crystals and Liquid Crystals Science and Technology. Molecular Crystals and Liquid Crystals Section A 367, 379-386 (2001).

59. Yamamoto, J., Yokoyama, H., & Watanabe, J. Zero surface anchoring liquid crystal orientation methods and its liquid crystal device. Japanese Patent No.4053530 (2007.12.14).

60. Ejaz, M., Yamamoto, S., Ohno, K., Tsujii, Y., & Fukuda, T. Controlled graft polymerization of methyl methacrylate on silicon substrate by the combined use of the Langmuir–Blodgett and atom transfer radical polymerization techniques. Macromolecules 31, 5934-5936 (1998).

61. Yamamoto, S., Ejaz, M., Tsujii, Y., Matsumoto, M., & Fukuda, T. Surface interaction forces of well-defined, high-density polymer brushes studied by atomic force microscopy. 2. Effect of graft density. Macromolecules 33, 5608-5612 (2000).

62. Yamamoto, S., Ejaz, M., Tsujii, Y., Matsumoto, M., & Fukuda, T. Surface interaction forces of well-defined, high-density polymer brushes studied by atomic force microscopy. 1. Effect of chain length. Macromolecules 33, 5602-5607 (2000).

63. Sakata, H., Kobayashi, M., Otsuka, H., & Takahara, A. Tribological properties of poly(methyl methacrylate) brushes prepared by surface-initiated atom transfer radical polymerization, Polymer Journal 37, 767-775 (2005).

64. Kuramoto, M., Okayasu, K., Ohno, K., Tsujii,Y., & Fukuda, T. Frictional Properties of Concentrated Polymer Brushes Studied by Rheometer. Polymer Preprints, Japan 55 (2), 4042 (2006).

65. Yoshikawa, C., Goto, A., Tsujii Y., Fukuda, T., Kimura, K., Yamamoto, K., & Kishida, K. Protein Repellency of Well-Defined, Concentrated Poly(2-hydroxyethyl methacrylate) Brushes by the Size-Exclusion Effect. Macromolecules 39, 2284-2290 (2006).

66. Okayasu, K., Yamamoto, S., Tsujii,Y., Fukuda, T., Torikai, N., & Takeda, M. Segmental Distribution of Blockcopolymer Brushes Studied by Neutron Reflectometry. Polymer Preprints, Japan 54 (1), 921 (2005).

67. Ohno, K., Morinaga, T., Koh, K., Tsujii,Y., & Fukuda, T. Synthesis of monodisperse silica particles coated with well-defined, high-density polymer brushes by surface-initiated atom transfer radical polymerization. Macromolecules 38, 2137-2142 (2005).

68. Ohno, K., Morinaga, T., Takeno, S., Tsujii, Y., & Fukuda, T. Suspensions of silica particles grafted with concentrated polymer brush: A new family of colloidal crystals. Macromolecules 39, 1245-1249 (2006).

Table 1-1. History of the research and development of LCDs[9,16,17]

Year	Content	Inventor	Nation
1888	Discovery of liquid crystal[18]	F. Reinitzer	Austria
1961	Article on TFT	RCA Laboratories	USA
1962	Patent application for DS mode	RCA Laboratories	USA
1968	Article on DS mode[20]	RCA Laboratories	USA
1968	Article on guest–host mode[21]	RCA Laboratories	USA
1970	Article on ECB mode[13]	Xerox	USA
1971	Article on TN mode[15]	Hoffman-La Roche	Switzerland
1971	Patent application for TN mode	Hoffman-La Roche	Switzerland
1971	Article on two-frequency driving method in DS LCD	Brown Boveri Research Center General Electric	Switzerland USA
1971	Article on active matrix driving system[23]	RCA Laboratories	USA
1971	Development of wristwatch equipped with DS LCD	Suwa Seikosha	Japan
1972	Article on ECB mode matrix-type LCD	Thomson-CSF	France
1972	Patent application for 1/3 bias voltage equalizing method	Hitachi	Japan
1972	Article applying the voltage equalizing method in an LCD	Texas Instruments	USA
1973	Article on LCD with interdigital electrode system[22]	Sperry Research Center	USA
1973	Article on 1/3 bias voltage equalizing method	Hitachi	Japan
1973	Article on trial manufacture of CdSe TFT matrix-type LCD[24]	Westinghouse Research Laboratories	USA
1973	Launch of electronic calculator equipped with DS LCD	Sharp	Japan
1973	Launch of electronic wristwatch equipped with TN LCD	Hattori Seiko	Japan

1973	Patent application for arbitrary bias voltage equalizing method	Hitachi	Japan
1974	Article on line sequential driving method (the effective value of dependency was taken into consideration)	IBM	USA
1974	Patent application for arbitrary bias voltage equalizing method	Hitachi	Japan
1975	Article on trial manufacture of DS mode matrix-type LCD	Hitachi Asahi Glass Dai Nippon Toryo	Japan
1976	Article on trial manufacture of TN mode matrix-type LCD[25]	Hitachi	Japan
1978	Launch of TN mode matrix-type LCD	Hitachi	Japan
1979	Article on development of orthogonal functions expression of driving waveform of matrix-type LCD	Brown Boveri Research Center	Switzerland
1979	Article on trial manufacture of a-Si TFT[12]	Dundee University	UK
1980	Article on trial manufacture of a-Si TFT matrix-type LCD[37]	Dundee University	UK
1981	Article on trial manufacture of LTPS[14]	Hitachi	Japan
1981	Patent application for LTPS	Hitachi	Japan
1981	Article on color filter system LCD[31]	Tohoku University	Japan
1983	Article that suggested that the voltage–transmittance characteristic curve should be made steep[26,27]	Royal Signals and Radar Establishment Brown Boveri Research Center	UK Switzerland
1983	Patent application for STN LCD	Royal Signals and Radar Establishment Brown Boveri Research Center	UK Switzerland
1984	Launch of color TV equipped with HTPS LCD	Hattori Seiko	Japan
1985	Article on trial manufacture of STN mode matrix-type LCD[28,29]	Brown Boveri Research Center	Switzerland
1986	Article on STN mode matrix-type LCD manufactured by rubbing method[30]	Hitachi	Japan
1986	Launch of STN mode matrix-type LCD	Hitachi	Japan

1986	Article on method of controlling high pre-tilt angles by rubbing	Tokyo University of Agriculture and Technology	Japan
1986	Launch of color TV equipped with a-Si TFT matrix-type LCD	Matsushita Electric Industrial	Japan
1987	Patent application for double-layered STN (D-STN) mode matrix-type LCD	Seiko Epson	Japan
1987	Launch of laptop computer equipped with D-STN mode matrix-type LCD	Seiko Epson	Japan
1988	Article on trial manufacture of D-STN mode matrix-type color LCD[32–34]	Sharp Asahi Glass Seiko Epson	Japan Japan Japan
1988	Article on trial manufacture of 14-inch a-Si TFT matrix-type color LCD	Sharp	Japan
1988	Patent application for film-compensated STN (F-STN) mode matrix-type LCD	Seiko Epson	Japan
1988	Launch of F-STN mode matrix-type LCD	Seiko Epson	Japan
1989	Launch of notebook computer equipped with F-STN mode matrix-type LCD	Toshiba	Japan
1990	Launch of laptop computer equipped with F-STN mode matrix-type color LCD	NEC	Japan
1991	Launch of notebook computer equipped with a-Si TFT matrix-type color LCD	NEC IBM Japan	Japan Japan
1995	Article on IPS mode TFT LCD[2]	Hitachi	Japan
1997	Article on MVA mode TFT LCD[3]	Fujitsu	Japan
1997	Article on EVA mode TFT LCD[38]	Sanyo Electric	Japan
1998	Article on PVA mode TFT LCD[39]	Samsung Electronics	Korea
1999	Launch of 20-inch color LCD TV	Sharp	Japan
2001	Article on FFS mode TFT LCD[40]	Hyundai Electronics Industries	Korea

a) The classification by the light source

- Transmissive
- Reflective
- Semi-transmissive

b) The classification by the LCD mode

- TN (Twisted Nematic)
- STN (Super Twisted Nematic)
- IPS (In-Plane Switching)
- VA (Vertical Alignment)

c) The classification by the driving system

- Segment addressing
  - Static addressing
  - Dynamic addressing
- Matrix addressing
  - Passive matrix addressing
  - Active matrix addressing
    - Thin Film Transistor (TFT)
      - Amorphous-Silicon TFT (a-Si TFT)
      - Low Temperature Poly-Silicon TFT (LTPS)
      - High Temperature Poly-Silicon TFT (HTPS)
      - Oxide TFT
    - Thin Film Diode (TFD)

Figure 1-1. Classification of LCDs[9]

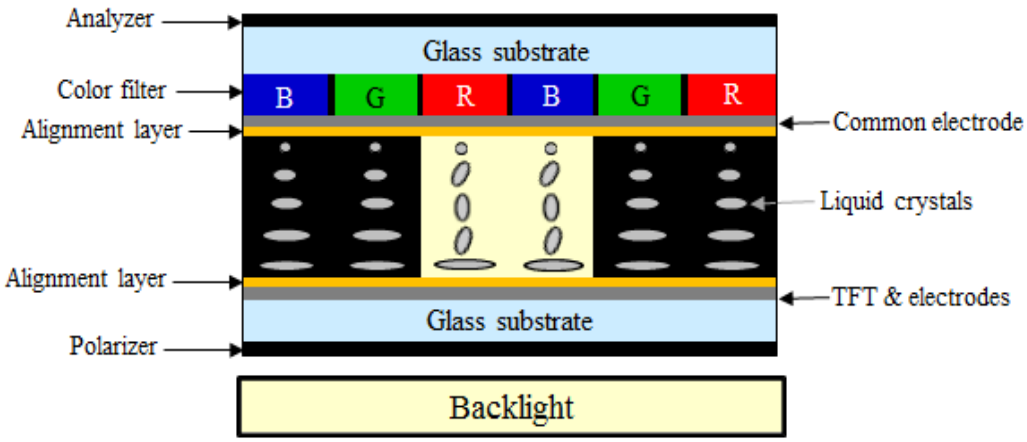

Figure 1-2. Structure of an LCD[10]

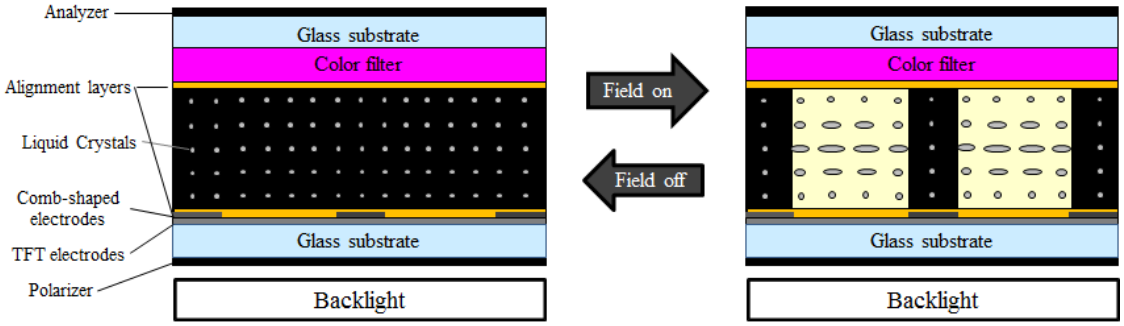

Figure 1-3. Structure of an IPS LCD

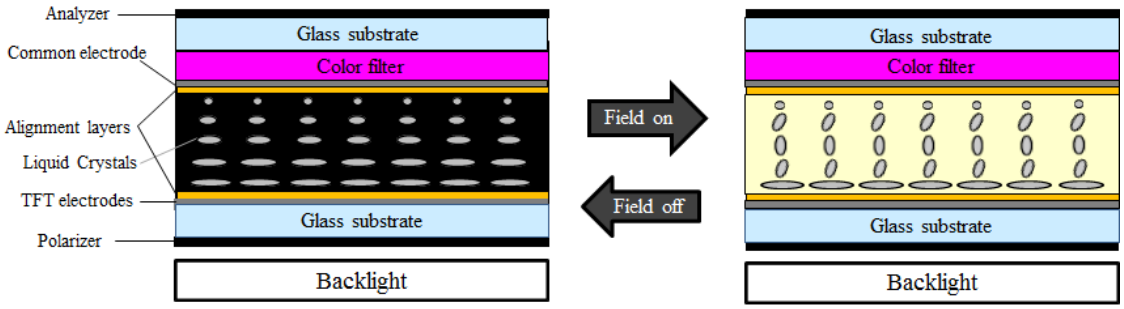

Figure 1-4. Structure of a TN LCD

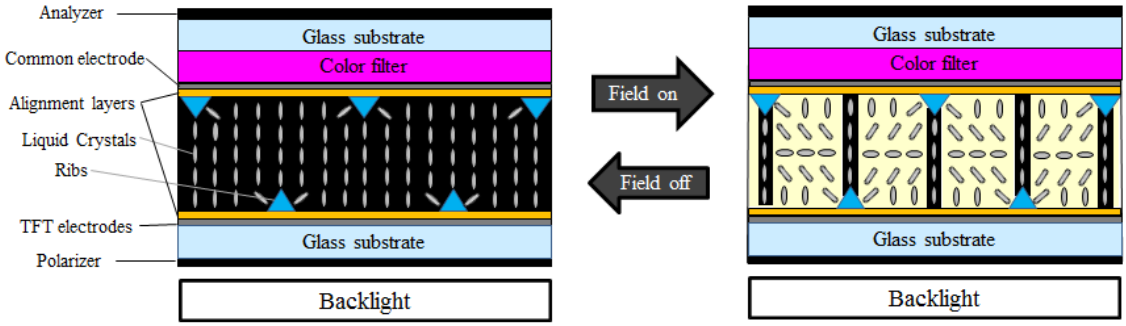

Figure 1-5. Structure of an MVA LCD

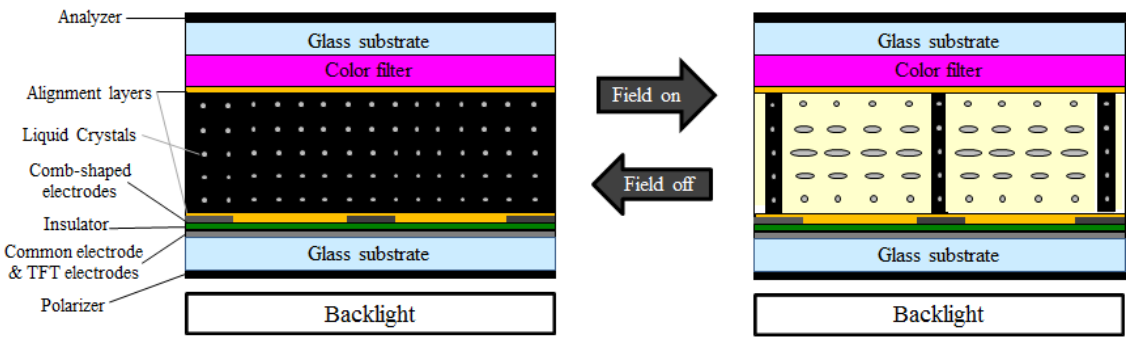

Figure 1-6. Structure of an FFS LCD

Chapter 2

High-density Polymer Brushes as Anchoring Surfaces of Nematic Liquid Crystals

Abstract

The orientation behavior of a nematic liquid crystal (LC) was examined in a cell consisting of two substrates on which the same kind of high-density polymer brushes were grafted. The nematic LC was injected into cells consisting of two substrates on which poly(methyl methacrylate) (PMMA) brushes with a density of 0.299 chains nm^{-2} or polystyrene (PS) brushes with a density of 0.43 chains nm^{-2} were grafted. The LC molecules displayed degenerate planar orientation, which became uniform on cooling from 120 °C in a magnetic field of 1 T. At ambient temperature, the aligned LC cells exhibited typical electro-optical properties when driven in in-plane switching (IPS) mode, which indicated that the LC molecules were anchored to the brushes with their director parallel to the magnetic field direction. In contrast, they functioned as a viscoelastic anchoring surface at higher temperatures. Moreover, at 110 °C (near the isotropization temperature of the bulk nematic) the PS brushes provided a near-zero-azimuth anchoring surface on which an anchoring force in the direction of an azimuthal angle did not exist, although a force existed in an angular direction. Zero anchoring is useful not only for the development of new liquid crystal display modes with novel non-contact orientation capabilities but also for the formation of an interface with ultralow friction with potential applications in a number of fields.

2-1 Introduction

Surface graft polymerization produces polymer brushes that are polymer chains tethered with one chain end to a solid substrate and modify solid surfaces effectively. By applying atom transfer radical polymerization (ATRP), chain length and distribution can be controlled and the graft density has been increased up to 0.7 chains nm^{-2} in the case of poly(methyl methacrylate) (PMMA) brushes[1-5]. Such high-density PMMA brushes have characteristic structures and properties that differ from polymer brushes with a moderate density of 0.001 - 0.05 chain nm^{-2}. In the solvent-swollen state, the polymer chains are highly extended, nearly to their full length, and highly resistant against compression[3]. Even in the dry state, the polymer chains are so extended that the thickness of the polymer brushes reaches 35 % of the fully extended chain length[4]. Such high-density brushes grafted on the surface provide an exceptionally good dispersibility in solvents for silica colloids[6,7] and a low friction coefficient between substrates[8,9].

In this chapter, I report the anchoring of a nematic liquid crystal (LC) to high-density PMMA brushes with σ = 0.299 chains nm^{-2} and polystyrene (PS) brushes with a high density of 0.43 chains nm^{-2}. The nematic LC was injected into a cell consisting of two substrates with polymer brushes. They aligned the director in the plane parallel to the substrate with the azimuthal angle being arbitrary. The director direction was along a preferred azimuthal direction by applying a magnetic field to the cell cooled from temperature of 120 ◦C, which was higher than the isotropization temperature of the nematic LC and as high as the glass transition temperature (T_g) of the brushes. The cell can be driven in the in-plane switching (IPS) mode with electro-optic characteristics similar to these of a conventional cell with rubbed polyimide (PI)-coated substrates at ambient temperature. On increasing temperature, in contrast, the transmittance became time-dependent, suggesting that the LC molecules anchoring to the brushes rotated toward the electric field direction. The brushes thus function as ‘‘soft’’

anchoring surfaces for the nematic LC. In addition, at 110 ◦C (near the isotropisation temperature (*T*i) of the bulk nematic), the PS brushes showed the near-zero azimuthal anchoring surface in which an anchoring force in the direction of an azimuthal angle does not exist, although the force exists in an angular direction.

2-2 Experimental Procedure

High-density PMMA brushes were prepared by surface initiated ATRP on two glass substrates, one of which had comb-shaped indium-tin oxide (ITO) electrodes for the IPS of the LC orientation[10-12]. The initiator of (2-bromo-2-methyl) propionyloxyhexyltriethoxysilane (BHE) was synthesized by the method described in the literature[6]. BHE (0.4 g) dissolved in ethanol (17.6 g) was added to a mixture of ammonia solution (28 % NH_3 aqueous solution, 2 g) and ethanol (20 g), and then stirred. In the resulting solution, the glass substrates cleaned by UV/ozone treatment were immersed for 12 h at ambient temperature to bond BHE to the surface. The modified glass substrates were cleaned by sonication in chloroform, rinsed in acetone, and then dried. Polymerization was performed by dipping the BHE-immobilized substrate in a degassed solution of methyl methacrylate (37.5 g, 0.37 mol), CuBr (0.53 g, 3.75 mmol), 4,4'-dinonyl-2,2’-bipyridine (3.67 g, 8.97 mmol), anisole (37.5 g, 0.35 mol), and 2-bromoisobutylic acid ethyl ester (0.067 g, 0.34 mmol) as a free initiator at 90 ◦C for 3 h. The number average molecular weight M_n and the polydispersity index M_w/M_n of the brushes were 1.12×10^5 and 1.17, respectively, as estimated from the gel permeation chromatogram of the freely initiated PMMA[1,3,4]. The thickness *h* of the brushes was determined on the basis of X-ray reflectivity (Rigaku UltimaIV) to be 46.8 nm (Figure 2-1). The graft density σ was estimated to be 0.299 chains nm^{-2} using the relationship $\sigma = \rho h N_A/M_n$ and assuming that the brush density ρ is equal to the density of the bulk PMMA (1.188 g cm^{-3})[4].

High density PS brushes were also prepared by surface initiated ATRP on two glass substrates, one of which had the same comb-shaped ITO as above. The initiator (2-bromo-2-methyl) propionyloxyhexyltriethoxysilane (BHE) was synthesized as described in the literature[6]. BHE (0.4 g) dissolved in ethanol (17.6 g) was added to a mixture of ammonia solution (28 % NH_3 aqueous solution, 2 g) and ethanol (20 g), and the resulting mixture was stirred to form a solution. The glass substrates cleaned by ultra-violet (UV)/ozone treatment were immersed in this solution for 12 h at ambient temperature to bond BHE with the surface. The modified glass substrates were cleaned by sonication in chloroform, rinsed in acetone and then dried. Polymerisation was performed by dipping the BHE-immobilized substrate in a degassed solution of styrene (44.9 g, 0.43 mol), CuBr (0.61 g, 4.26 mmol), 4,4'-dinonyl-2,2'-bipyridine (3.31 g, 8.10 mmol) and 2-bromoisobutylic acid ethyl ester (0.081 g, 0.41 mmol) as a free initiator at 110 ◦C for 3 h. The number average molecular weight (M_n) and polydispersity index (M_w/M_n) of the PS brushes were 7.06×10^4 and 1.21, respectively, as estimated from the gel permeation chromatogram of the freely initiated PS in the same vessel[1,3,4]. The thickness h of the brushes was determined to be 48.2 nm on the basis of X-ray reflectivity (Rigaku UltimaIV, Figure 2-2). The graft density σ was estimated to be 0.43 chains nm^{-2} by using the relationship $\sigma = \rho h N_A/M_n$ and assuming that the brush density ρ is equal to the density of the bulk PS (1.05 g cm^{-3})[4]. The polymerization conditions and the characteristics of the PMMA and PS brushes are summarized in Table 2-1 and 2-2, respectively.

An experimental cells were fabricated by injecting a nematic LC (JNC JC-5051XX with a nematic-isotropic transition temperature, T_{NI} = 112.7 ◦C) between two plates of PMMA or PS-grafted glass with a gap of 3 μm by capillary action at ambient temperature. A conventional cell was also prepared using two rubbed PI (JSR AL16301)-coated substrates with the same gap as the experimental cells. Here, the experimental cells with PMMA brush and PS brush and the

conventional cell were designated as PMMA-B cell, PS-B cell and rubbed PI (RPI) cell, respectively. Both of the magnetic field directions in the PMMA-B and PS-B cells and the rubbing direction in RPI cell were tilted by 20 ° with respect to the comb-shaped electrodes (Figure 2-3(a)), and a typical IPS mode was adopted, in which the electric field induced the twisted arrangement of molecules from the parallel arrangement as illustrated in Figure 2-3(c). The electro-optical properties of the LC cells were measured using Otsuka Electronics LCD-5200. The intensity of incident light near the surface of the LC cell was about 2.2 million cd/m^2. Polarized optical microscopy (POM) observation was performed by Olympus BX50P microscopy.

2-3 Results

2-3-1 Uniform Planar Alignment of Nematic LC by Magnetic Field

The nematic LC as-injected into the PMMA-B and PS-B cells showed Schlieren texture under POM (Figure 2-4(a) and 2-5(a), respectively), indicating that the nematic LC on the PMMA and PS brushes had a degenerate planar orientation. To obtain a uniform planar LC alignment in the cell, a magnetic field of 1 T was applied in the direction parallel to the substrates. Although the magnetic orientation of the LC orientation was not achieved at ambient temperature both in the PMMA-B and PS-B cells, it was attained when the cells were heated to 120 ◦C and then cooled gradually. Such a macroscopic nematic director orientation was confirmed by POM observations (Figure 2-4(b) and 2-5(b), respectively).

It is interesting that the temperature determined whether the magnetic orientation of the LC was achieved. The lowest temperature at which the magnetic orientation can be achieved in the PMMA-B cell was determined by the following procedure. At the magnetic field, the cell was first heated to a predetermined temperature, annealed for 20 min, and then cooled to

ambient temperature at a rate of 3 ◦C min^{-1}. The LC orientation was confirmed by POM. When the temperature was set to 30 ◦C and increased in 10 ◦C steps, the uniform planar orientation was completed only when the cell was heated to temperatures higher than 120 ◦C. This characteristic temperature is as high as the glass transition (T_g) of neat high-density PMMA brushes[5] and is higher than the T_{NI} of the nematic LC.

2-3-2 In-Plane Switching of PMMA-B Cell at Ambient Temperature

The PMMA-B cell was driven in the IPS mode at ambient temperature. Figure 2-6 (a) shows the voltage-light transmittance (*V*-*T*) curves of the PMMA-B and RPI cells at 25 ◦C. Here, the cells were set with the nematic LC director direction coinciding with the polarizer direction. The transmittance was represented by the relative values taking the transmittances in the electric-field-off state and at its maximum as 0 and 100 %, respectively. The curves were almost identical in shape but slightly different in voltage showing the maximum transmittance V_{max}, which was determined to be 8.5 V for the PMMA-B cell and 9.1 V for the RPI cell. Figure 2-6 (b) shows the transmittance responses of the PMMA-B and RPI cells upon switching the voltage on and off. The response times on switching the voltage on and off were 13.2 and 22.5 ms for the PMMA-B cell, respectively, which were similar to those (12.1 and 20.2 ms) observed for the RPI cell. Figure 2-6 (c) shows the time dependence of the transmittance observed when V_{max} was applied to the PMMA-B cell over a period of 10,000 s and then switched off. The transmittance changed sharply on switching on and off the voltage and was persistently time-independent during both on and off states, indicating the durability of the anchoring effect. These results show that the PMMA brushes function as anchoring surfaces, such as the rubbed PI.

2-3-3 In-Plane Switching of PS-B Cell at Ambient Temperature

Figure 2-7(a) shows the voltage–light transmittance curves of the PS-B and RPI cells driven in the IPS mode at 25 ◦C. Here the cells were set originally such that the nematic LC director coincided with the polarizer direction leading to complete darkness, and the transmittance is represented as the relative values taking the transmittance value in the electric field-off state and at maximum field strength as 0 and 100 %, respectively. The curves are almost identical in shape, although they slightly differ for the voltage showing a maximum transmittance (V_{max}), which was determined to be 8.0 V for the PS-B cell and 9.1 V for the RPI cell. Figure 2-7 (b) shows the time dependence of the transmittance observed when V_{max} was applied to the PS-B cell for 10,000 s and then the voltage was switched off. The transmittance changed sharply on switching the voltage on and off and was persistently time independent during both on and off states, indicating the durability of the anchoring effect. These results show that the PS brushes also function as anchoring surfaces at ambient temperature similar to the rubbed PI.

2-3-4 Temperature Dependency of Anchoring Characteristics of PMMA Brushes

The LC anchoring effect of the PMMA brushes was not as heat-resistant as that of the rubbed PI. Figure 2-8 shows the time dependence of the transmittance of the PMMA-B cell at 45, 65, and 85 ◦C. Unlike the RPI cell, the transmittance of the PMMA-B cell became time-dependent when the temperature increased. While the transmittance remained constant at temperatures up to 45 ◦C (Figure 2-8(a)), it became time dependent at 65 and 85 ◦C (Figure 2-8(b) and (c)). The time-dependent transmittance changes were observed clearly at 85 ◦C during the first 10,000 s in the field-on state and the following 20,000 s after switching off the voltage. In the field-on state, the transmittance increased and then decreased with time to show a

maximum at about 500 s. After switching off the voltage, the transmittance initially increased with time, reached the maximum value of 35 %, and then decreased.

2-3-5 Temperature Dependency of Anchoring Characteristics of PS Brushes

Similarly to the PMMA brushes, the LC anchoring on the PS brushes is not as heat-resistant as that on the rubbed PI. A strong anchoring effect was assured only in a temperature range below 35 ◦C and the transmittance became time-dependent as the temperature increased. The typical examples of time-dependent transmittance are shown in Figure 2-9(a), (b) and (c), which were measured at 45, 65 and 85 ◦C, respectively.

The time-dependence of the transmittance at 45 ◦C in Figure 2-9(a) is similar to that of the PMMA-B cell observed at the higher temperature of 85 ◦C. In the 10,000 s field-on state, the transmittance increased and then decreased with time showing a maximum at approximately 3,100 s. After switching off the voltage, the transmittance initially increased, reached the maximum value of 30 % and then decreased.

2-3-6 Zero Anchoring Surface of PS Brushes Resulting in Spontaneous Alignment of LC Molecules

The orientation behaviour at high temperatures in the PS-B cell exhibits two interesting cell properties: (1) the comb-shaped electrodes function as anchoring substrates and (2) the PS brushes provide a near-zero azimuthal anchoring surface. Anchoring by the electrodes at high temperature could also be recognized when the PS-B cell was heated to the isotropic temperature of 115 ◦C and then cooled to the nematic phase at 110 ◦C. Figure 2-10 shows the optical textures for the nematic phase thus prepared. The LC molecules were found to align uniformly in the direction parallel to the electrodes immediately following the transformation to

the nematic phase, whereas the polydomain schlieren texture appeared in the region without electrodes. Considering that the electrodes offer only a very small surface anisotropy (thickness, 55 nm; width, 4 μm and distance between neighbouring electrodes, 10 μm) or a negligibly small elastic force, the distinctly perfect alignment along the electrodes can only be allowed by a near-zero azimuthal anchoring nature[13] of the PS brushes at 110 ◦C.

2-4 Discussion

2-4-1 A Uniform Planar Orientation Obtained by Magnetic Field

The uniform planar orientation in PMMA-B cell was completed only when the cell was heated to temperatures higher than 120 ◦C. A fundamental question arises as to why the magnetic orientation was achieved on cooling the cell from a temperature higher than 120 ◦C. The temperature of 120 ◦C was as high as the T_g of the PMMA brushes; thus, the brushes exhibited micro-Brownian motions. At the same temperature, the LC was in the isotropic liquid state. Thus, the LC could be miscible with PMMA enough to seep into the brushes (Figure 2-11(a)). On the following cooling, the LC would decrease its miscibility with PMMA owing to its transformation into the nematic state; however, some LC molecules still seeped into the interface and oriented along the magnetic field direction. The magnetic orientation seems to require the LC molecules to seep into the PMMA bushes. On further cooling, the LC molecules were clamped by the polymer brushes losing mobility so as to anchor the LC molecules to the brushes (Figure 2-11(b)). In PS-B cell, the uniform planar orientation was considered to have been achieved by the same mechanism as above. In addition, this anchoring effect may be similar to memory effect of the nematic LC on polymer alignment layers[14-18].

2-4-2 Planar LC Orientation Generated on PMMA and PS Brushes

The nematic LC on the PMMA and PS brushes preferentially oriented such that its director was parallel to the surface, contrary to the expectation that it would be arranged in a perpendicular fashion (homeotropic alignment) because of steric interactions between the LC molecules and the aliphatic chains, similar to the surfactant-treated nematic LCs[19]. This can be explained by assuming that the segments of the brushes in the LC-molecule swelling area are parallel to the substrate. The polymer brushes possess some molecular weight distribution; little stretching out was observed near the end of the brushes because the polymer density near the end of the brushes is not as high as that near the center. When the LC molecules seeped into the brush region, the mobility of the brushes in the LC-molecule swelling area greatly increased owing to the plasticizing effect of the LC. As a result, the brushes entangled with the surrounding brushes, as depicted in Figure 2-11. The LC molecules, thus, mostly interfaced with the side of the brushes, which caused them to orient themselves parallel to the surface.

2-4-3 Time-Dependent Transmittance Changes of PMMA-B Cell at High Temperature

The anchoring molecules rotated toward the electric field and tended to recover the initial orientation after turning off the field above 65 ◦C. This can explain the time-dependent transmittances of the PMMA-B cell at high temperature shown in Figure 2-8. The angle at which the electric field rotated the anchoring molecules can be estimated from the extinction direction of the cell that was quenched to ambient temperature on switching off the voltage. Here, it was assumed that the LC molecules between the substrates immediately became parallel to the anchoring ones on switching off the voltage. The extinction direction did not alter at 45 ◦C, but rotated anticlockwise by 6.5 and 56 ° relative to the initial ones at 65 and 85 ◦C, respectively, as illustrated on the right-hand side of Figure 2-8(a), (b) and (c). After switching

off the voltage, all the LC molecules rotated toward the initial position. During this process at 85 ◦C, the director direction passed through the diagonal position of the crossed Nicoles to produce the transmittance maximum. In contrast, such a recovery of the orientation direction did not take place at all when the cell was quenched to ambient temperature on switching off the field and the LC maintained the director direction for at least more than over one month. The anchoring molecules thus can rotate at high temperatures to produce time-dependent transmittances in the field-on and following field-off states. The azimuthal angle φ of the anchoring molecules in the voltage-on and -off states can be estimated from the transmittance. φ is defined as the counter-clockwise angle from the initial orientation direction. To determine φ in the voltage-on state, the relative transmittance was calculated using 2D optical calculation by assuming the continuously twisting director configuration where the director directions in the middle of the substrates and on the brush surface are parallel to the electric field and φ, respectively[20]. The calculated transmittance T is approximated as a quadratic function of φ, $T = (-2.89\times10^{-4})\,\varphi^2 + (1.56\times10^{-2})\,\varphi + 0.789$, where T is the transmittance normalized by the maximum value. Φ can be estimated by solving the quadratic equation where T is equated with the observed transmittance normalized by the maximum value. On the other hand, φ in the following field-off state can be estimated simply by assuming that the transmittance is proportional to $\sin^2(2\varphi)$ because all the molecules lie along one direction. Here, I shall focus on the transmittance at 85 ◦C because it shows clear maxima in both the voltage-on and off states that can give clues to the identity of the director configuration in the PMMA-B cell. In Figure 2-12, the φ values thus estimated in the electric field-on and off states are plotted against the elapsed time. In the field-on state, φ increases gradually to reach 54 ° with the application of an electric field for 10,000 s. This angle agrees with that estimated by the extinction direction measured for the cell on turning off the voltage. In the following field-off state, φ decays

exponentially with time. These time dependences of φ in the field-on and off states are similar to the strains of the viscoelastic materials loaded and unloaded, respectively, suggesting that the PMMA brushes behave as a viscoelastic solid[21]. The electric field exerted force on the anchoring molecules to rotate their long axis to the field direction. This azimuthal rotation of the anchoring molecules involved the viscoelastic deformation of the polymer brushes; thus it occurred gradually. Upon switching on the field, the elastic energy generated by the deformation of the brushes was balanced by the energy generated by the forces exerted on the anchoring molecules that were nonparallel to both the LC between the substrates and the electric field direction. After switching off the voltage, the forces exerted on the anchoring molecules disappeared and the elastic energy exerted force on the brushes to recover their original configuration. The recovery of the brush configuration affected the orientation of the anchoring LC molecules. The PMMA brushes thus serve as viscoelastic anchoring surfaces for the nematic LC; hence, their anchoring effect on the LC is temperature-dependent.

2-4-4 Time-Dependent Transmittance Changes of PS-B Cell at High Temperature

The time-dependent transmittance changes of PS-B cell at 45 ◦C can be explained according to the model illustrated on the right in Figure 2-9(a). As proposed for the PMMA-B cell, the molecules anchored by the PS brushes are forced to rotate towards the electric field in the field-on state causing the transmittance to initially increase and then decrease with time. On switching off the voltage, the LC molecules in the bulk aligned immediately parallel to the anchored ones on the surface, which had been rotated from their initial orientation direction. During this process, the director direction passed through the diagonal position of the crossed Nicols to maximize the transmittance at point D in Figure 2-9(a). The temperature at which time-dependent transmittance appeared in the PS-B cell was significantly lower than that for the

PMMA-B cell. This is presumed to be because there is greater compatibility between the PS brushes and LC molecules than between the PMMA brushes and LC molecules, i.e. there is a larger depression of the glass transition temperature in the PS brushes than in the PMMA ones.

On further heating to 65 ◦C and then to 85 ◦C, as observed in Figures 2-9(b) and 2-9(c), respectively, the transmittance began to decrease immediately after switching on the voltage and approached a constant value. The transmittance changes in the field-on state at 65 ◦C and 85 ◦ C are considered to be essentially the same as those observed at 45 ◦C; however, these changes take place in different time scales, i.e. very rapidly. In the field-off state, on the other hand, a distinct behaviour is observed at these high temperatures; the transmittance increased rapidly up to the maximum value and then decreased as observed at 45 ◦C, but began to increase again after reaching the minimum zero value at approximately 15,000 s and 1 s for 65 ◦C and 85 ◦C, respectively. In the final stage after 30,000 s at 85 ◦C, the transmittance was approximately 6 %, which is expected when the nematic director is parallel to the comb-shaped electrodes (refer to the molecular arrangements illustrated on the right in Figure 2-9(c)). In practice, this peculiar orientation along the electrodes was easily confirmed by POM observations. Thus, I conclude that at higher temperatures the LC molecules are rotated all the way to the position parallel to the comb-shaped electrodes, advancing beyond the orientation direction initially set by the magnetic field.

At 110 ◦C (near the T_i), this trend becomes remarkable; after switching off the voltage, the molecules immediately aligned parallel to the comb-shaped electrodes. The zero anchoring state is presumed to occur because of the low T_g of the PS-B surface, which results from the compatibility between the PS brushes and LC molecules; i.e. because the LC molecules, at least those in the interface between the PS brushes and bulk nematic LC, acquired sufficient mobility (close to that of a liquid) at 110 ◦C. Therefore, the orientation behaviour is considered to be

constant in the temperature range of 65 - 110 ◦C. However, the response time is different because of the temperature-dependent viscoelastic properties of the PS brushes.

2-5 Conclusions

The high-density PMMA and PS brushes functioned as anchoring surfaces for the nematic LC. The nematic LC injected into the PMMA and PS-B cells showed a degenerate planer orientation, which became uniform upon the LC cooling from 120 °C in a magnetic field of 1 T. During this process, an LC in the isotropic liquid state seeped into the brushes and transformed into the nematic phase with its director oriented with the magnetic field direction. The LC molecules were fixed when the brushes lost mobility upon further cooling. At ambient temperatures, the LC was driven in IPS mode with electro-optical properties typical for LC cells.

In contrast, at temperatures higher than 45 °C for the PS-B cell and 65 °C for the PMMA-B cell, time dependency for the transmittance was observed. In the field-on state, the anchoring molecules were rotated toward the field direction by the elastic force produced between the anchoring molecules and the bulk LCs, which were aligned by the electric field. In the subsequent field-off state, the anchoring molecules were rotated all the way to the position parallel to the comb-shaped electrodes by the elastic force produced between the anchoring molecules and the bulk LCs, which were aligned along the comb-shaped electrodes. These resulted in time-dependent transmittances. The viscoelasticity of the polymer brushes could explain the temperature-dependent LC anchoring.

Furthermore, the PS brushes approached near-zero anchoring at 110 °C. The zero-anchoring state was presumed to occur because of the presence of a liquid-like layer in the interface zone between the PS brushes and the bulk nematic LC. Due to the existence of the

liquid-like layer, the bulk LCs could intercept the anchoring influence from the substrate and could rotate freely on the liquid-like layer.

The zero- azimuth anchoring technology has potential not only for the development of new LCD modes with novel non-contact orientation capabilities but also for the formation of an ultra-low friction interface with potential applications in number of fields.

References

1. Ejaz, M., Yamamoto, S., Ohno, K., Tsujii, Y., & Fukuda, T. Controlled graft polymerization of methyl methacrylate on silicon substrate by the combined use of the Langmuir-Blodgett and atom transfer radical polymerization techniques. Macromolecules 31, 5934-5936 (1998).
2. Ejaz, M., Ohno, K., Tsujii, Y., & Fukuda, T. Controlled grafting of a well-defined glycopolymer on a solid surface by surface-initiated atom transfer radical polymerization. Macromolecules 33, 2870-2874 (2000).
3. Yamamoto, S., Ejaz, M., Tsujii, Y., Matsumoto, M., & Fukuda, T. Surface interaction forces of well-defined, high-density polymer brushes studied by atomic force microscopy. 1. Effect of chain length. Macromolecules 33, 5602-5607 (2000).
4. Yamamoto, S., Ejaz, M., Tsujii, Y., Matsumoto, M., & Fukuda, T. Surface interaction forces of well-defined, high-density polymer brushes studied by atomic force microscopy. 2. Effect of graft density. Macromolecules 33, 5608-5612 (2000).
5. Yamamoto, S., Tsujii, Y., & Fukuda, T. Glass transition temperatures of high-density poly(methylmethacrylate) brushes. Macromolecules 35, 6077-6079 (2002).
6. Ohno, K., Morinaga, T., Koh, K., Tsujii, Y., & Fukuda, T. Synthesis of monodisperse silica particles coated with well-defined, high-density polymer brushes by surface-initiated atom transfer radical polymerization. Macromolecules 38, 2137-2142 (2005).
7. Ohno, K., Morinaga, T., Takeno, S., Tsujii, Y., & Fukuda, T. Suspensions of silica particles grafted with concentrated polymer brush: A new family of colloidal crystals. Macromolecules 39, 1245-1249 (2006).

8. Sakata, H., Kobayashi, M., Otsuka, H., & Takahara, A. Tribological properties of poly(methyl methacrylate) brushes prepared by surface-initiated atom transfer radical polymerization. Polymer Journal 37, 767-775 (2005).

9. Kuramoto, K., Okayasu, K., Ohno, K., Tsujii,Y., & Fukuda, T. Polymer Preprints, Japan 55, 4042 (2006).

10. Oh-e, M., & Kondo, K. Response mechanism of nematic liquid crystals using the in-plane switching mode. Applied Physics Letters 69, 623-625 (1996).

11. Oh-e, M., & Kondo, K. The in-plane switching of homogeneously aligned nematic liquid crystals. Liquid Crystals 22, 379-390 (1997).

12. Oh-e, M. In-plane switching electro-optical effect of nematic liquid crystals. Liquid Crystals Today 10 (2), 6-10 (2010).

13. Yamamoto, J., Yokoyama, H., & Watanabe, J. Zero surface anchoring liquid crystal orientation methods and its liquid crystal device. Japanese Patent No.4053530 (2007.12.14).

14. Clark, N.A. Surface memory effects in liquid crystals: Influence of surface composition. Physical Review Letters 55, 292-295 (1985).

15. Nose, T., Masuda, S., & Sato, S. Memory Effects in Nematic Liquid Crystals by a Surface Molecular Reorientation. Japanese Journal of Applied Physics 30 (12R), 3450 (1991).

16. Ouch, Y., Feller, M.B., Moses, T., & Shen, Y.R. Surface memory effect at the liquid-crystal–polymer interface. Physical Review Letters 68, 3040-3043 (1992).

17. Vetter, P., Ohmura, Y., & Uchida, T. Study of memory alignment of nematic liquid crystals on polyvinyl alcohol coatings. Japanese Journal of Applied Physics 32, L1239-L1241 (1993).

18. Zhou, Y., & Sato, S. Electrooptical and Response/Relaxation Properties of Liquid Crystal Cells in In-plane Switching Mode with Polyvinylcinnamate Photoinduced Alignment Layer. Japanese Journal of Applied Physics 37, 4439 (1998).

19. Dierking, I. in *Textures of Liquid Crystals* Ch.2 (John Wiley & Sons, Weinheim, 2003).

20. The transmittance was calculated using LCD Master (Shintech, Inc., Japan) for the LC cell with a gap of 3 μm with the following parameters: refractive indexes n_e = 1.5696 and n_o = 1.4886; relative permitivities $\varepsilon_{\parallel}$ = 8.4 and $\varepsilon_{\perp}$ = 3.7; elastic constants K_{11} = 10.1 pN, K_{22} = 12.8 pN, and K_{33} = 28.2 pN; rotational viscosity γ = 0.1 Pa s. The azimuthal angle of the molecules anchoring to the substrate with the electrodes is approximated to be equal to that of the molecules anchoring to the other substrate so as to eliminate the complex procedure for determining the angle, though a stronger electric field near the electrode may make the former angle larger than the latter one.

21. Ward, I. M., & Sweeney, J. *An Introduction to the Mechanical Properties of Solid Polymers* 2nd ed., 55 (Wiley, Chichester, U.K., 2004) .

Table 2-1. Polymerization condition of PMMA and PS brushes

Polymer brush	Monomer (mol)	Initiator (mmol)	Catalyst (mmol)	Solvent (mol)	Temp. (◦C)	Period (h)
PMMA	methyl methacrylate /0.37	2-bromoisobutylic acid ethyl ester [a] /0.34	CuBr/3.75 4,4'-dinonyl -2,2'-bipyridine/8.97	Anisole /0.35	90	3
PS	styrene /0.43	2-bromoisobutylic acid ethyl ester [a] /0.41	CuBr/4.26 4,4'-dinonyl -2,2'-bipyridine/8.10	-	110	3

[a] ethyl bromoisobutyrate

Table2-2. Characterization of PMMA and PS brush substrates

Polymer brush	M_n	M_w/M_n	Thickness h (nm)	Graft density σ [a] (chains nm^{-2})
PMMA	112,000	1.17	46.8	0.299
PS	70,600	1.21	48.2	0.43

[a] estimated assuming the density ρ is equal to that of the bulk polymers. PMMA: 1.188 g cm^{-3}, PS: 1.05 g cm^{-3}.

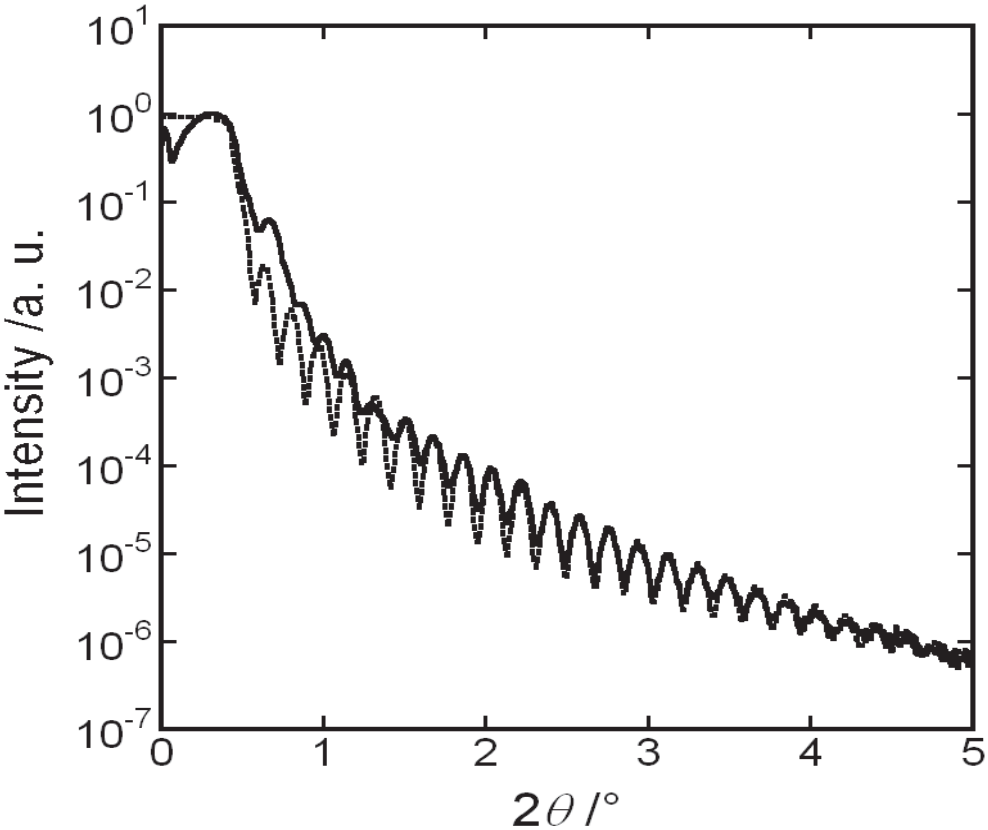

Figure 2-1. X-ray reflectivity curve of PMMA brushes on glass substrate. The experimental data was fitted by setting the brush and BHE layer thicknesses to 46.8 and 1.60 nm, respectively. The densities (ρ) of the layers were assumed to be 1.188 (equal to ρ of the bulk PMMA) and 1.126 g cm^{-3}, respectively.

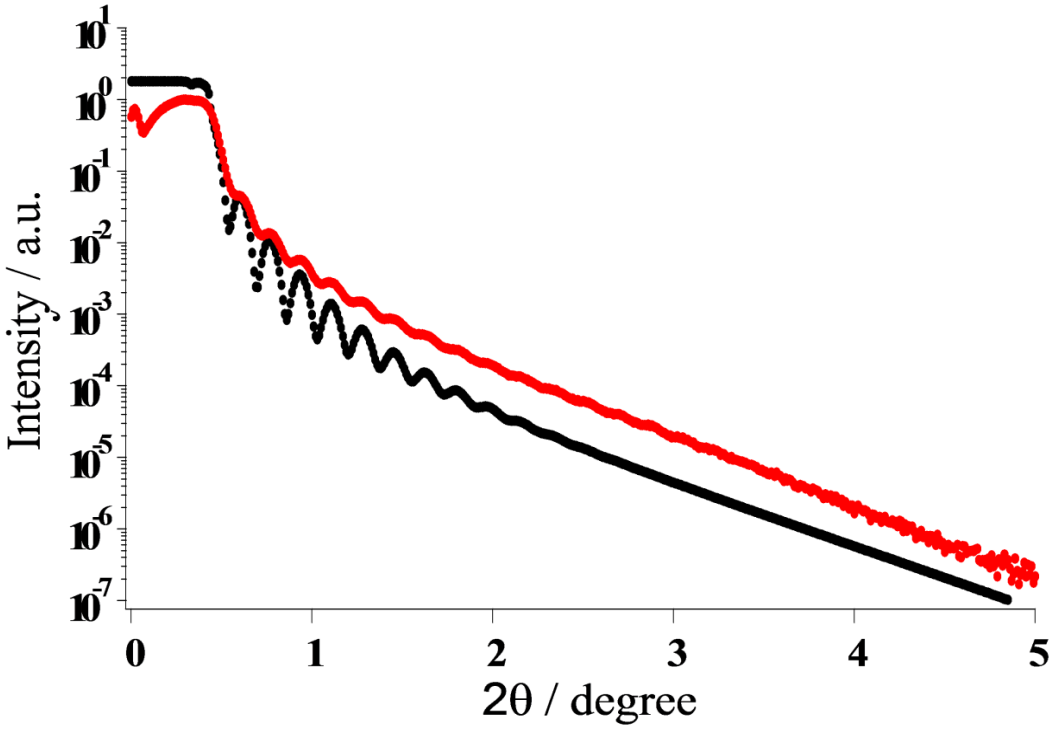

Figure 2-2. X-ray reflectivity curve of PS brushes on glass substrate. The experimental data was fitted by setting the brush to 48.2 nm. The density (ρ) of the PS layer was assumed to be 1.05 g cm^{-3} (equal to ρ of the bulk PS).

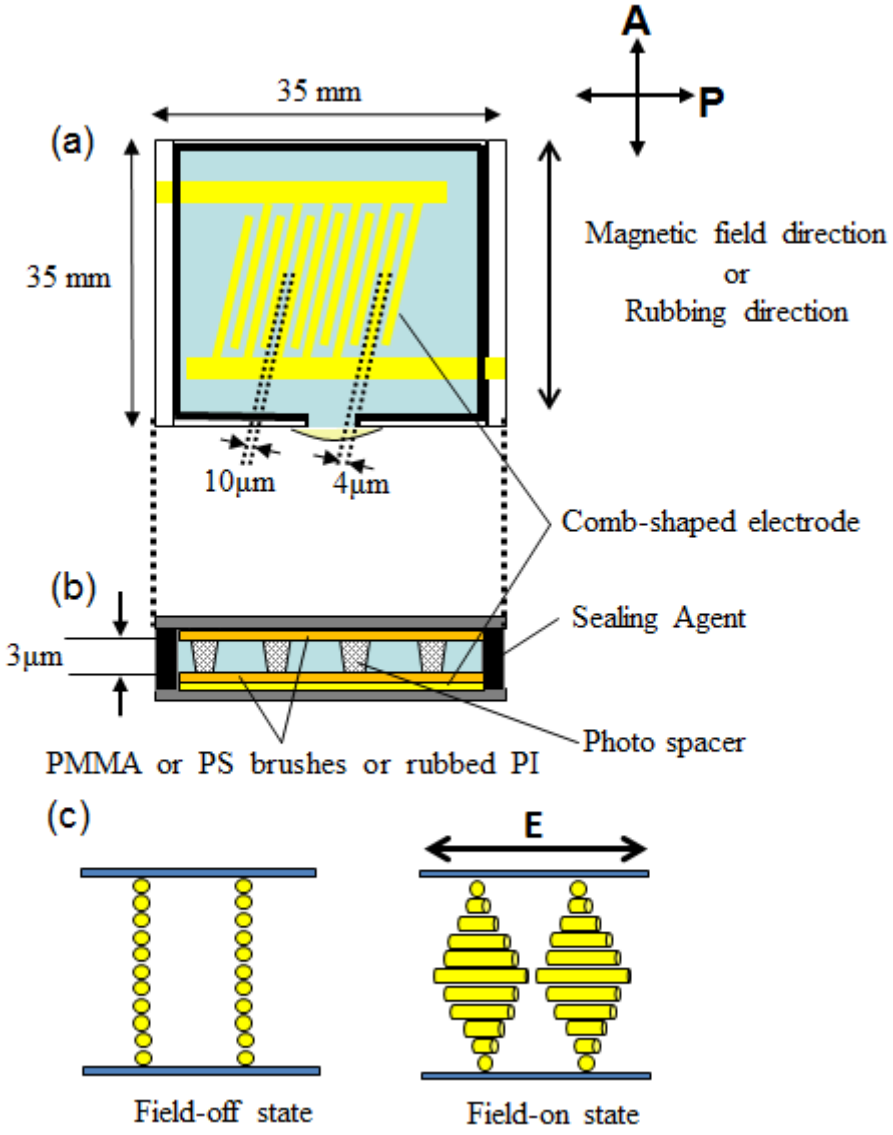

Figure 2-3. Schematic diagram of the PMMA-B cell and PS-B cell: (a) front and (b) side views, and (c) molecule alignments in field-on and -off states viewed from the side. In the field-on state, the molecules at the center of the cell are oriented to the field, and the rest of the molecules are twisted continuously between two orientations on the anchoring surface and at the center.

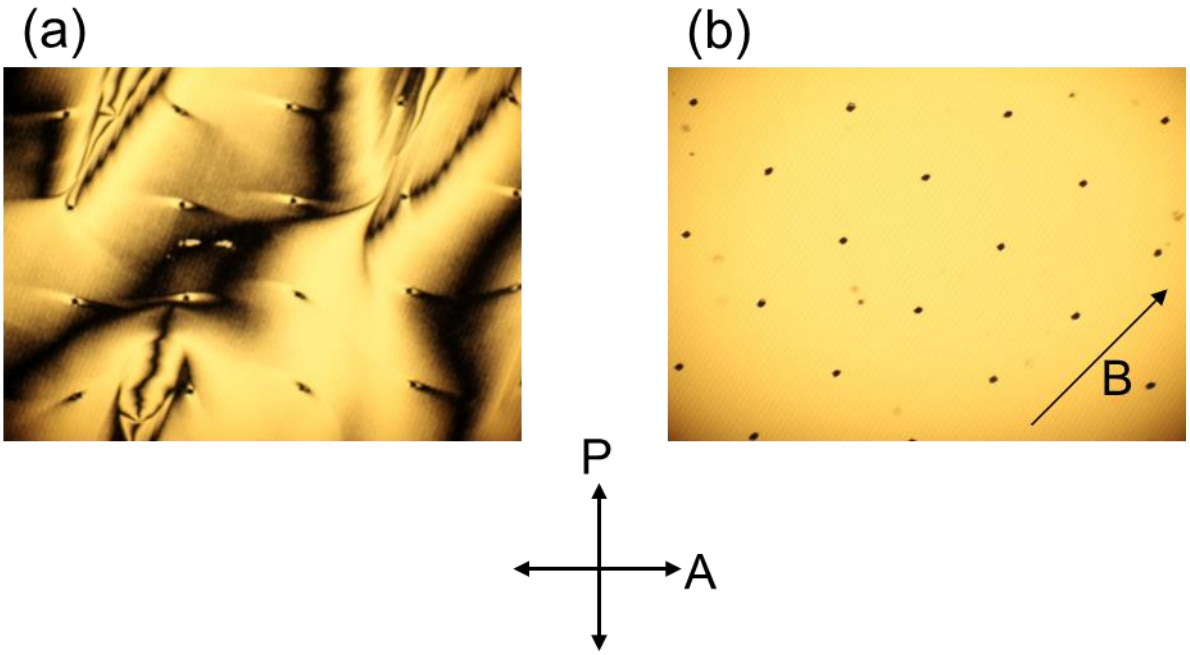

Figure 2-4. Optical images taken with a polarizing microscope. (a) The PMMA-B cell just filled with the nematic LC, then (b) cooled to ambient temperature at the rate of 3 ◦C min^{-1} under a magnetic field of 1 T after annealing at 120 ◦C for 20 min. P and A indicate the polariser and analyser, respectively. In (b), the arrow indicates the direction of the magnetic field and the dark dots represent the spacers set within the cell.

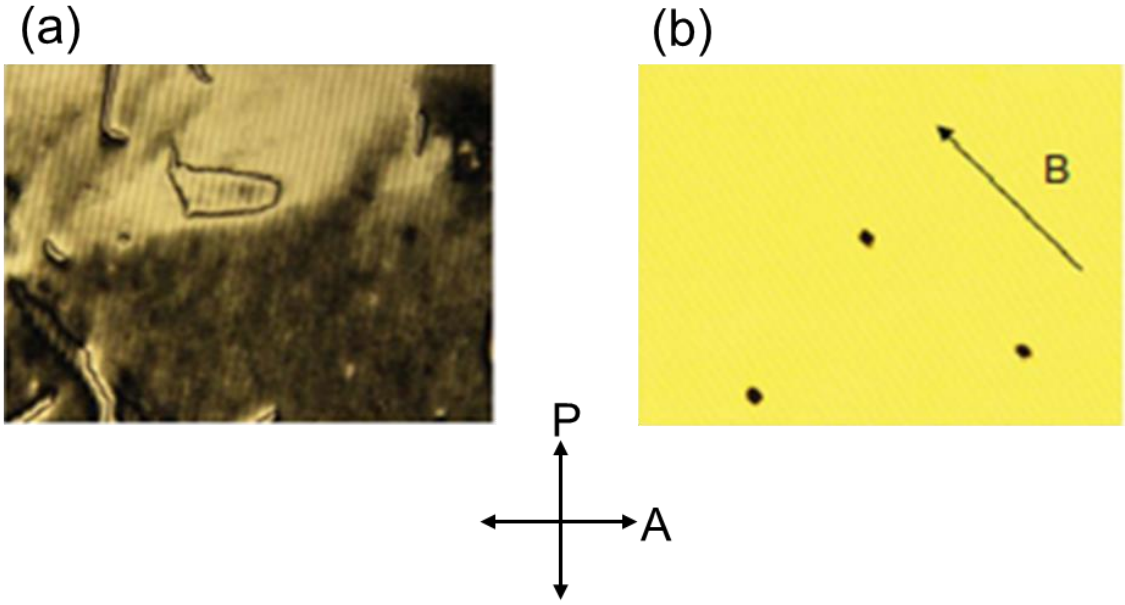

Figure 2-5. Optical images of the PS-B cell captured with a polarising microscope. (a) Cell just filled with the nematic LC. (b) Cell cooled to ambient temperature at the rate of 3 ◦C min^{-1} under a magnetic field of 1 T after annealing at 120 ◦C for 20 min. P and A indicate the polariser and analyser, respectively. In (b), the arrow indicates the direction of the magnetic field and the dark dots represent the spacers set within the cell.

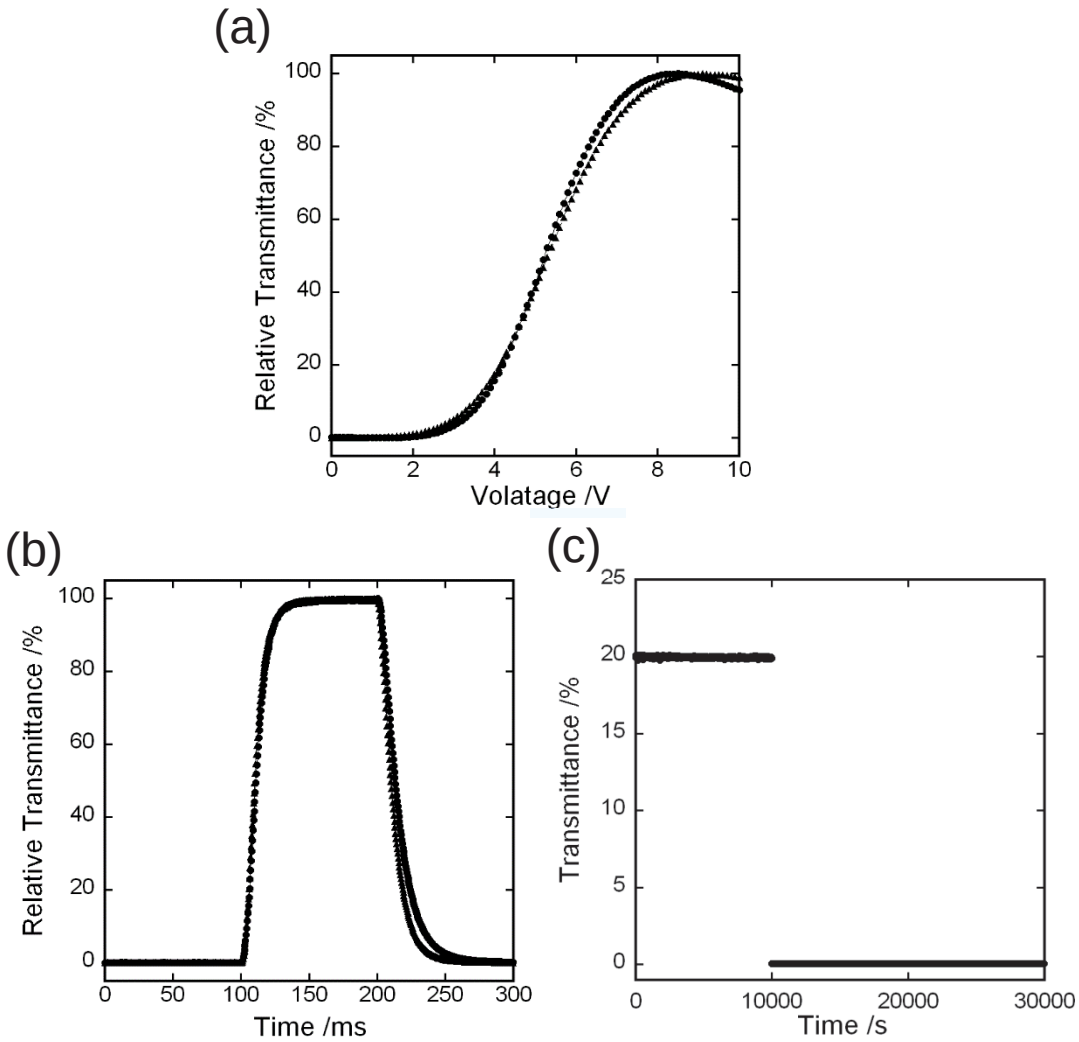

Figure 2-6. (a) Voltage–light transmittance characteristics of the PMMA-B (circles) and the RPI (triangles) cells. The cells were set with the nematic LC director direction coinciding with that of one of the crossed Nicole polarizers and the light transmittance was observed in the IPS switching mode. (b) Optical response measured by applying AC voltage with amplitude of V_{max} at frequency of 60 Hz to the cells. The response time was the period required for the change in normalized transmittance between 10 and 90 %. (c) Time dependence of the transmittance of the PMMA-B cell measured by applying the voltage of V_{max} in the first 10,000 s and then switching off at 25 ◦C. In (a) and (b), the transmittance is normalized as 100 % at V_{max}, and in (c), it is given as the transmittance measured without the cell to be 100 %.

(a)

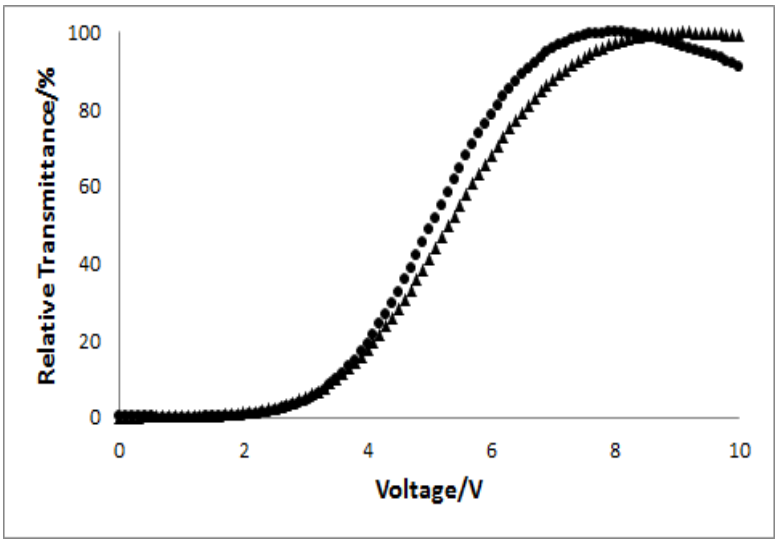

(b)

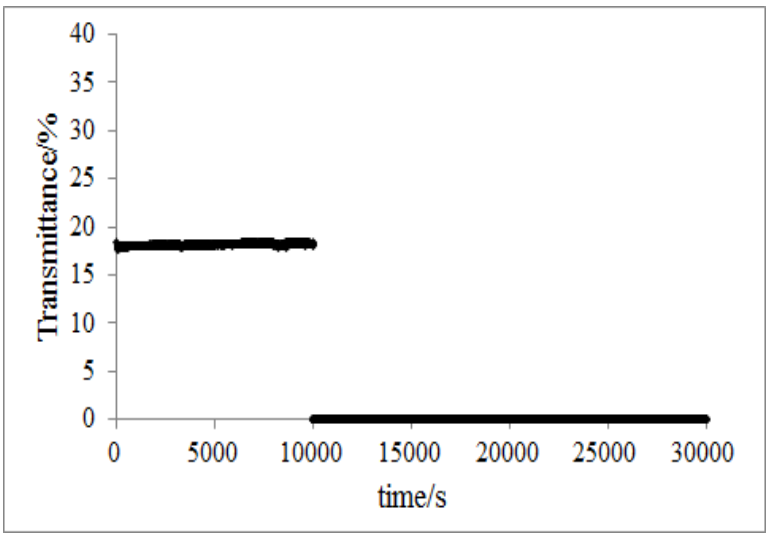

Figure 2-7. (a) Voltage–light transmittance characteristics of the PS-B (circles) and RPI (triangles) cells. (b) Time dependence of the transmittance of the PS-B cell at 25 ◦C measured after applying the voltage of V_{max} for the first 10,000 s and then switching off the voltage. In (a), the transmittance is normalised to 100 % at V_{max}. In (b), the transmittance measured without the cell is normalised to 100 %.

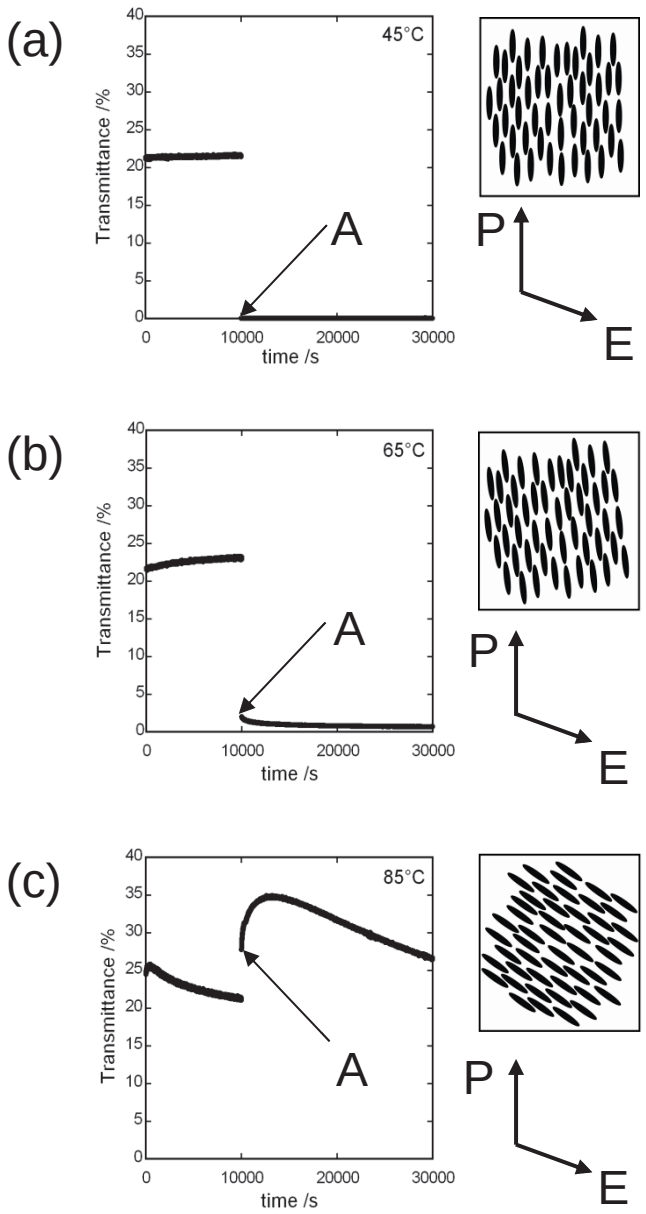

Figure 2-8. Time dependence of the transmittance of the PMMA-B cell measured by applying the voltage of V_{max} in the first 10,000 s and then switching off at temperatures of (a) 45, (b) 65, and (c) 85 ◦C. Illustrations on the right-hand side show the anchored molecules rotated during the application of the electric field for 10,000 s (see the text). The angles can be determined from the extinction direction measured between crossed polarizers for the homogeneously aligned sample at point A. The arrows P and E show the direction of the polarizer axis and the electric field applied, respectively.

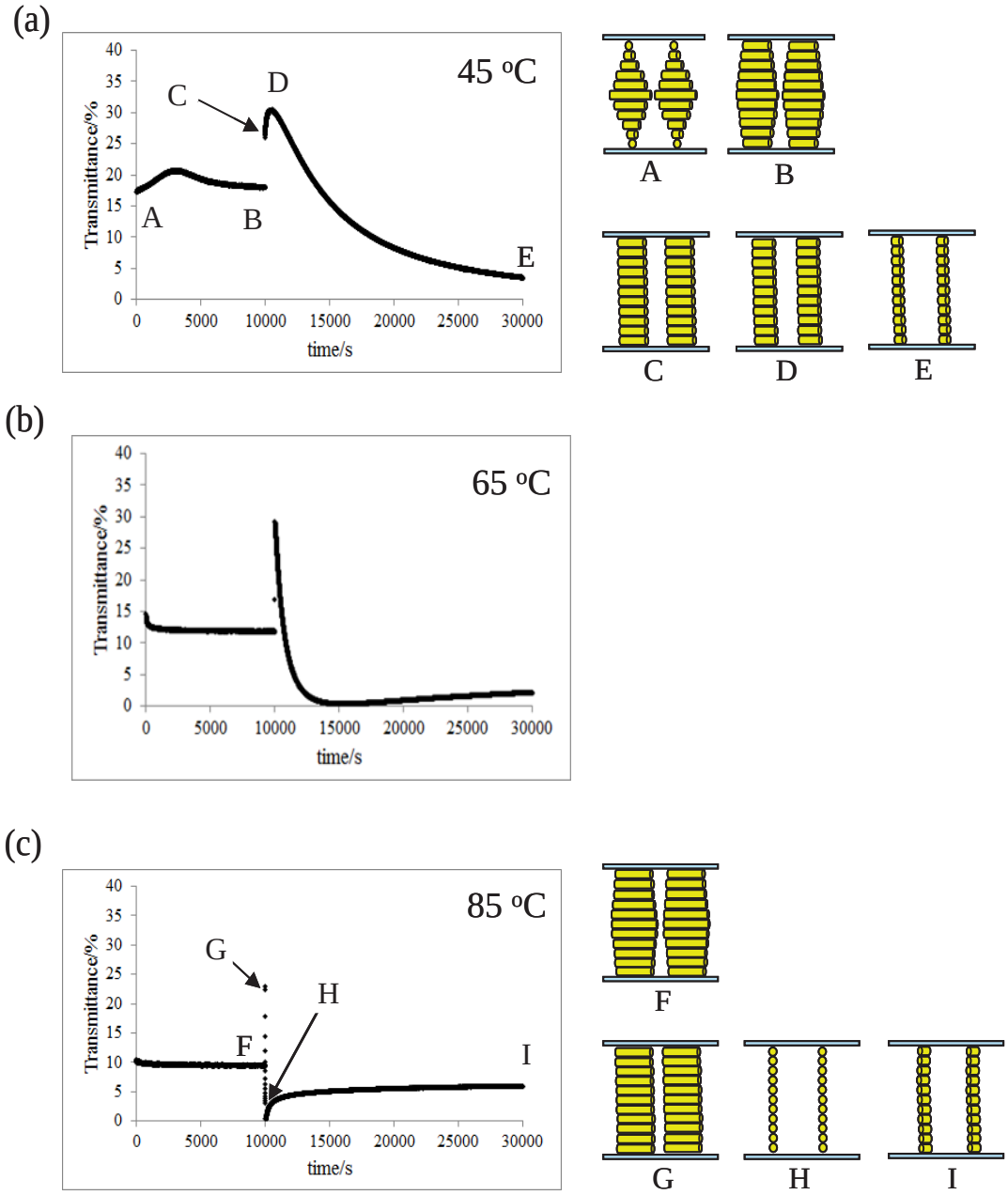

Figure 2-9. Time-dependence of the transmittance of the PS-B cell measured after applying the voltage of V_{max} in the first 10,000 s and then switching off the voltage at temperatures of (a) 45 ◦C, (b) 65 ◦C and (c) 85 ◦C. The molecular alignments are illustrated at the A - I points in the field-on and field-off states on the right in (a) and (c).

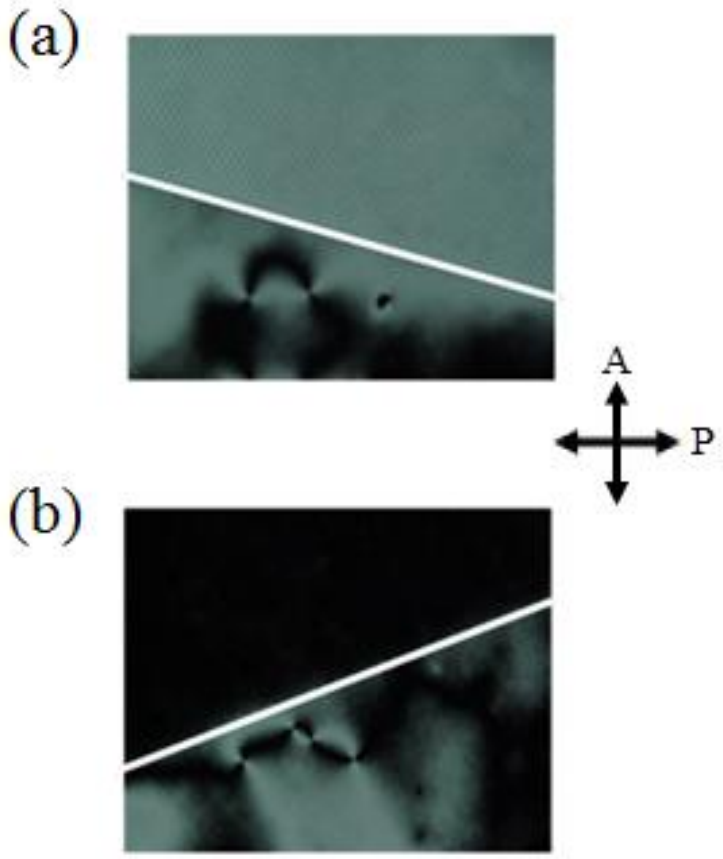

Figure 2-10. Optical images of the PS-B cell captured with a polarising microscope just after transforming from the isotropic phase (115 ◦C) to the nematic phase (110 ◦C). (a) The electrodes did not coincide with the polariser direction. (b) The electrodes coincided with the polariser direction. The region above the white line is the area where the electrodes existed and that below the white line is the area where no electrodes were present.

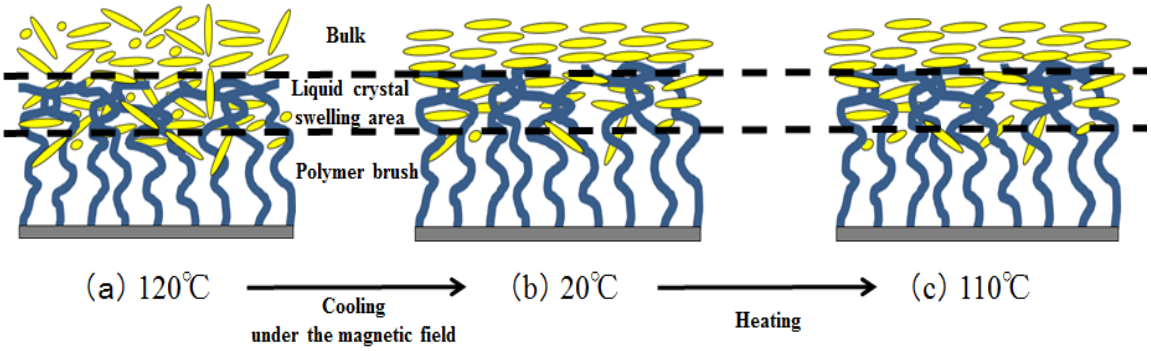

Figure 2-11. Illustration of the LC molecules immersed in the PMMA or PS brushes. At 120 ◦C, the LC molecules in the isotropic state seep in the part of the PMMA or PS brush, as show in (a). On cooling under the magnetic field, the LC molecules immersed in the brushes and bulk LC molecules are transformed into the nematic LC state, aligning uniformly with the director corresponding to the field direction, as shown in (b).When the PS-B cell is heated to the high temperature (for example 110 ◦C) near the T_i of the bulk nematic LC, the interface zone between the PS brushes and the bulk nematic LC becomes liquid-like to offer the nearly zero anchoring surface as shown in (c).

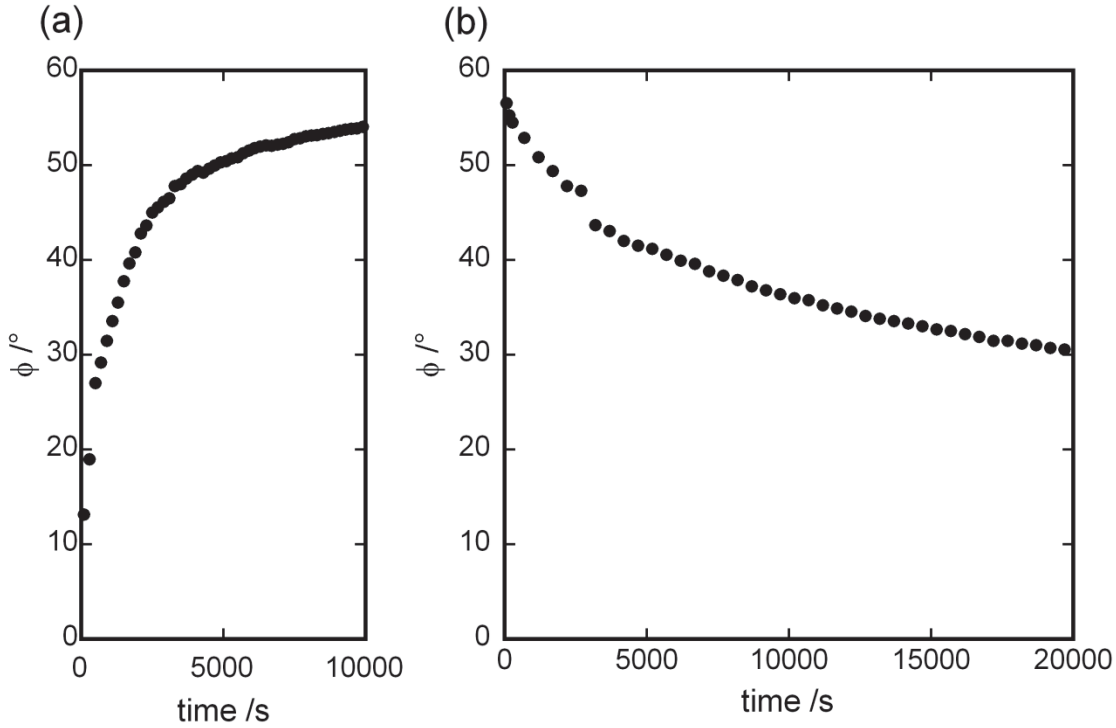

Figure 2-12. Time dependence of the angle φ between the nematic director direction in the PMMA-B cell and the polarizer axis (a) in the field-on state for 10,000 s and (b) the subsequent field-off states at 85 ◦C. The strength of the field applied was equal to V_{max}.

Chapter 3

Nematic Liquid Crystal Anchoring Strengths of High-density Polymer Brush Surfaces

Abstract

The azimuthal anchoring coefficient (A_2) of a nematic liquid crystal (NLC) on high-density polymer brushes (PBs) was investigated using the threshold voltage for in-plane switching of liquid crystal (LC) cells consisting of polymer-grafted substrates. The value of A_2 was affected by the glass transition temperature (T_g) of the grafted polymers and decreased with an increase in temperature. NLCs on poly(methyl methacrylate) (PMMA), poly(ethyl methacrylate) (PEMA), and polystyrene (PS) brushes had an A_2 value of 10^{-5} J m^{-2} at 25 °C. In contrast, high-density poly(hexyl methacrylate) (PHMA) brushes provided a near-zero-azimuth anchoring surface for NLCs at room temperature. NLCs in a cell with PHMA-grafted substrates aligned along the comb-shaped electrodes after a slight push owing to the unevenness of the brush surface. The LC cell was driven at a threshold voltage of one-fifth that of a conventional cell and the NLCs on PHMA brushes exhibited a small A_2 value (1.1×10^{-6} J m^{-2}) at 25 °C. With an increase in temperature to 90 °C, the A_2 values of the NLCs on the PEMA and PS brushes decreased to 10^{-7} J m^{-2}, and the NLCs were oriented in a similar way to that in the PHMA brush cell. Although the T_g values of PMMA and PS are similar, at 90 °C the A_2 value of the NLCs on the PMMA brushes was 4.5×10^{-6} J m^{-2} and a magnetic field was required for orientation of the LC. Such a difference in the A_2 value is explained by the fact that PS has better compatibility with the NLCs than PMMA.

3-1 Introduction

In liquid crystal displays (LCDs), the LC molecules at the interface with the substrate are strongly anchored. The director alignment is not influenced by the external-field-induced deformation of the LCs and allows the deformed LCs to recover their orientation in the absence of the field. If the LC molecules are not anchored to the substrates, the director can be aligned in an arbitrary direction by an external field and memorized in the absence of the field. Such a zero-anchoring surface may enable the development of new LCD modes with novel noncontact orientation capabilities[1]. Substrates coated with polymers at sufficiently high temperatures have offered weak azimuthal anchoring surfaces[2-6]. When nematic LCs (NLCs) between two polymer-coated substrates were heated to the isotropic phase and cooled slowly to the nematic phase, they were in degenerate planar alignment. An external field applied during the heating and cooling processes can align the NLC director and the resulting orientation can be memorized at low temperatures. At moderate temperatures, the coated polymer offers a viscoelastic surface to the anchoring LC molecules and the LC director gradually rotates towards the field direction[7-10].

While polymer-coated substrates may not avoid the exfoliation of polymer films from the glass substrates, surface grafting of polymer chains onto the substrate via covalent bonding yields thin polymer films that cannot be detached from substrates. Grafted polymer chains can reform surfaces and control the orientations of LCs on surfaces[11,12]. In previous chapter, I constructed in-plane switching (IPS) LC cells by grafting poly(methyl methacrylate) (PMMA) and polystyrene (PS) to substrate surfaces and examined the orientation behaviours and voltage-transmittance (*V*-*T*) properties of the IPS LC cells[11,12]. Polymer chains grafted on glass substrates by surface-initiated atom transfer radical polymerisation (ATRP) at high density (0.3 - 0.5 chains nm^{-2}) form thin layers with a thickness of 40 - 50 nm. NLCs within the cells were

in a homogeneous planar orientation when slowly cooled from the isotropic phase with a magnetic field. At room temperature, the aligned LC cell showed typical electro-optical properties, indicating that the LC molecules are strongly anchored to the brushes. With increasing temperature, the cell showed time-dependent transmittance on long-period driving, which is attributed to the rotation of the anchored molecules towards the electric field direction. For cells with PS-grafted substrates, NLCs tended to orient along the comb-shaped electrodes. Thus, the anchoring force of the polymer brush (PB) surfaces decreases with increasing temperature, similar to that in substrates coated with polymers via spin coating and dipping.

Such a decrease in the anchoring force of LCs on polymer films may be connected to the micro-Brownian motions of polymer chains that are released at the glass transition temperature (T_g). The T_g values of PMMA and PS are approximately 100 °C, which can be decreased by mixing with NLCs at the interface. Comparatively, T_g of PS decreases more significantly because PS bearing benzene rings can be more miscible with NLCs. LC molecules are strongly anchored to polymer surfaces at $T < T_g$, whereas the molecules can be rotated by aligning fields at $T > T_g$. These LC orientation behaviours in the PB cells suggest that the LC anchoring force of the PB surface decreases with increasing temperature. Thus, polymers with a T_g that is sufficiently lower than room temperature are expected to offer zero azimuthal anchoring surfaces at room temperature. These trends agree with the temperature dependence of the threshold voltage (V_{th}) of the PB cells.

In this chapter, I treat the LC anchoring force of polymer brushes quantitatively using V_{th} in the IPS mode. The V_{th} is related to the twist anchoring coefficient A_2 as shown in the following equation[13]:

$$V_{\mathrm{th}} = \frac{\pi l}{d + 2\,K_2/A_2}\sqrt{\frac{K_2}{\varepsilon_0 \Delta\varepsilon}} \tag{3.1}$$

where l is the electrode distance; d, the cell gap; K_2, the twist elastic constant of the LC; ε_0, the dielectric constant in free space; and $\Delta\varepsilon$, the dielectric constant anisotropy of the LC.

PB cells were fabricated with substrates onto which PMMA, poly(ethyl methacrylate) (PEMA), PHMA and PS chains with different T_gs were grafted. The T_gs of bulk PMMA, PEMA, PHMA and PS are 105 °C, 65 °C, −5 °C and 100 °C, respectively[14]. Although the A_2 values of the PEMA-B and PS-B cells at 25 °C were more than ten times larger than that of the PHMA-B cell to exhibit V_{th} comparable to that of a rubbed polyimide (RPI) cell, they decreased to a value comparable to the A_2 of the PHMA-B cell at 25 °C with increasing temperature, indicating that the LC molecules were barely anchored to the PEMA-B and PS-B brushes at high temperature.

3-2 Experimental Procedure

PMMA, PEMA, PHMA and PS brushes were grafted on two glass substrates, one of which had comb-shaped indium tin oxide (ITO) electrodes for driving the IPS mode of the NLC orientation, via surface-initiated ATRP. The ITO electrodes were 55 nm thick and had lines and spaces that were 4 μm and 10 μm, respectively. The initiator (2-bromo-2-methyl) propionyloxyhexyltriethoxysilane (BHE) was synthesized as described in the literature[15] and immobilized on the substrates. Polymerization was performed by dipping the substrate with immobilized BHE in a degassed polymerization solution of the monomer, a free ATRP initiator (2-bromoisobutylic acid ethyl ester), catalyst and solvent. The number average molecular weight (M_n) and polydispersity index (M_w/M_n) of each polymer brush were estimated from the gel permeation chromatogram of the freely initiated polymer in the same vessel[16-18]. The thickness (h) of each brush was determined based on its X-ray reflectivity (Rigaku UltimaIV, Figure 2-1, 3-1 and 3-2 for PMMA, PEMA and PHMA brushes, respectively). The graft density (σ) of each brush was estimated using the relationship $\sigma = \rho h N_A/M_n$, assuming that the brush

density (ρ) was equal to the density of each bulk polymer[18]. The polymerization conditions and key characteristics of the polymer brushes are summarized in Tables 3-1 and 3-2, respectively.

The PB cells were fabricated by injecting a nematic LC (JC-5051XX, JNC Corporation; nematic-isotropic transition temperature T_{NI} = 112 °C) between the two plates of the polymer-grafted glass with a gap of d = 3 μm via capillary action at ambient temperature. A reference cell was prepared using two rubbed polyimide (AL16301, JSR Corporation)-coated substrates with the same gap as that of the experimental cells. The rubbing direction was parallel to the electrode direction. Hereafter, the reference cell is referred to as the RPI cell. Outlines of the LC cells used in this study are shown in Figure 3-3.

The electro-optical properties of the LC cells were measured using an LCD-5200 (Otsuka Electronics). The intensity of incident light near the surface of the LC cell was about 2.2 million cd/m^2. Polarized optical microscopy (POM) observation of the LC cells was performed using an Olympus BX50P microscope. The level differences of the comb-shaped electrodes and the polymer brush surfaces in the electrode regions of the PHMA-B cells were measured using an Olympus OLS4100 laser scanning microscope. Differential scanning calorimetry (DSC) was performed using a PerkinElmer DSC-7 differential scanning calorimeter at a heating rate of 20 °C min^{-1}.

3-3 Results and Discussion

The nematic LC as-injected into the PMMA-B, PEMA-B and PS-B cells showed Schlieren texture under polarized optical microscopy, indicating that the nematic LC on these brushes had a degenerate planar orientation. The uniform planar LC orientation in the PMMA-B cell was achieved by applying a magnetic field of 1 T along the electrode direction during cooling from the isotropic liquid state (see Figure 3-4(a)). In the PEMA-B and PS-B cells, it

was accomplished by new noncontact orientation method which was shown in the second chapter: by heating to the isotropic temperature and then cooled to room temperature (nematic phase). Figure 3-4(b) and (c) show the polarized optical microscope images of the PEMA-B and PS-B cells, respectively, cooled at a rate of 1 °C min^{-1} from the isotropic liquid state. Although no orientation treatment was performed, the LCs in these PEMA-B and PS-B cells exhibited uniaxial orientation in the electrode regions and had extinction positions upon rotation of the cells between the crossed Nicol polarisers, while the LCs in the regions without the electrodes exhibited schlieren texture. The existence of extinction positions indicated that the directors of the NLCs were arranged uniformly parallel to the comb-shaped electrodes.

On the other hand, The NLCs in PHMA-B cell showed the specific behavior which was not seen in other PB-cells. Figure 3-5 shows images of the PHMA-B cell positioned between crossed Nicol polarisers. Immediately upon filling the cell, the LC exhibited the schlieren texture, a satisfactory indication of degenerate planar alignment, although the cell was filled with LC in the nematic phase. On closer inspection, two ‘brushes’ emerged from most of the defect cores in the region without the electrodes (left of the dashed line in Figure 3-5 (a)), whereas four brushes emerged from most of the cores in the region with the electrodes. The latter brushes represent a so called Néel wall, which is observed for NLCs on weak anchoring surfaces[19]. On pushing the cell surface lightly at room temperature, the schlieren texture in the region with the electrodes changed into a uniform texture, while the schlieren texture was maintained in the region without the electrodes (Figure 3-5 (b) and 3-5 (c)). The extinction positions on rotation of the cell between the crossed polarizers and the retardation indicate that the LC in the region with the electrode arranged the director parallel to the electrodes. The spontaneous LC orientation in the PEMA-B and PS-B cells upon cooling from the isotropic liquid state and PHMA-B cell on pushing the cell surface lightly at room temperature is related

to the level differences in the electrode regions. The level difference at the substrate surface of a PHMA-B cell was confirmed to be similar to that of the electrodes (4 μm-wide, 40 - 50 nm-tall and 10 μm-long) via confocal laser microscopy (Figure 3-6). Although such surface grooves can induce LC orientation near hills, the observed homogeneous orientation requires propagation of the local LC orientation between the hills at a distance of 10 μm, which is 20,000 times greater than the lateral distance of the neighbouring LC molecules (0.5 nm). The conditions are thus not always sufficient for LC alignment, and the propagation is typically limited by interfacial interactions such as anchoring forces[20]. Hence, LC orientation in the regions with the electrodes suggests that the LC anchoring forces of these polymer brush surfaces were negligible at temperatures as high as 90 °C. The LC in the PHMA-B cell was aligned simply by lightly pushing the substrate, suggesting that the LC was barely anchored to the PHMA-B surface at 25 °C.

The differences in the surface anchoring of the LC molecules between the PB surfaces influenced the voltage–transmittance (*V-T*) properties for driving the cells in the IPS mode. Figure 3-7 shows the *V-T* curves of the RPI and PB cells measured at various temperatures. With increasing applied voltage, the transmittance of each of the cells began to increase at a certain voltage, which is defined as the threshold voltage (V_{th}), and then reached a maximum at a voltage V_{max}. At 25 °C, the *V-T* curves of all of the PB cells, except the PHMA-B cell, resembled that of the RPI cell. However, while the *V-T* curves of the RPI cell were independent of temperature, the values for both V_{th} and V_{max} of the PB cells shifted to lower voltages with increasing temperature. When the cells were heated from 25 °C to 90 °C, V_{max} for the RPI cell remained nearly constant at 8.5 V, whereas V_{max} for the PB cells decreased. The PHMA-B cell exhibited a distinct *V-T* curve even at 25 °C with a V_{max} of 1.7 V, which is significantly lower than V_{max} for other cells. In addition, when cooled to −15 °C, V_{max} for the PHMA-B cell

increased to 5.3 V, but did not reach V_{max} for the other cells at 25 °C. Moreover when the voltage was increased beyond V_{max}, the transmittance decreased to zero, indicating that the LC molecules at the PHMA brush interface as well as those between the substrates arranged their long axis in the electric field direction.

The anchoring forces of the polymer brushes can be treated quantitatively by examining V_{th}. Assuming that the RPI cell is within the strong anchoring limit, the twist anchoring coefficient A_2 was calculated according to the following equation:

$$A_2 = \frac{2K_2}{\left(\frac{V_{\mathrm{th,RPI}}}{V_{\mathrm{th}}} - 1\right)d} \tag{3.2}$$

where $V_{th,\,RPI}$ is the V_{th} of the RPI cell (4.70 V). Here V_{th} is approximated to be the voltage at which the transmittance is 2 % of the maximum transmittance at V_{max} and the values are listed in Table 3-3 which also includes the temperature-dependent K_2 values provided by JNC Corporation. The estimated values for A_2 are plotted as a function of temperature in Figure 3-8. At temperatures below 25 °C, the A_2 values of the PB cells, except for the PHMA-B cell, were each on the order of 10^{-5} Jm^{-2}. Although these A_2 values are smaller than the A_2 of the RPI cell (3.3×10^{-4} J m^{-2})[21], the LCs can be as strongly anchored to the surfaces of the polymer brushes as the LC on the RPI cell to exhibit V_{th} comparable to each other. In contrast, the PHMA-B cell exhibited an A_2 value of 1.1×10^{-6} J m^{-2} at 25 °C. Such a low A_2 value is assumed to be a typical value for a surface to which the NLC molecules are barely anchored. In addition, with increasing temperature up to 90 °C, the A_2 of the PEMA-B and PS-B cells decreased to values smaller than 1×10^{-6} J m^{-2}, indicating that the LC was barely anchored to the PEMA-B and PS-B surfaces at higher temperatures and thus could be aligned by the surface unevenness. On the other hand, the A_2 of the PMMA-B cell decreased to 4.5×10^{-6} J m^{-2} and still required an external field for LC orientation, even at 90 °C.

Such temperature-dependent anchoring forces for the polymer brushes also influenced the response times of the LC cells. The optical response time of an LC cell after switching off the voltage (τ_{off}) increases as A_2 decreases according to the following equation[22];

$$\tau_{\mathrm{off}} = \frac{\gamma_1\left(d+2K_2/A_2\right)^2}{\pi^2 K_2} \tag{3.3}$$

where γ_1 is the twist viscosity of the LC. Figure 3-9 shows the temperature dependence of τ_{off} for the PB and RPI cells after a voltage of V_{max} was applied for 100 ms and then switched off. The value of τ_{off} was approximated as the period required for a change in the normalized transmittance to 90 %. In the temperature range investigated, the τ_{off} of the RPI cell was approximately 10 ms, while that of the PHMA-B cell was approximately 1,000 ms. These τ_{off} values for the RPI and PHMA-B cells are assumed to be typical values for the strong and weak anchoring limits, respectively. In addition, the τ_{off} of the PMMA-B cell was slightly larger than that of the RPI cell over the entire temperature range, indicating that the LC molecules were anchored to the PMMA brushes at the interface. On the other hand, the values of τ_{off} of the PEMA-B and PS-B cells were comparable to that of the PMMA-B cell at temperatures below 45 °C, and then increased tenfold between 45 °C and 65 °C to become comparable to τ_{off} of the PHMA-B cell at temperatures above 65 °C. Thus, the LC anchoring forces for the PEMA and PS brushes decreased drastically as the temperature increased from 45 °C to 65 °C.

The temperature at which A_2 began to decrease (T_{d}) increased in the order PHMA (lower than 25 °C) < PEMA and PS (~ 35 °C) < PMMA (65 °C). Notably, this order for the T_{d} values for the poly(methyl methacrylate) is the same as that of the T_{g} values for the bulk polymers: PHMA (−5 °C) < PEMA (65 °C) < PMMA (105 °C). Such an agreement in the order of the T_{d} and T_{g} values suggests that the decrease in the LC anchoring force of the polymer brushes is related to the T_{g}s of the polymers. In addition, the fact that the T_{d} values are

significantly lower than the corresponding T_g values suggests that the LC, which had a low T_g, permeated into the surfaces of the brushes. Furthermore, the significantly lower value for T_d of the PS brushes compared to that of the PMMA brushes is reasonable even though the T_g of PS (100 °C) is comparable to that of PMMA, because PS is more miscible with the NLC than PMMA is, as confirmed by a decrease in T_g upon mixing the NLC into the polymer. Specifically, the T_gs of mixtures of the NLC and each polymer were measured by DSC as a function of the weight fraction of NLC (Figure 3-10). With increasing LC fraction, the T_g of the NLC/PS mixture decreased more significantly than that of the NLC/PMMA mixture. In addition, when the NLC fraction was increased to 15 wt%, the T_g of the PS/ LC mixture was 20 °C, while that of the PMMA/LC mixture was 70 °C. Such trends suggest that PS has a higher compatibility with the NLC than PMMA does. At the interface with the NLC, the T_g of the PS brush was therefore decreased more efficiently than that of the PMMA brush. Consequently, the decrease in the LC anchoring force for the polymer brushes is associated with the T_g of each polymer brush at the interface with the NLC. This T_g at the interface depends on the T_g of the polymer and decreases as the miscibility of the polymer with the NLC increases.

3-4 Conclusions

Our results demonstrate that the LC anchoring coefficient A_2 of high-density polymer brushes decreases above the T_g of the polymers at the interface with the NLC. The A_2 values of the polymer brushes decreased with increasing temperature. At 25 °C, PB cells with PMMA, PEMA and PS brushes each exhibited an A_2 on the order of 10^{-5} J m^{-2}, as well as *V*-*T* curves and τ_{off} values similar to those of the reference RPI cell. At the same temperature, the PHMA-B cell exhibited a lower V_{th} and longer τ_{off} than the other cells, along with a lower A_2 of 1×10^{-6} J m^{-2}. The LC in the PHMA cell was aligned along the electrode by only slightly pushing the

substrate, and when the voltage was increased beyond V_{max}, the transmittance decreased to zero, indicating that the LC was barely anchored to the brush surface. Thus, this A_2 value is assumed to be typical for weak LC anchoring. In addition, with increasing temperature, the A_2 values of the PEMA-B and PS-B cells began to decrease at T_d = 35 °C and reached a value on the order of 10^{-7} J m^{-2} at 90 °C. The LCs in these cells were thus barely anchored to the brushes and aligned along the electrode after cooling from the isotropic liquid phase. On the other hand, the A_2 of the PMMA-B cell only decreased to 5×10^{-6} J m^{-2} at 90 °C, and a magnetic field was required to align the LC upon cooling from the isotropic phase. The τ_{off} values of the PB cells also varied in relation to A_2 in the range from 10^1 to 10^3 ms.

The decrease in the A_2 values of the PB cells is associated with the glass transition of each PB at the interface with the NLC. The order of the T_d values of the PMMA, PEMA and PHMA brushes is the same as that of the T_g values of the corresponding bulk polymers, although the T_d values are much lower than the T_g values. In addition, the lower T_d value of the PS-B cell than that of the PMMA-B cell, even though the T_g of PS is similar to that of PMMA, suggests that the NLC, which has a low T_g, permeated into the brushes to decrease the T_g at the interface. PS is more compatible with the NLC than PMMA is, and thus the T_d of the PS-B cell was lowered more efficiently than that of the PMMA-B cell. These results demonstrate that the LC anchoring force for the PB surface depends on the T_g of the bulk polymer, but can be decreased when the compatibility of the polymer with the NLC is high.

These results demonstrate that weak azimuthal anchoring of LC molecules at room temperature can be achieved by coating the substrate surface with polymers exhibiting a subzero T_g. Because the T_g of PHMA is −5 °C, the surface of the PHMA grafted substrate remains in the liquid state at room temperature. I believe that a durable surface with weak azimuthal anchoring can be provided only by polymer brushes. Spin-coated or dip-coated polymer films in the liquid

state can more or less mix with NLCs and can be easily exfoliated from the substrate. In contrast, polymer brushes composed of polymer chains bonded covalently to substrates are durable and can permanently offer ultra-weak LC anchoring surfaces. The ultra-weak LC anchoring surfaces at room temperature are expected to contribute greatly to the development of not only new LCD modes with novel noncontact orientation capabilities but also new applicable fields such as an ultra-low friction interfaces.

References

1. Yamamoto, J., Yokoyama, H., & Watanabe, J. Zero surface anchoring liquid crystal orientation methods and its liquid crystal device. Japanese Patent No.4053530 (2007.12.14).
2. Nemoto, F., Nishiyama, I., Takanishi, Y., & Yamamoto, J. Anchoring and alignment in a liquid crystal cell: selfalignment of homogeneous nematic. Soft Matter 8, 11526-11530 (2012).
3. Syed, I.M., Carbone, G., Rosenblatt, C., & Wen, B. Planar degenerate substrate for micro-and nanopatternednematic liquid-crystal cells. Journal of Applied Physics 98, 034303 (2005).
4. Bryan-Brown, G.P., Wood, E.L., & Sage, I.C. Weak surface anchoring of liquid crystals. Nature 399, 338-340 (1999).
5. Oswald, P., Dequidt, A., & Żywociński, A. Sliding planar anchoring and viscous surface torque in a cholesteric liquid crystal. Physical Review E 77, 061703 (2008).
6. Nespoulous, M., Blanc, C., & Nobili, M. Ultraweak azimuthal anchoring of a nematic liquid crystal on a planar orienting photopolymer. Journal of Applied Physics 102, 073519 (2007).
7. Jánossy, I. Kinetics of director gliding on a polymer- liquid-crystal interface. Physical Review E. 81, 031714 (2010).
8. Vetter, P., Ohmura, Y., & Uchida, T. Study of memory alignment of nematic liquid crystals on polyvinyl alcohol coatings. Japanese Journal of Applied Physics, L1239-L1241 (1993).
9. Stoenescu, D.N., Dozov, I., & Martinot-Lagarde, P. Longtime behavior of the azimuthal anchoring strength and easy axis gliding of nematic liquid crystal. Molecular Crystals and Liquid Crystals Science and Technology. Section A 351, 427-434 (2000).

10. Yamaguchi, R., & Sato, S. Tortional torque effects of twisted nematic bulk on the polymer surface alignment. Molecular Crystals and Liquid Crystals Science and Technology. Section A 367, 379-386 (2001).

11. Tokita, M., Sato, O., Inagaki, Y., Nomura, A., Tsujii, Y., Kang, S., Fukuda, T., & Watanabe, J. High-density poly (methyl methacrylate) brushes as anchoring surfaces of nematic liquid crystals. Japanese Journal of Applied Physics 50, 071701 (2011).

12. Sato, O., Kasai, T., Nomura, A., Tsujii, Y., Kang, S., Tokita, M., & Watanabe, J. Viscoelastic PS brush surface offering strong anchoring at low temperature and near-zero anchoring at high temperature for LC molecules. Liquid Crystals 40, 221-227 (2013).

13. Yoneya, M., Iwasaki, K., Tomioka, Y., & Kondo, K. Cell gap margin enlargement of in-plane switching mode liquid crystal displays using weak-anchoring effects. Applied Physics Letters 74, 803-805 (1999).

14. Brandrup, J., Immergut, E.H., & Grulke, E.A. (Eds.) *Polymer handbook.* 4th ed. (Wiley, New York, 1999).

15. Ohno, K., Morinaga, T., Koh, K., Tsujii, Y., & Fukuda T. Synthesis of monodisperse silica particles coated with well-defined, high-density polymer brushes by surface initiated atom transfer radical polymerization. Macromolecules 38, 2137-2142 (2005).

16. Ejaz, M., Yamamoto, S., Ohno, K., Tsujii, Y., & Fukuda, T. Controlled graft polymerization of methyl methacrylate on silicon substrate by the combined use of the Langmuir-Blodgett and atom transfer radical polymerization techniques. Macromolecules 31, 5934-5936 (1998).

17. Yamamoto, S., Ejaz, M., Tsujii, Y., Matsumoto, M., & Fukuda, T. Surface interaction forces of well-defined, high-density polymer brushes studied by atomic force microscopy. 1. Effect of chain length. Macromolecules 33, 5602-5607 (2000).

18. Yamamoto, S., Ejaz, M., Tsujii, Y., Matsumoto, M., & Fukuda, T. Surface interaction forces of well-defined, high-density polymer brushes studied by atomic force microscopy. 2. Effect of graft density. Macromolecules 33, 5608-5612 (2000).

19. Ryschenkow, G., & Kleman, M. Surface defects and structural transitions in very low anchoring energy nematic thin films. Journal of Chemical Physics 64, 404-412 (1976).

20. Cheng, J., & Boyd, G.D. The liquid-crystal alignment properties of photolithographic gratings. Applied Physics Letters 35, 444-446 (1979).

21. Faetti, S., & Marianelli, P. Strong azimuthal anchoring energy at a nematic-polyimide interface. Physical Review E 72, 051708 (2005).

22. Oh-e, M., & Kondo, K. Response mechanism of nematic liquid crystals using the in-plane switching mode. Applied Physics Letters 69, 623-625 (1996).

Table 3-1. Polymerization condition of polymer brushes

Polymer Brush	Monomer (mol)	Initiator [a] (mmol)	Catalyst (mmol)		Solvent (mol)	Temp. (°C)	Period (h)
PMMA	0.37	0.34	CuBr DNbipy [b]	3.75 8.97	anisole 0.35	90	3.0
PEMA	0.13	0.13	CuBr DNbipy [b]	1.58 1.22	anisole 0.14	90	4.0
PHMA	0.10	0.23	CuBr PMDETA[c]	0.67 0.96	anisole 0.16	90	14.0
PS	0.43	0.44	CuBr DNbipy [b]	4.33 8.66	-	110	3.3

[a] 2-bromoisoisobutylic acid ethyl ester
[b] 4,4′-dinonyl-2,2′-bipyridine
[c] N,N,N′,N″,N″-pentamethyldiethylenetriamine

.

Table 3-2. Characterization of PB substrates

Brush	M_n	M_w/M_n	Thickness h (nm)	Graft density σ [a] (chains nm^{-2})
PMMA-B	112,000	1.17	46.8	0.299
PEMA-B	95,900	1.31	42.0	0.314
PHMA-B	69,000	1.36	44.5	0.388
PS-B	64,300	1.21	36.5	0.359

[a] estimated assuming the density ρ is equal to that of the bulk polymers. PMMA: 1.19 g cm^{-3}, PEMA: 1.19 g cm^{-3}, PHMA: 1.01 g cm^{-3}, PS: 1.05 g cm^{-3}.

Table 3-3. K_2 of NLC and and $V_{th}(V_{2\%})$ of PB-cells at various temperatures

Temperature (°C)	K_2 [a] (pN)	V_{th} (V)			
		PMMA-B	PEMA-B	PHMA-B	PS-B
−15	7.9		4.38	1.81	3.98
5	7.5		4.34	1.34	3.90
25	6.9	3.84	4.48	0.89	3.56
45	6.5	3.79	3.80	0.62	2.72
65	6.0	3.62	2.23	0.57	0.88
90	5.5	2.60	0.94	0.32	0.54

[a] provided by JNC Corporation.

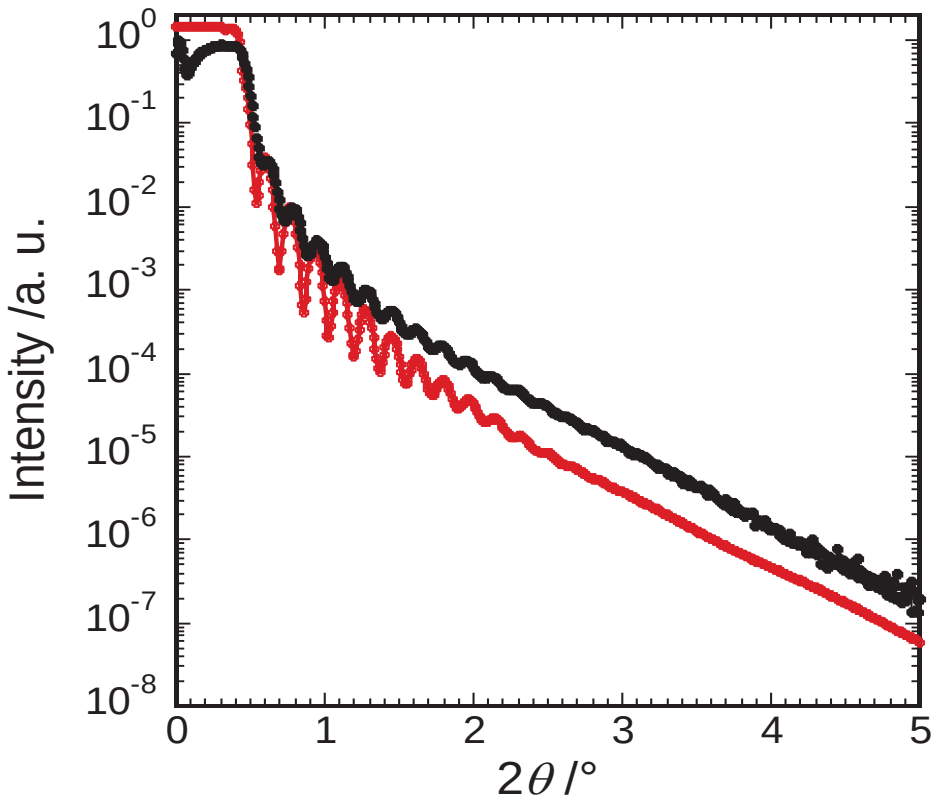

Figure 3-1. X-ray reflectivity curve of PEMA brushes on glass substrate. The experimental data was fitted by setting the brush to 42.0 nm. The density (ρ) of the PEMA layer was assumed to be 1.19 g cm^{-3} (equal to ρ of the bulk PEMA).

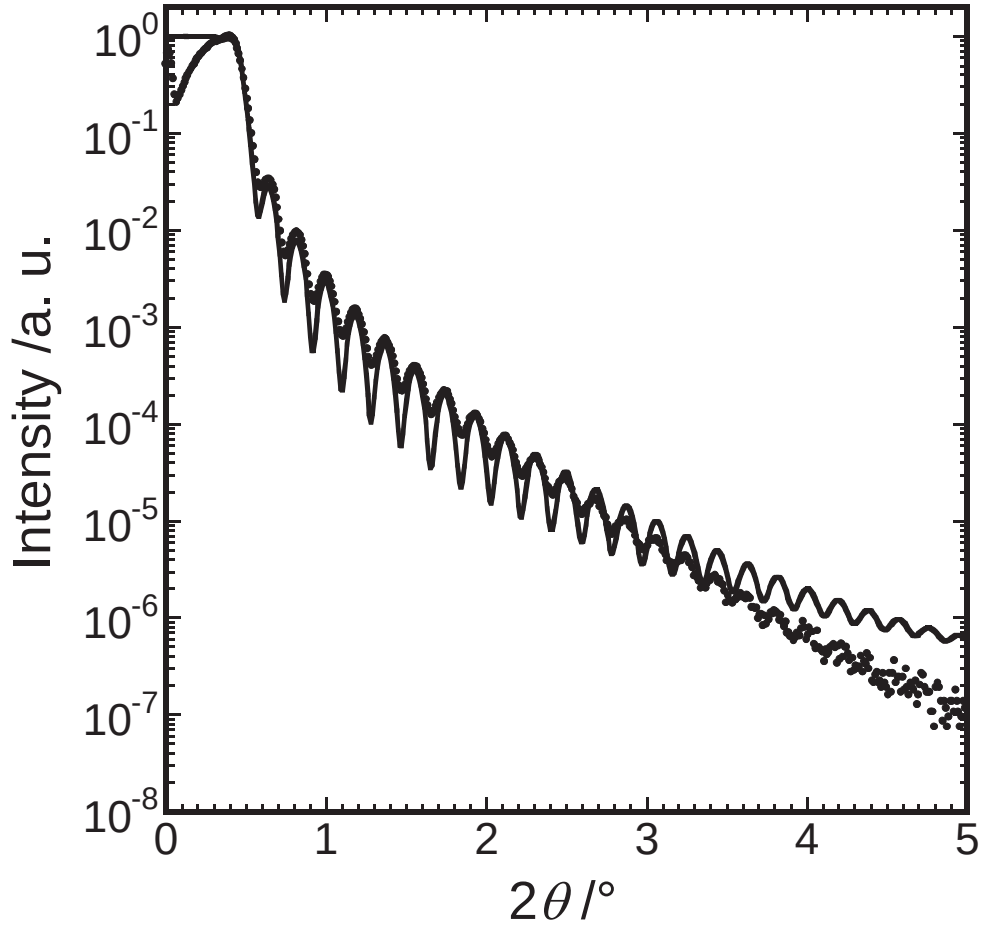

Figure 3-2. X-ray reflectivity curve of PHMA brushes on glass substrate. The experimental data was fitted by setting the brush and BHE layer thicknesses to 44.5 and 0.90 nm, respectively. The densities (ρ) of the layers are assumed to be 1.01 (equal to ρ of the bulk PHMA) and 1.301 g cm^{-3}, respectively.

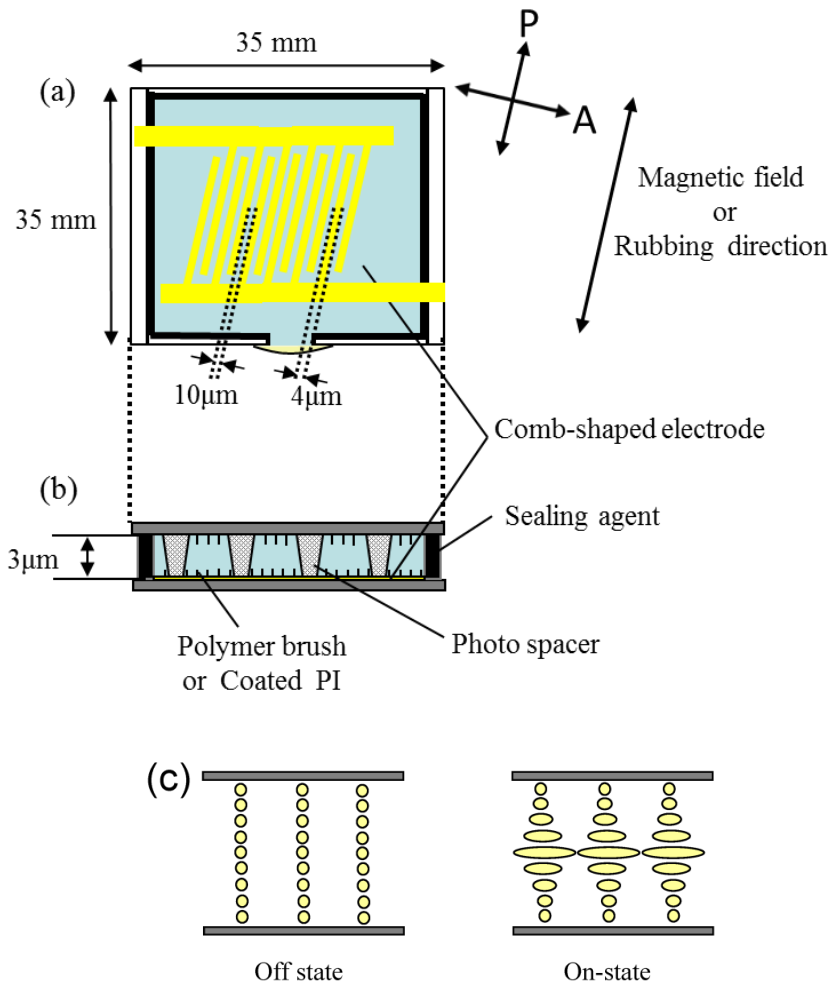

Figure 3-3. Schematic diagram of the RPI and PB cells: (a) front and (b) side views. The aligned axes are parallel to the comb-shaped electrodes. (c) Molecular alignments in the electric field-on and field-off states for the IPS switching mode viewed from the side and a perspective perpendicular to the initial aligned direction. In the field-on state, the molecules at the centre of the cell are oriented with the field, and the rest of the molecules are twisted continuously between two orientations at the anchoring surface and at the centre, if the anchoring functions properly. The cells were set such that the initially aligned nematic LC director coincided with the direction of one of the crossed Nicol polarisers, and the light transmittance was observed in the IPS switching mode. Under this condition, there is no light transmittance in the field-off state, while there is a significant transmittance in the field-on state.

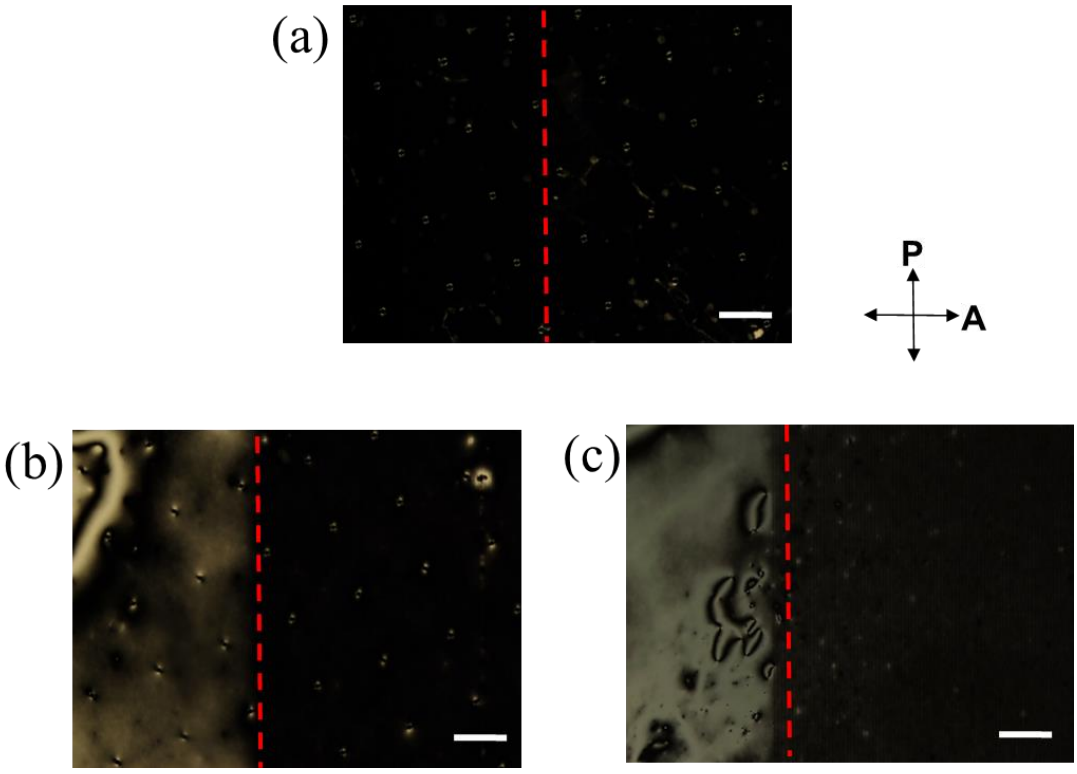

Figure 3-4. POM images of the (a) PMMA-B cell which was applied a magnetic field of 1 T parallel to the electrode direction, and (b) PEMA-B cell and (c) PS-B cell after cooling from the isotropic liquid state. Comb-shaped electrodes can be seen only to the right of the dashed line and are parallel to the line. Scale bar: 200 μm.

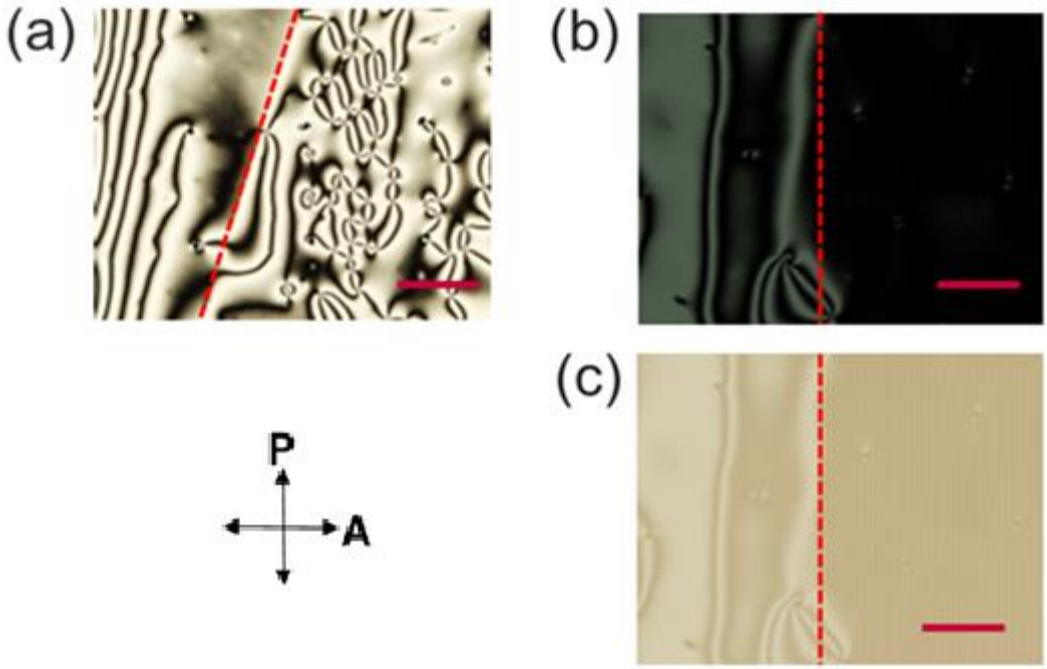

Figure 3-5. Optical images captured with a polarizing microscope of the PHMA-B cells filled with LCs (a) before and (b) after a light push. (c) The same area as in that in (b) observed with the analyser removed. Comb-shaped electrodes are seen only to the right of the dashed line and are parallel to the line. Scale bar, 200 μm.

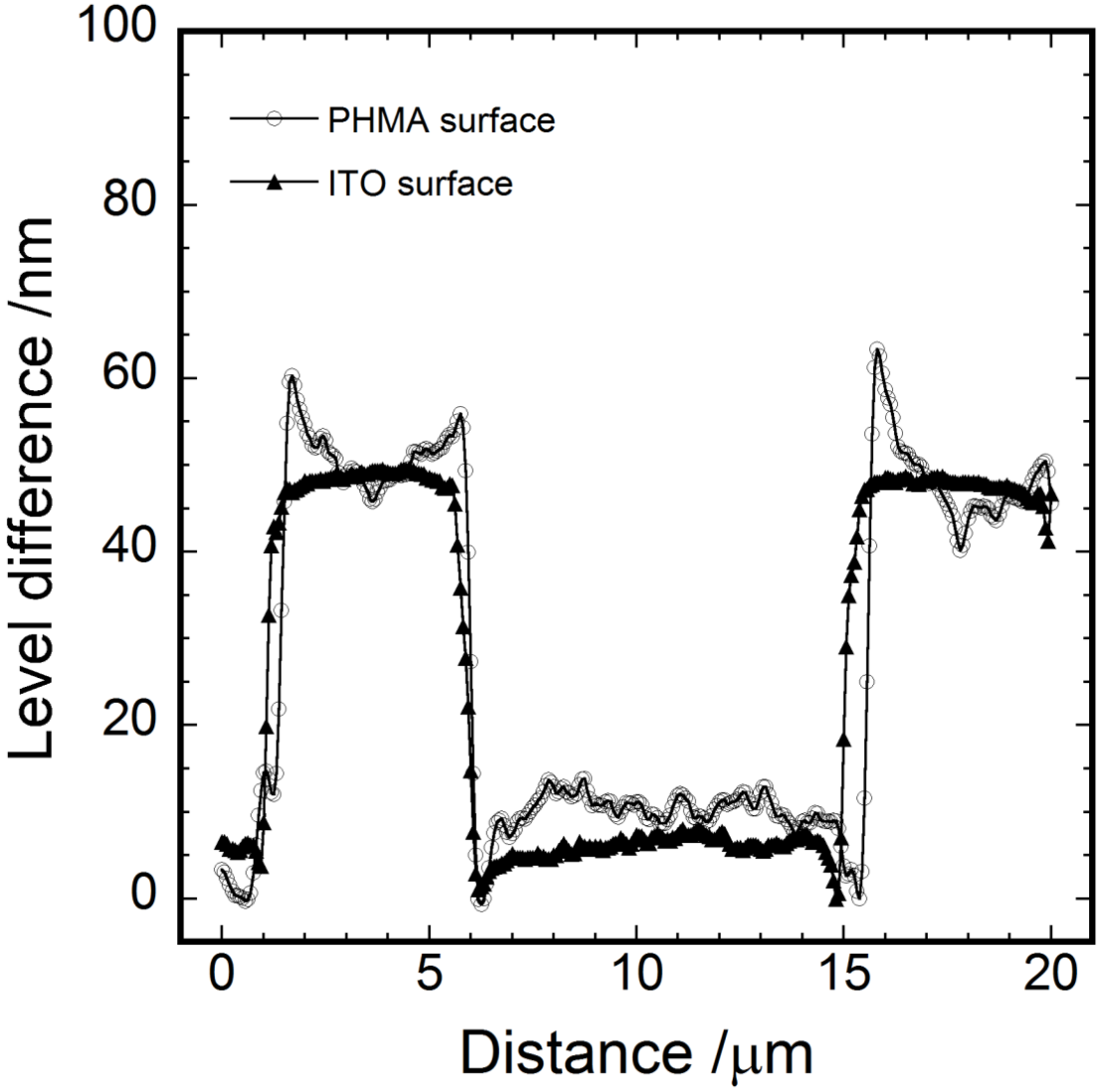

Figure 3-6. Level differences for the PHMA brush (open circles) and ITO comb-shaped electrode (closed triangles) surfaces determined via laser scanning microscopy.

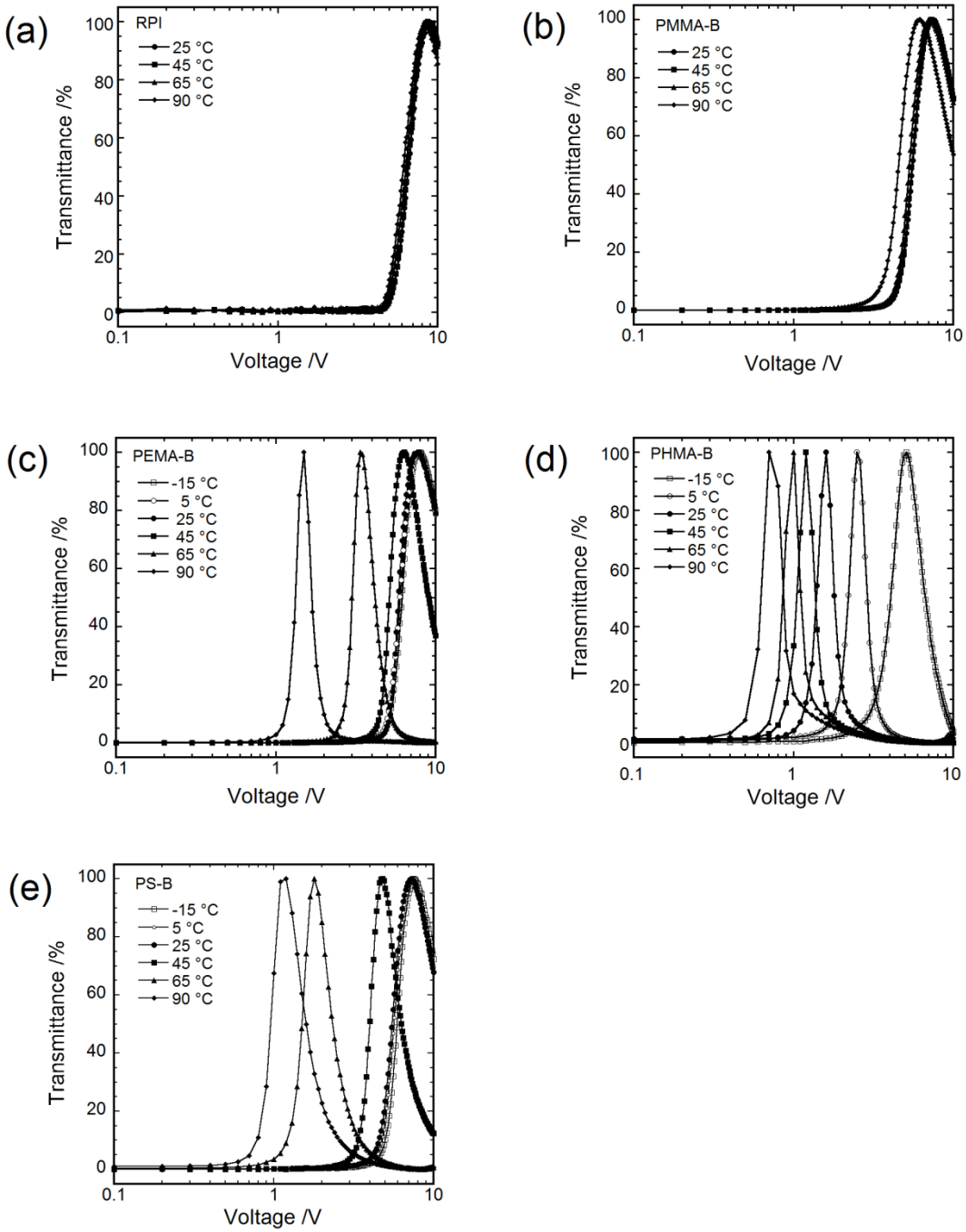

Figure 3-7. *V-T* curves for each cell measured at the indicated temperatures: (a) RPI cell, (b) PMMA-B cell, (c) PEMA-B cell, (d) PHMA-B cell and (e) PS-B cell.

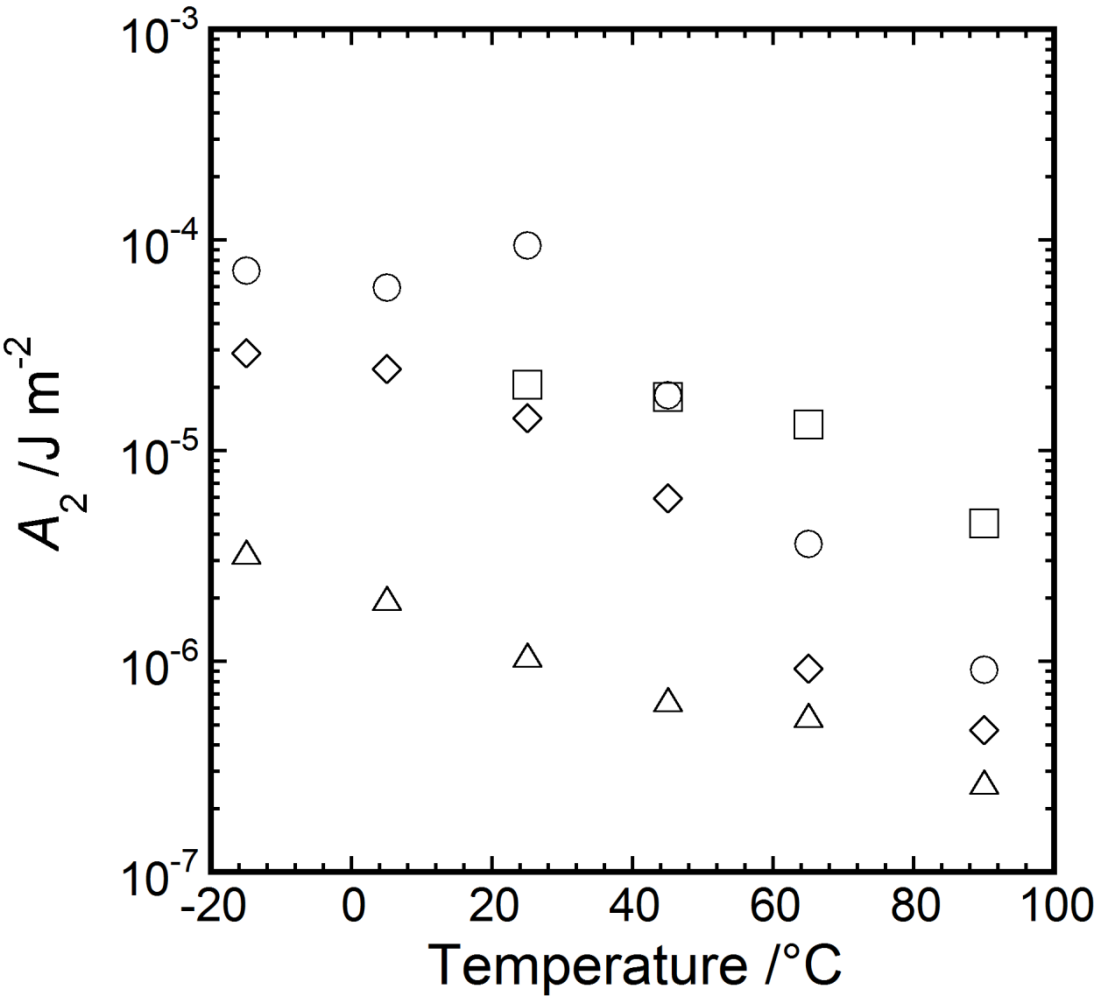

Figure 3-8. Temperature dependence of the twist anchoring coefficient A_2 for the PMMA (squares), PEMA (circles), PHMA (triangles) and PS (lozenges) brushes.

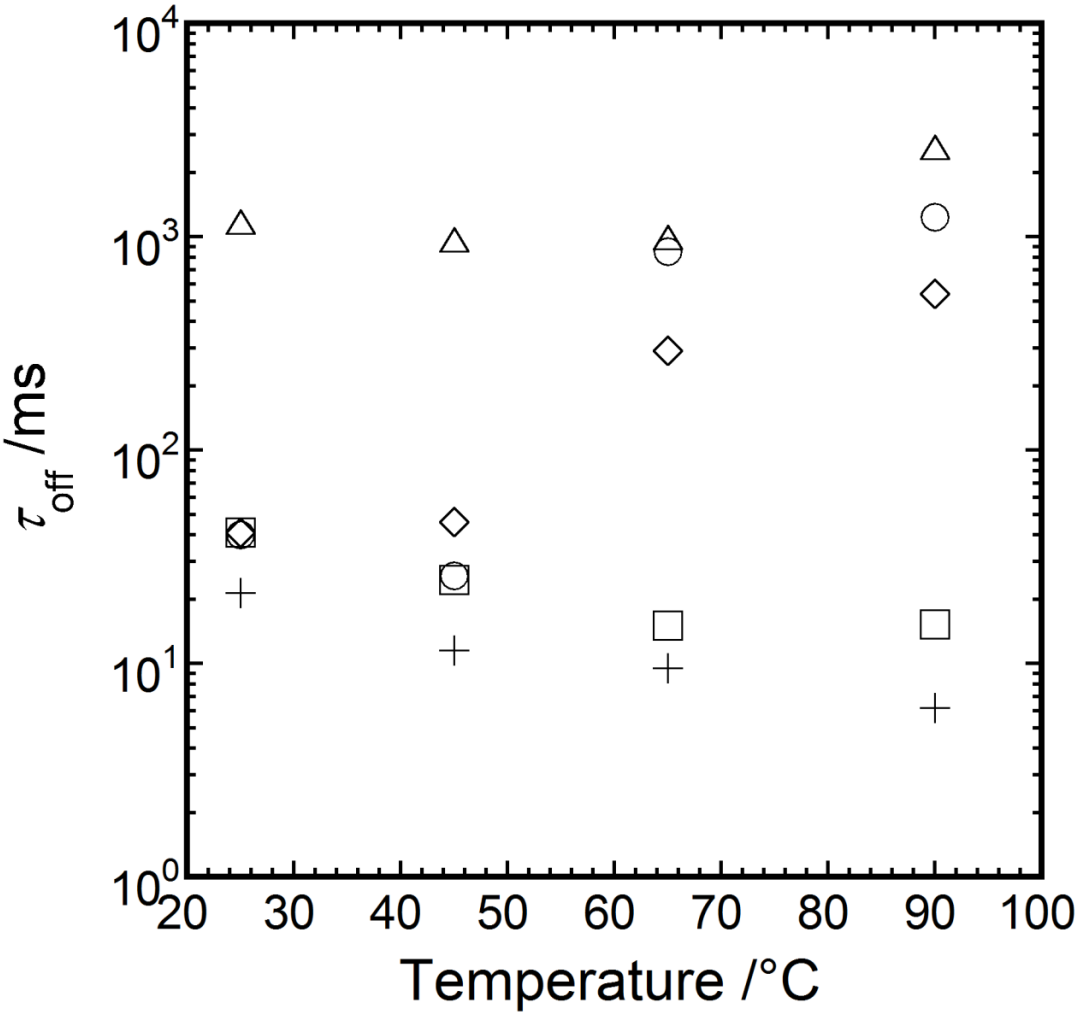

Figure 3-9. Temperature dependence of the relaxation time τ_{off} of the PMMA-B (square), PEMA-B (circle), PHMA-B (triangle), PS-B (lozenge) and RPI (cross) cells. The value of τ_{off} was measured by applying V_{max} at the measurement temperature and then turning off the voltage.

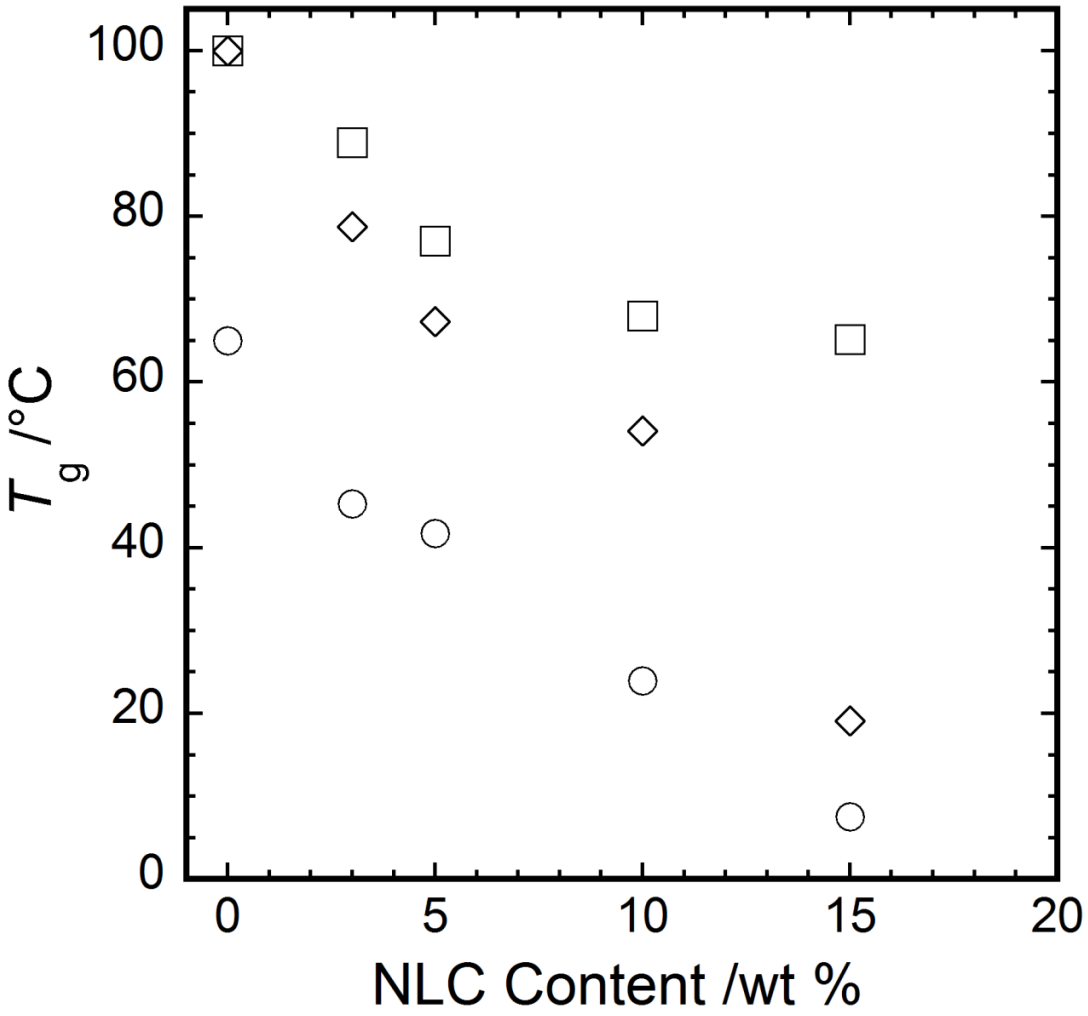

Figure 3-10. Glass transition temperature of mixtures of polymers and the NLC as a function of the weight fraction of NLC: PMMA (square), PS (lozenge) and PEMA (circle). The M_n (M_w/M_n) values for the PMMA, PS and PEMA polymers were 50,500 (1.26), 54,000 (1.17) and 88,000 (1.40), respectively.

Chapter 4

An In-plane Switching Liquid Crystal Cell with Weakly Anchored Liquid Crystals on the Electrode Substrates

Abstract

A new “one side zero-azimuth anchoring in-plane switching” (OZ-IPS) mode of liquid crystal (LC) display featuring low driving voltage, higher transmittance efficiency, and higher contrast ratio than that of the conventional IPS LCD has been established. The OZ-IPS mode LC cell is assembled from an electrode substrate to which polymer chains are grafted and a counter substrate coated with a rubbed polyimide film where the rubbing direction is parallel to the interdigital electrodes. LC molecules filling the cell are strongly anchored to the counter substrate whereas they are hardly anchored to the electrode substrate so that the LC director is parallel to the rubbing direction under the crossed polarizers and the cell exhibits 20% smaller transmittance than the conventional IPS cell in the voltage-off state. In the voltage-on state, the LC director is twisted in going from the counter substrate to the electrode substrate and the transmittance starts to increase and becomes the maximum with increasing the voltage up to a threshold voltage (V_{th}) and at a voltage (V_{max}), respectively, which are two times lower than that in the conventional IPS cell. When a voltage of V_{max} is applied to the cell, linearly polarizing light incident on the counter substrate passing the cell rotates the polarizing direction by 90 ° so that the emitted light entirely passes the analyzer. To this switching process the area above the electrodes contributes. Thus this OZ-IPS mode LCD has almost two times greater maximum

transmittance and 2.3 times higher contrast ratio than the conventional IPS-LCD although a longer turn-off response time is intrinsic due to the lower V_{th}.

4-1 Introduction

While organic light emitting diode (OLED) displays have been put to practical use, liquid crystal display (LCD) industries need a new LCD mode for further improvement of the characteristics such as higher transmittance and contrast ratio, lower driving voltage, and better viewing characteristic. The in-plane switching (IPS) mode LCD has taken place of the twisted nematic (TN) mode LCD because of their surpassing viewing angle characteristics, i.e., uniform gray levels and colors in a large range of viewing angle;[1-3] however, it has lower transmittance than the TN LCD[4]. The area above the electrodes does not contribute to the switching process to decrease the aperture. Above the electrodes molecules are not switched by the electric field between interdigital electrodes. The electrical field lines above the electrodes lie almost perpendicular to the electrodes, so there exists a week in-plane electric field. Such an intrinsic problem has been overcome in the fringe-field switching (FFS) LCDs[5,6]. Stripe electrodes having the same electric potential are placed on a common electrode insulated with a passivation layer. When the electrode space is shorter than both the electrode width and the cell gap, an in-plane field between a stripe electrode and the common electrode becomes strong enough to rotate molecules above the electrodes. On the other hand, the transmittance is decreased by the absorption and reflection of light in each layer and at the layer interface, respectively. Therefore, a higher transmittance efficiency is expected for the IPS mode rather than the FFS mode in the case of displays with the resolution as high as that in the television in which the ratio of the stripe electrode area to the pixel area is not very great.

Considering the above-mentioned backgrounds, I propose a new IPS mode LCD in which LC molecules are strongly anchored to the counter substrate which is the uniaxial orientation treatment whereas they are hardly anchored to the electrode substrate. When applying voltage to the NLC filling the cell via the electrodes, the positive dielectric anisotropy NLC molecules tend to change their alignment from parallel to perpendicular to the electrodes. While NLC molecules on the counter substrate anchored strongly to the rubbed PI, molecules on the electrode substrate can rotate and align along the electric field by extremely low voltage. Thus, the electric field can twist the director of NLC contained in the cell to make the molecular orientation similar to that in the TN cell in the voltage-off state. If the optical design of a TN mode is applied to new mode LCD, realization of LCD which has both high transmissivity and extremely low driving voltage characteristics can be expected.

4-2 Experimental Procedure

The new mode LCD cell, hereafter designated as “type-I cell” (Figure 4-1(a)). A peculiarity of the type-I cell is that the electrode substrate is coated with poly(hexyl methacrylate) (PHMA) brush to offer a zero-azimuth anchoring surface. The high-density PHMA brush surface exhibited an NLC anchoring energy 1/300 lower than that of the rubbed PI at room temperature[7,8]. PHMA brushes were polymerized by the following methods. The initiator 2-bromo-2-methyl-N-(3-(triethoxysilyl) propanamide (BPA) (0.05 g), ethanol (4.7 g) and ammonia solution (28 % NH_3 aqueous solution, 0.25 g) was mixed, and the resulting mixture was stirred to form a solution. The glass substrates cleaned by ultra-violet (UV)/ozone treatment were immersed in this solution for 12 h at ambient temperature to bond BPA with the surface. The modified glass substrates were cleaned by sonication in acetone and then dried. Polymerization was performed by dipping the BPA-immobilized substrate in a degassed

solution of hexyl methacrylate (29.74 g, 174.7 mmol), CuBr (152.2 mg, 1.06 mmol), N,N',N",N"-Pentamethyldiethylenetriamine (PMDETA) (243.8 mg, 1.41 mmol), ethyl-2-bromoisobutyrate (EBIB) (68.7 mg, 0.35 mmol) as a free initiator and anisole (29.97 g, 277 mmol) at 70 °C for 7 h. The number average molecular weight (M_n) and polydispersity index (M_w/M_n) of PHMA brushes were 88,900 and 1.74, respectively, as estimated from the gel permeation chromatogram with PMMA standards of the freely initiated PHMA in the same vessel[9-11]. The thickness h of the brushes was determined on the basis of X-ray reflectivity (Rigaku UltimaIV) to be 18.0 nm (Figure 4-2). The graft density was estimated to be 0.123 chains nm^{-2} using the relationship $\sigma = \rho h N_A/M_n$ and assuming that the brush density ρ is equal to the density of the bulk PHMA (1.01 g cm^{-3})[11]. The polymerization conditions and key characteristics of the PHMA brushes are summarized in Tables 4-1 and 4-2, respectively. On the other hand, PI (JSR, AL-16301) was coated as the alignment layer on the counter substrate on which 6 μm-high photo spacers were formed. The rubbing treatment was executed to PI on the counter substrate so that NLCs might be homogeneous alignment in the direction parallel to the comb-shaped electrodes in LC cell. The electrode and the counter substrates were stuck by the sealant, and it was cured by heating the cell at 120 °C for 2 h under nitrogen atmosphere. NLC was injected via capillary action into the cell and the inlet of NLC was sealed with the UV curing type sealing agent. The electrode substrate has comb-shaped ITO electrodes (thickness: 55 nm, lines and spaces: 4 μm and 10 μm, respectively), and photo spacers were formed on the counter substrate similarly to the conventional IPS LCD cell. The cell gap was set at 6.0 μm so that the first minimum condition[12] might be fulfilled.

To understand the characteristics of the cell, other two type reference cells were prepared. Schematics of these reference cells are show in Figure 4-1(b) and 4-1(c), respectively. The reference type-II cell was produced to compare the response time. It differs from the type-I cell

in that the electrode substrate is coated with PI film. The type-III cell is the same as the cell in the practical IPS-LCD. Both substrates were coated with PI film rubbed in the direction tilted by 20 ° with respect to the electrodes. The cell gap of the type-III cell was set at 3.4 μm so that Δnd equals $\lambda/2$ (λ = 550 nm). Type-II and type-III cells were fabricated at the same process as type-I cell except that the sealant was cured at 150 °C for 2 hours. All the three cells were filled with the NLC (JNC, JC-5051XX, a nematic-isotropic transition temperature: 112.7 °C and Δn = 0.081) and were placed between linear polarizer **P** and analyzer **A** with P ⊥ A and P is on the counter side with the axis parallel to the rubbing direction.

The voltage-transmittance (*V*-*T*) curves, the viewing angle characteristic and the response time were measured at 25 °C by Otsuka Electronics LCD-5200. The intensity of the incident light near the surface of the LC cell was about 2.2 million cd/m^2. The transmittance of each cell was given as the transmittance measured without the cell to be 100 %. The viewing angle characteristics of type-I and type-III cells were measured with applied voltage of 0 V and V_{max} for the off and on states, respectively. The response times of type-I and type-II cells were measured by applying AC voltage with amplitude of V_{max} at frequency 60 Hz to the cell. τ_{on} was the period from the application of the voltage until the transmittance was reached to 90 % in normalized transmittance. On the other hand, τ_{off} was the period from the removal of the voltage until the transmittance was reached to 10 % in normalized transmittance.

The normalized Stokes parameter measurement when arbitrary electric field was applied to type-I cell was performed using green light (λ = 546nm) by LCD Analyzer (Meiryo technical co., ltd. LCA-LU4As10) at room temperature. To determine the Stokes parameters, the linearly polarized light perpendicular to the rubbing direction (*x*-direction) was normally incident on the counter substrate and the transmitted light intensity I_{ij} were measured with inserting a quarter-wave plate (QWP) and an analyzer behind the LC cell where *i* and *j* refer the fast axis

direction of the quarter-wave plate and the analyzer axis, respectively. *i* and *j* are either of *x*, *y*, and *d*, where *y* is orthogonal to the *x*-direction and d is the direction at 45 ° with respect to the *x*-axis (see Figure 4-3). The Stokes parameters are defined as follows[13].

$$S_1 = (I_{xx} - I_{yy}) / (I_{xx} + I_{yy}) \tag{4.1}$$

$$S_2 = [2I_{dd} - (I_{xx} + I_{yy})] / (I_{xx} + I_{yy}) \tag{4.2}$$

$$S_3 = [2I_{yd} - (I_{xx} + I_{yy})] / (I_{xx} + I_{yy}) \tag{4.3}$$

Polarized optical microscopy (POM) observation was performed by Olympus BX50P microscopy.

4-3 Results and Discussion

The NLCs as-injected into type-I cell arranged uniformly the director parallel to the comb-shaped electrodes. Considering that the anchoring induced by the unevenness of the comb-shaped electrodes[14] is two orders of magnitude smaller than the anchoring induced by rubbing treatment[15], the uniform orientation in type-I cell is considered to be achieved by the rubbing treatment mainly.

Figure 4-4 shows the voltage-transmittance (*V*-*T*) curves of type-I and type-III cells at 25 ◦C. With increasing voltage, the transmittance starts to increase at a threshold voltage (V_{th}) and becomes the maximum at a voltage (V_{max}). Here V_{th} is defined as the voltage at 2 % of the maximum transmittance (T_{max}). V_{th} and V_{max} of the type-I cell are 1.7 and 4.3 V, respectively, which are significantly lower than that of the type-III cell (V_{th} = 2.6 V, V_{max} = 8.8 V). Thus the type-I cell can be driven with lower voltage than the type-III cell. T_{max} of the type-I cell is 33.2 %, almost two times greater than T_{max} of the type-III cell (18.1 %). The transmittance efficiency (*TE*), which is defined as the ratio of T_{max} to the transmittance measured with setting the two polarizers parallel, is 86 % for the type-I cell, which is comparable to that of the TN-LCD. On the other hand, in the voltage-off state, the transmittance of the type-I cell is 20 %

lower than that of the type-III cell. The lower transmittance in the voltage-off state, in addition to the high transmittance efficiency in the voltage-on state, produces the higher contrast ratio (*CR*). The contrast ratio of the type-I cell is 2.3 times higher than that of the type-III cell. The lower transmittance of the type-I cell in the voltage-off state is attributed to the uniaxial orientation of LC along the rubbing direction in the voltage-off state. In the conventional IPS cells, LC tends to twist to cause slight transmittance in the voltage-off state because of small difference in rubbing direction between the two substrates. In the type-I cell, LC is hardly anchored to the electrode substrate and oriented along the rubbing direction of the counter substrate. Moreover, reflecting the in-plane LC orientation change, the type-I cell exhibited excellent viewing angle characteristics equivalent to the conventional IPS cell. In addition, the region with high-contrast-ratio over 300 of the type-I cell were about 5 times wider than that of the type-III cell reflecting the contrast ratio improvement (Figure 4-5).

The high transmittance efficiency of the type-I cell is attributed to the following two points. First, the type-I cell has a higher aperture ratio than the conventional IPS LCDs. The electrode region in the type-I cell transmits light in the voltage-on state although that in the conventional IPS LC cell (type-III) does not (Figure 4-6). Although in the IPS LCDs the in-plane electric field above the electrodes is too small to rotate molecules, the molecules in the type-I cell are hardly anchored to the electrode substrate surface covered with PHMA chains so that LC molecules above the electrodes can be rotated by the small in-plane electric field to transmit light and by the elastic torque with the LC between electrodes. Thus in the voltage-on state, the type-I cell has larger aperture than the conventional IPS LC cell.

Second, at $V_{\mathrm{appl}} = V_{\mathrm{max}}$, the type-I cell emits light linearly polarizing along the analyzer direction. Figure 4-7 shows the voltage dependence of the Stokes parameters measured for the type-I cell. At $V_{\mathrm{appl}} = 0$ V, $S_1 = -1.0$, $S_2 = 0$, and $S_3 = 0$ are consistent with the homogeneous director alignment along the *x*-direction. Over the range of V_{appl} investigated, S_3 is almost constant at zero, indicating that the light passing the cell is linearly polarized, whereas S_1 and S_2

vary in value, suggesting the polarization direction is dependent on V_{appl}. At $V_{appl} = V_{th} = 1$ V, S_1 and S_2 begin to increase and decrease, respectively. At $V_{appl} = 2$ V, $S_1 = 0$ and $S_2 = -1$ showing that the polarization direction is in the direction at an angle of 45 ° with respect to the *x*-direction. With further increasing V_{appl} greater than 4.5 V (close to $V_{max} = 4.3$ V), $S_1 = 1$ and S_2 is close to zero, indicating that the polarization direction is along the *y*-direction. Thus, in a measured voltage range, the light passing through the type-I cell is linearly polarized. When viewed from the electrode substrate side, the polarization direction of the light emitted from the cell rotates with increasing V_{appl} in the counterclockwise direction from the rubbing direction and becomes parallel to the analyzer axis so that the light entirely passes the analyzer. This rotation of the polarizing direction of light emitted from the LC cell is associated with the director of nematic LC rotating preferentially counterclockwise in going from the counter substrate to the electrode substrate. This counterclockwise twisting of LC director direction can be ascribed to a slight displacement of the rubbing direction from the electrode direction.

A drawback of the type-I cell is longer response times. The response times (τ_{on} and τ_{off}) on voltage-on and off were measured for the type-I and type-II cells at 25 °C and plotted against the applied voltage (V_{appl}) in Figure 4-8(a) and 4-8(b), respectively. When V_{appl} was set at V_{max} for each cell (4.3 V and 7.3 V for the type-I and type-II cells, respectively), τ_{on} of the type-I cell was 144 ms, which was 2.3 times longer than that of the type-II cell (62.8 ms). Such longer τ_{on} of the type-I cell is a side effect of the lower V_{th} and V_{max}. τ_{on} of conventional IPS-LCD in which the LC was assumed to be anchored strongly to both substrates is inversely proportional to $V_{appl}^2 - V_{th}^2$ [2 2]. When the V_{appl} for the type-I cell was set at 6.73 V so as to equate the value of $V_{appl}^2 - V_{th}^2$, τ_{on} became 42.3 ms, 30 % shorter than that of the type-II cell. The response speed on voltage-on of type-I cell is essentially considered to be faster than that of the type-II cell. It may be attributed to the weak LC anchoring of the electrode substrate surface in the type-I cell.

On the other hand, the longer τ_{off} is intrinsic to the type-I cell. Theoretical calculation of response in IPS mode shows that τ_{off} is inversely proportional to the square of the threshold

electric field (E_{th}^2) assuming strong LC anchoring to both substrates[2]. Thus, τ_{off} of the IPS LC cells with the same electrode distance is inversely proportional to V_{th}^2 and independent on V_{appl}. In contrast, the type-I cell increases τ_{off} with increasing V_{appl} and becomes 540 ms at V_{max}, which is 7.7 times longer than that of the type-II cell (70 ms). Such a V_{appl} dependence of τ_{off} is expected because the twist angle increases with increasing V_{appl}. A long τ_{off} of the type-I cell may be attributed both to a low V_{th} and to a large twisting angle of the LC molecules on the weak LC anchoring substrate.

4-4 Conclusions

In summary, a new IPS mode LC cell is assembled from electrode and counter substrates which are coated with grafted polymer chains and rubbed polyimide film, respectively, to feature lower driving voltage, higher transmittance efficiency, and higher contrast ratio than that of the conventional IPS LC cell. In the new IPS mode cell in the voltage-off state, LC is oriented along the direction of rubbing of the counter substrate and appears to be black under crossed polarizers at 20 % smaller transmittance than that of the conventional IPS cell. With increasing applied voltage, the transmittance starts increasing at V_{th} and then becomes maximum at V_{max}. These V_{th} and V_{max} are two times smaller than that of the conventional IPS cell. The polarizing direction of the light incident on the counter substrate is rotated by 90 ° at $V_{appl} = V_{max}$. To this switching process the molecules above the electrodes contribute to make the aperture greater than that of the conventional IPS cell. Thus, the transmittance efficiency becomes as large as that of the TN-LCD and the contrast ratio is 2.3 times higher than the conventional IPS cell. On the other hand, the lower V_{th} results in an intrinsic longer turn-off response time. This new mode IPS is termed as “one side zero-azimuth anchoring in-plane switching (OZ-IPS) mode”.

References

1. Oh-e, M., & Kondo, K. Electro-optical characteristics and switching behavior of the in-plane switching mode. Applied physics letters 67, 3895-3897 (1995).

2. Oh-e, M., & Kondo, K. Response mechanism of nematic liquid crystals using the in-plane switching mode. Applied physics letters 69, 623-625 (1996).

3. Oh-e, M., Yoneya, M., & Kondo, K. Switching of negative and positive dielectro-anisotropic liquid crystals by in-plane electric fields. Journal of applied physics 82, 528-535 (1997).

4. Schadt, M., & Helfrich, W. Voltage-dependent optical activity of a twisted nematic liquid crystal. Applied Physics Letters 18, 127-128 (1971).

5. Lee, S. H., Lee, S. L., & Kim, H. Y. Electro-optic characteristics and switching principle of a nematic liquid crystal cell controlled by fringe-field switching. Applied physics letters 73, 2881-2883 (1998).

6. Kim, D. H., Lim, Y. J., Kim, D. E., Ren, H., Ahn, S. H., & Lee, S. H. Past, present, and future of fringe-field switching-liquid crystal display. Journal of Information Display 15, 99-106 (2014).

7. Sato, O., Kasai, T., Sato, M., Sakajiri, K., Tsujii, Y., Kang, S., Watanabe, J., & Tokita, M. High-density poly (hexyl methacrylate) brushes offering a surface for near-zero azimuthal anchoring of liquid crystals at room temperature. Journal of Materials Chemistry C 1 (48), 7992-7995 (2013).

8. Sato, O., Iwata, N., Kasai, T., Tsujii, Y., Kang, S., Watanabe, J., & Tokita, M. Nematic liquid crystal anchoring strengths of high density polymer brush surfaces. Liquid Crystals 42 (2), 181-188 (2015).

9. Ejaz, M., Yamamoto, S., Ohno, K., Tsujii, Y., & Fukuda, T. Controlled graft polymerization of methyl methacrylate on silicon substrate by the combined use of the Langmuir-Blodgett and atom transfer radical polymerization techniques. Macromolecules 31 (17), 5934-5936 (1998).

10. Yamamoto, S., Ejaz, M., Tsujii, Y., Matsumoto, M., & Fukuda, T. Surface interaction forces of well-defined, high-density polymer brushes studied by atomic force microscopy. 1. Effect of chain length. Macromolecules 33, 5602-5607 (2000).

11. Yamamoto, S., Ejaz, M., Tsujii, Y., Matsumoto, M., & Fukuda, T. Surface interaction forces of well-defined, high-density polymer brushes studied by atomic force microscopy. 2. Effect of graft density. Macromolecules 33, 5608-5612 (2000).

12. Gooch, C.H., & Tarry, H.A. The Optical Properties of twisted nematic liquid crystal structures with twist angle less than or equal to 90 degrees. Journal of Physics D: Applied Physics 8, 1575 (1975).

13. Zhou, Y., He, Z., & Sato, S. A novel method for determining the cell thickness and twist angle of a twisted nematic cell by Stokes parameter measurement. Japanese journal of applied physics 36, 2760 (1997).

14. Berreman, D.W. Solid surface shape and the alignment of an adjacent nematic liquid crystals. Physical Review Letters 28, 1683-1686 (1972).

15. Lee, E.S., Saito, Y., & Uchida, T. Detailed Morphology of Rubbed Alignment Layers and Surface Anchoring of Liquid Crystals. Japanese journal of applied physics 32, L1822 (1993).

Table 4-1. Polymerization condition of PHMA brushes

Polymer	Monomer (mmol)	Initiator [a] (mmol)	Catalyst (mmol)		Solvent (mmol)	Temp. (°C)	Period (h)
PHMA	174.7	0.35	CuBr PMDETA[b]	1.06 1.41	anisole 277	70	7

[a] ethyl-2- bromoisobutyrate
[b] N,N,N′,N″,N″-pentamethyldiethylenetriamine

Table 4-2. Characterization of PHMA brush substrates

Brush	M_n	M_w/M_n	Thickness h (nm)	Graft density σ [a] (chains nm^{-2})
PHMA-B	88,900	1.74	18.0	0.123

[a] estimated assuming the density ρ is equal to that of the bulk PHMA: 1.01 g cm^{-3}.

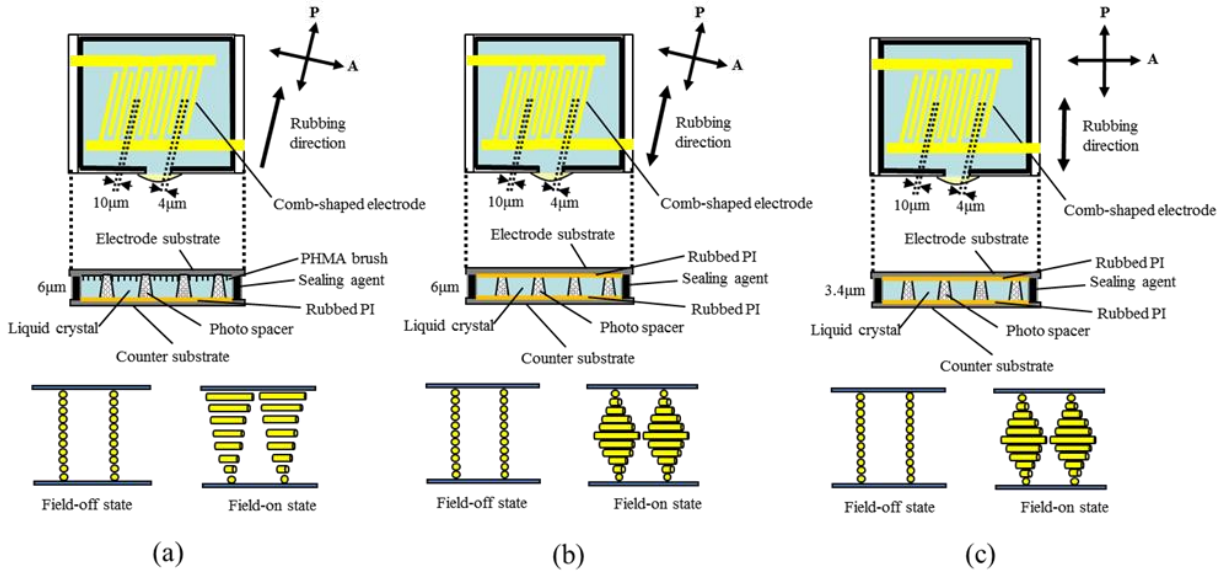

Figure 4-1. Schematics of the (a) type-I, (b) type II, and (c) type-III cells. In the upper and middle parts of each panel, the front and side views are shown, respectively. In the lower part of each panel, the molecular alignments are shown for the electric field-on and field-off states (viewed side-on). Light sequentially propagates through the polarizer, counter substrate, LC, electrode substrate, and analyser. In each cell, the polarizer and analyser axes are parallel and perpendicular, respectively, to the polyimide (PI) rubbing direction.

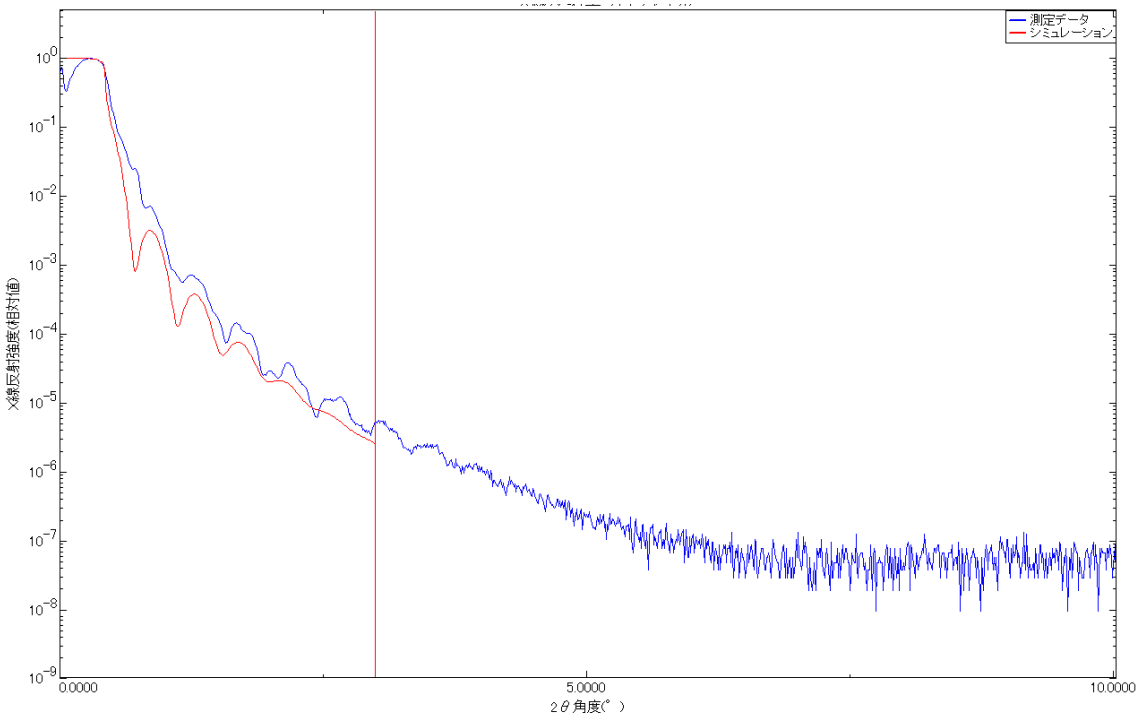

Figure 4-2. X-ray reflectivity curve of PHMA brushes on glass substrate. The experimental data was fitted by setting the brush to 18.0 nm. The density (ρ) of the PHMA layer was assumed to be 1.01 g cm^{-3} (equal to ρ of the bulk PHMA).

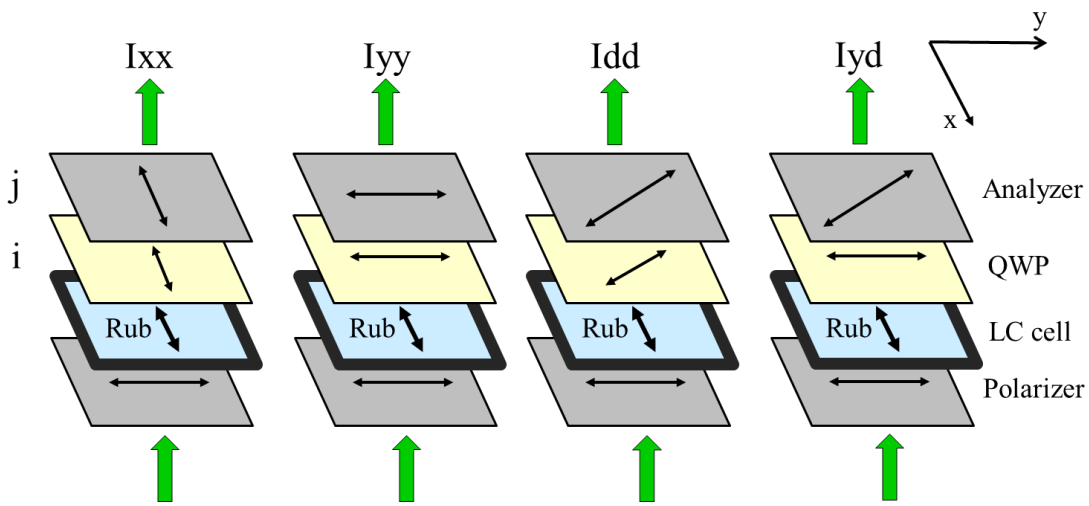

Figure 4-3. Schematic diagram of the optics setup for measuring the Storks Parameters.

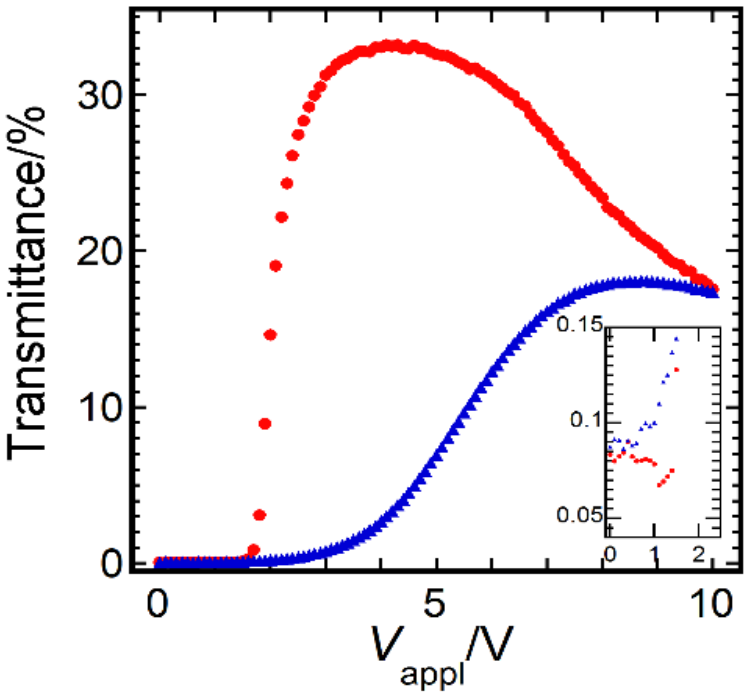

Figure 4-4. Voltage-transmittance characteristics of the type-I cell (circle) and type-III cell (triangle) measured at 25 °C.

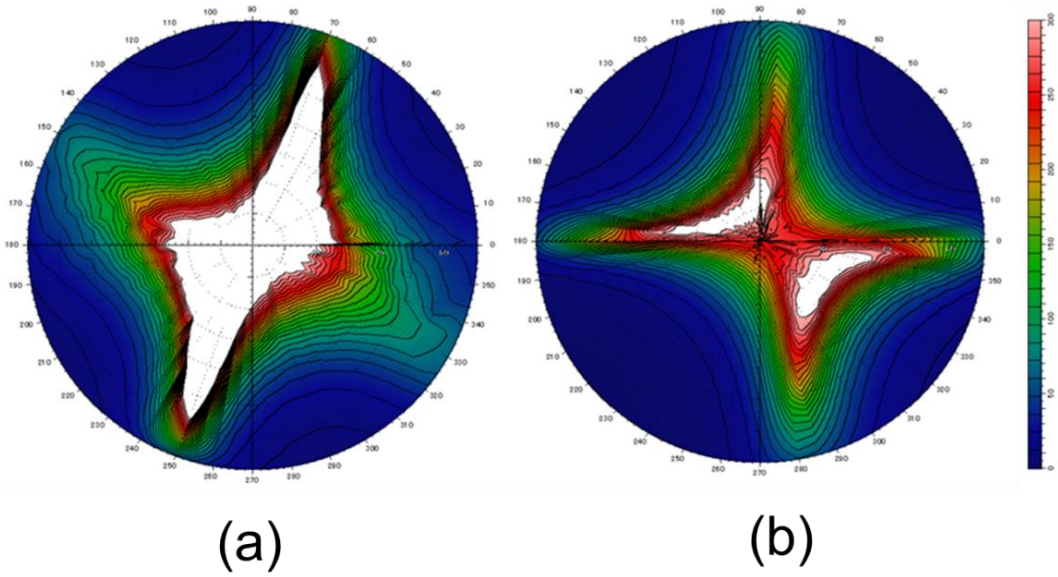

Figure 4-5. Contour map of the contrast ratio for (a) type-I cell and (b) type-III cell. The region with contrast ratios higher than 300 is shown by white color. A difference laid in the symmetry of the high contrast region, which was just 20 ° between the type-I and type- III cells. This corresponded to the differences of the cross Nicole and rubbing directions which differed just 20 ° between these cells (see Figure 4-1). The initial LC orientation directions of the type-I and type-III cells were 70 ° - 250 °, 90 ° - 270 ° directions, respectively.

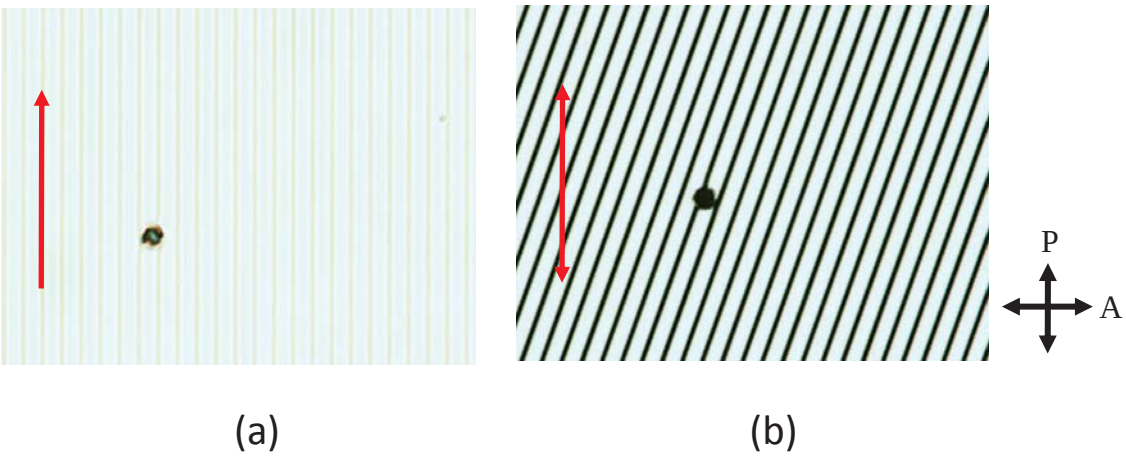

Figure 4-6. Polarizing optical microscopy image of (a) the type-I and (b) type-III cells applied a voltage of V_{max} at which the transmittance is maximum. Light did not transmit above the electrodes even in the field-on state in the type-III cell. In contrast, light transmitted in the field-on state in all area including above electrodes in the type-I cell. Red arrows indicate the rubbing direction.

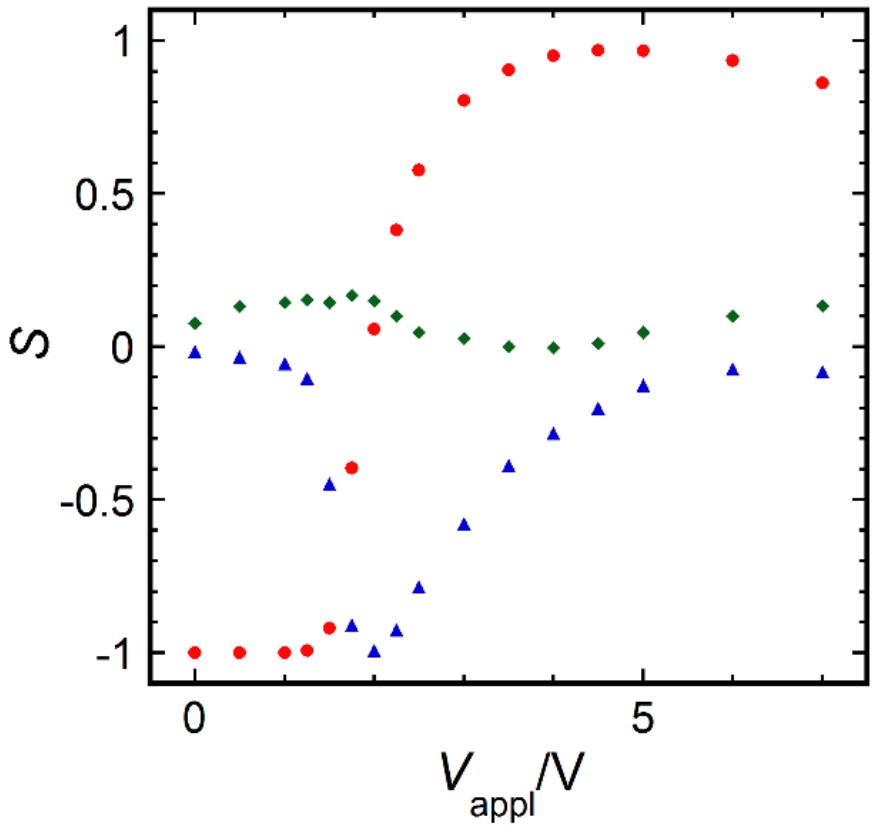

Figure 4-7. The Stokes parameters of S_1 (circle), S_2 (triangle), and S_3 (lozenge) measured for the type-I cell driven at voltages ranging from 0 to 7 V at room temperature.

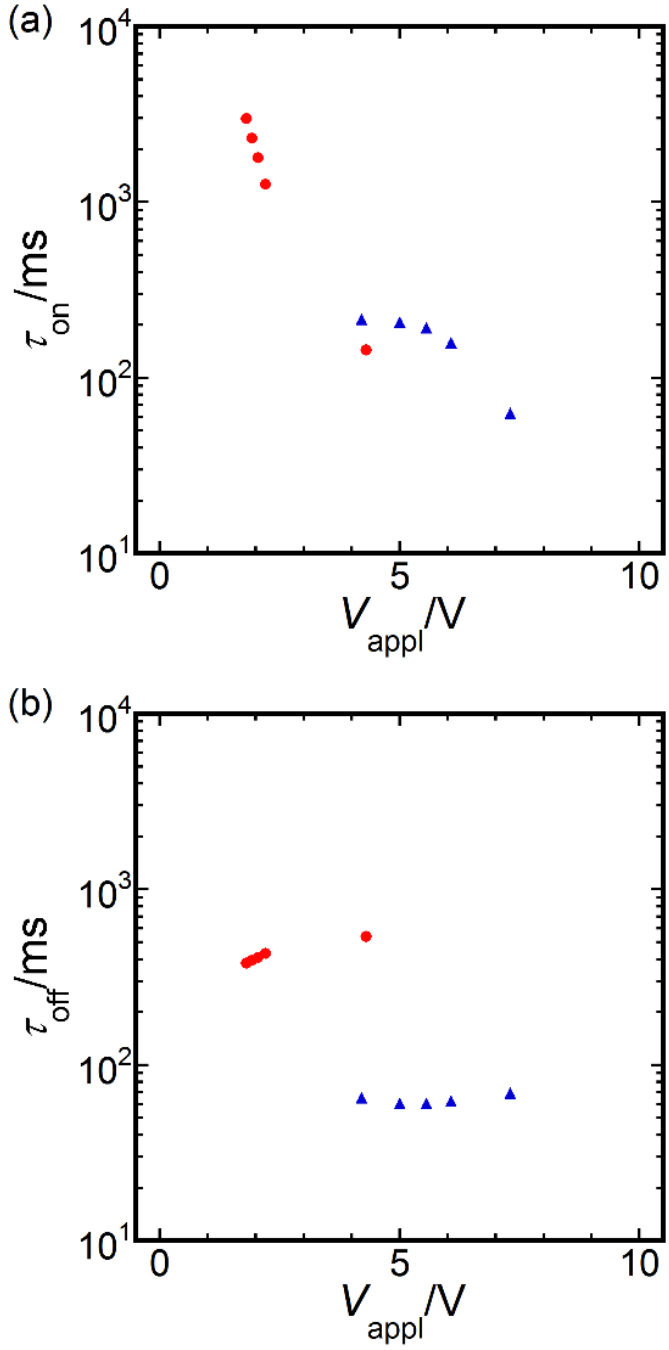

Figure 4-8. Applied voltage dependence of the response times of (a) τ_{on} and (b) τ_{off} for the type-I cell (circle) and the type-II (triangle) at 25 °C.

Chapter 5

General Conclusions

5-1 Conclusions

The purpose of this research was to investigate the following three subjects:

1) Elucidation of the anchoring behavior between high-density polymer brushes and nematic liquid crystals (NLCs);
2) Achievement of a zero-azimuth anchoring state using high-density polymer brushes; and
3) Creation of a new liquid crystal display (LCD) mode driven by in-plane switching (IPS) that utilizes the zero-azimuth anchoring state.

The following five conclusions were reached as the results of this research:

1) The NLCs on the high-density polymer brushes have a degenerate planar orientation. A uniform planar alignment of the NLCs on the high-density polymer brushes can be attained when the NLCs are slowly cooled from the isotropic phase in a magnetic field.
2) The anchoring state at the interface between the high-density polymer brushes and NLCs changes to the following three states on changes in temperature: a strong anchoring state equivalent to rubbed polyimide, a viscoelastic state, and a near-zero-azimuth anchoring state, in which anchoring in the direction of the azimuthal angle was mostly lost. Moreover, the temperature of the transition between each state changes with the kind of polymer brush and LC. The anchoring force of the LC on the polymer brush surface depends on the glass

transition temperature of the polymer brush, but can be decreased when the polymer brush is highly compatible with the NLC.

3) The interface between the high-density polymer brushes and LCs provides a strong anchoring state when the azimuthal anchoring coefficient (A_2) is over 10^{-5} J m^{-2}, a near-zero-azimuth anchoring state when the A_2 value is below about 1×10^{-6} J m^{-2}, and a viscoelastic state between these A_2 values.

4) High-density poly(hexyl methacrylate) provides stable near-zero-azimuth anchoring for NLCs at ambient temperature.

5) A new LCD mode by IPS which utilized the zero-azimuth anchoring state was succeeded in developing. An LC cell with NLCs injected between a substrate with a near-zero-azimuth anchoring interface and a substrate with a strong anchoring interface has a driving voltage reduced by almost half, 1.8 times greater maximum transmittance, and 2.3 times higher contrast ratio than a conventional IPS LCD. Such a drastic improvement in transmittance is achieved because NLCs above the comb-shaped electrodes rotate toward the electric field direction on the application of a voltage and the transmission of light above the electrodes. This new mode IPS is termed as “one side zero-azimuth anchoring in-plane switching (OZ-IPS) mode”.

5-2 Future Works

5-2-1 Basic Researches

The following two investigations are required as basic research:

1) A study of the state of the LC molecules in the high-density polymer brushes. It has not been fully examined whether LC molecules enter the polymer brushes. It will be an interesting

research task to determine the state of LC molecules in the polymer brushes, if LC molecules are present in the high-density polymer brushes.

2) A study of the density of polymer brushes that provide a zero-azimuth anchoring state. It has not been fully clarified whether a zero-azimuth anchoring state is achieved by low-density polymer brushes. This will represent an important research task, which will have a major influence on the direction of applied research.

5-2-2 Applied Researches

The study of the practical use of the new LCD mode by IPS, which utilizes the zero-azimuth anchoring state, is given as an example of applied research. The greatest challenge to its practical use is the development of a substitute material for high-density polymer brushes. Because the polymerization of polymer brushes takes a long time, it is difficult to carry out in the existing mass production of LCDs. In addition, because a substrate of which the side is about 3 m long must be immersed in a polymerization solution to form polymer brushes on the substrate, the development of new equipment and an immense amount of investment are required. With such a background, the development of a coating material that can provide the zero-azimuth anchoring state is very important. In addition, when compared with conventional IPS LCDs, there is a drawback in the new LCD mode, namely, that the response time on switching the voltage off (τ_{off}) is longer. In order to overcome this drawback, it will be necessary to also consider improvements based on innovative ideas, in addition to gradual improvements to existing knowledge such as making the cell gap thinner, reducing the viscosity of the LCs, and increasing the twist elastic modulus of LCs. At present, an innovative idea to reduce the value of τ_{off} has been suggested and the concrete design, material, and production process to achieve this are under examination.

Although the new LCD mode introduces a concept that changes completely the common idea of conventional LCDs, it has the merit that the structure of conventional IPS LCDs and many existing processes can be retained. I aim to accelerate the pace of the research described in this section and achieve a true innovation, i.e., a technological innovation with economic merit, in a short period of time.

List of Publications

1. Tokita, M., **Sato, O.**, Inagaki, Y., Nomura, A., Tsujii, Y., Kang, S., Fukuda, T., & Watanabe, J. High-Density Poly(methyl methacrylate) Brushes as Anchoring Surface of Nematic Liquid Crystals. Japanese Journal of Applied Physics 50, 071701(2011).
2. **Sato, O.**, Kasai, T., Nomura, A., Tsujii, Y., Kang, S., Tokita, M., & Watanabe, J. Viscoelastic PS brush surface offering strong anchoring at low temperature and near-zero anchoring at high temperature for LC molecules. Liquid Crystals 40 (2), 221-227 (2013).
3. **Sato, O.**, Kasai, T., Sato, M., Sakajiri, K., Tsujii, Y., Kang, S., Watanabe, J., & Tokita, M. High-density poly(hexyl methacrylate) brushes offering a surface for near-zero azimuthal anchoring of liquid crystals at room temperature. Journal of Materials Chemistry C 1, 992-7995 (2013).
4. **Sato, O.**, Iwata, N., Kasai, T., Tsujii, Y., Kang, S., Watanabe, J., & Tokita, M. Nematic Liquid Crystal Anchoring Strengths of High Density Polymer Brush Surfaces. Liquid Crystals 42 (2), 181-188 (2015).
5. **Sato, O.**, Iwata, N., Kawamura, J., Maeda, T., Tsujii, Y., Watanabe, J., & Tokita, M. An in-plane switching liquid crystal cell with weakly anchored liquid crystals on the electrode substrate. Journal of Materials Chemistry C 5, 4384-4387 (2017).

Publications not included in the thesis

1. **Sato, O.**, Inagaki, Y., Kang, S., Tokita, M., & Watanabe, J. Regular Network Pattern Evolution Observed in Phase Separation in Low-Molecular-Weight LC and LC Block Copolymer Mixture. Macromolecules 42 (15), 5442-5445 (2009).
2. Sugiyama, T., **Sato, O.**, Kang, S., Tokita, M., & Watanabe, J. Nematic-nematic phase separation from uniform nematic domain in polymer LC and low-molecular-weight LC mixture showing network lattice formation in pinning stage. Soft Matter 7, 6998-7002 (2011).
3. Momoi, Y., **Sato, O.**, Koda, T., Nishioka, A., Haba, O., & Yonetake, K. Surface rheology of rubbed polyimide film in liquid crystal display. Optical Materials Express 4 (5), 1057-1066 (2014).
4. Iwata, N., **Sato, O.**, Ohno, K., Sakajiri, K., Kang, S., & Tokita, M.Transparent and High Permittivity Films of Poly(Methyl methacrylate)-Grafted 7nm Barium Titanate Particles Prepared by Suraface-Initiated Atom Transfer Radical Polymerization. Polymer 81, 23-28 (2015).

Acknowledgment

It has been a great pleasure to complete this thesis here based on cooperative research with the Watanabe & Tokita Laboratory of the Department of Organic and Polymeric Materials, Faculty of Engineering, Tokyo Institute of Technology and the Tsujii Laboratory of the Institute for Chemical Research, Kyoto University.

The author would like to express deep appreciation to Masatoshi Tokita, an Associate Professor at the Tokyo Institute of Technology for his continuous guidance and invaluable discussions, as well as his constant encouragement throughout this thesis.

The author would like to express his gratitude to Emeritus Professor Junji Watanabe at the Tokyo Institute of Technology, Emeritus Professor Takeshi Fukuda and Professor Yoshinobu Tsujii at Kyoto University for their guidance and generous support.

The author would also like to show his appreciation to Professor Toshiaki Ougizawa, Professor Atsushi Shishido, Associate Professor Susumu Kawauchi, and Associate Professor Hidetoshi Matsumoto at the Tokyo Institute of Technology for their insightful comments and suggestions.

The author would like to offer his thanks to Assistant Professor Sungmin Kang and the members of the Watanabe & Tokita Laboratory and Assistant Professor Keita Sakakibara and the members of the Tsujii Laboratory for their useful advice and kind help.

In addition, the author would like to thank Dr. Tsuyoshi Maeda, Mr. Joji Kawamura, Ms. Harumi Okuno, Mr. Isao Adachi, and Mr. Hayato Ishiguro, who were his colleagues at the Japan Laboratory, LG Display Co., Ltd., for their useful suggestions and kind help.

Finally, the author expresses his heartfelt thanks to his wife and his parents for their continuous support and encouragement.

March 2018

Osamu Sato